DEVELOPMENT OF A "SELF-CLEANING" ENCAPSULATION TECHNOLOGY FOR IMPLANTABLE GLUCOSE MONITORING

A Dissertation

by

REBECCA MAY GANT

Submitted to the Office of Graduate Studies of
Texas A&M University
in partial fulfillment of the requirements for the degree of

DOCTOR OF PHILOSOPHY

December 2009

Major Subject: Biomedical Engineering

DEVELOPMENT OF A "SELF-CLEANING" ENCAPSULATION TECHNOLOGY FOR IMPLANTABLE GLUCOSE MONITORING

A Dissertation

by

REBECCA MAY GANT

Submitted to the Office of Graduate Studies of
Texas A&M University
in partial fulfillment of the requirements for the degree of

DOCTOR OF PHILOSOPHY

Approved by:

Co-Chairs of Committee,	Gerard L. Coté
	Melissa A. Grunlan
Committee Members,	Kenith Meissner
	Cynthia Meininger
Head of Department,	Gerard L. Coté

December 2009

Major Subject: Biomedical Engineering

ABSTRACT

Development of a “Self-Cleaning” Encapsulation Technology for Implantable Glucose Monitoring. (December 2009)

Rebecca May Gant, B.S., Cornell University;

M.E., Cornell University

Co-Chairs of Advisory Committee: Dr. Gerard L. Coté
Dr. Melissa A. Grunlan

The increasing prevalence of diabetes and the severity of long-term complications have emphasized the need for continuous glucose monitoring. Optically-based methods are advantageous as they have potential for noninvasive or minimally invasive detection. Fluorescence-based affinity assays, in particular, can be fast, reagentless, and highly specific. Poly(ethylene glycol) (PEG) microspheres have been used to encapsulate such fluorescently labeled molecules in a hydrogel matrix for implantation into the body. The matrix is designed to retain the sensing molecules while simultaneously allowing sufficient analyte diffusion. Sensing assays which depend upon a spatial displacement of molecules, however, experience limited motility and diminished sensor response in a dense matrix. In order to overcome this, a process of hydrogel microporation has been developed to create cavities within the PEG that contain the assay components in solution, providing improved motility for large sensing elements, while limiting leaching and increasing sensor lifetime.

For an implanted sensor to be successful *in vivo*, it should exhibit long-term stability and functionality. Even biocompatible materials that have no toxic effect on surrounding tissues elicit a host response. Over time, a fibrous capsule forms around the implant, slowing diffusion of the target analyte to the sensor and limiting optical signal propagation. To prevent this biofouling, a thermoresponsive nanocomposite hydrogel based on poly(*N*-isopropylacrylamide) was developed to create a self-cleaning sensor membrane. These hydrogels exist in a swollen state at temperatures below the volume phase transition temperature (VPTT) and become increasingly hydrophobic as the temperature is raised. Upon thermal cycling around the VPTT, these hydrogels exhibit significant cell release *in vitro*. However, the VPTT of the original formula was around 33-34°C, resulting in a gel that is in a collapsed state, ultimately limiting glucose diffusion at body temperature. The hydrogel was modified by introducing a hydrophilic comonomer, *N*-vinylpyrrolidone (NVP), to raise the VPTT above body temperature. The new formulation was optimized with regard to diffusion, mechanical strength, and cell releasing capabilities under physiological conditions. Overall, this system is a promising method to translate a glucose-sensitive assay from the cuvette to the clinic for minimally invasive continuous glucose sensing.

DEDICATION

To my husband, Alex, and our future child

ACKNOWLEDGEMENTS

I would like to thank my co-advisors, Dr. Coté and Dr. Grunlan, as well as my committee members, Dr. Meissner and Dr. Meininger, for their guidance and support throughout the course of this research. Thanks also go to my friends and fellow labmates, past and present, in the Optical Bio-sensing Laboratory. Your humor and vitality have made this an exciting and often unexpected ride. I am particularly grateful for assistance from Alex Abraham, who took over all of my “dangerous” chemical work and is always willing to lend a hand, even when he has a conference poster, a quiz, and homework due the next day.

I would also like to thank the many sources of funding that kept food on my table and wireless internet legal at my house, including the Department of Biomedical Engineering, the Dwight Look College of Engineering, NASA/Texas Space Grant Consortium, SPIE, and the NIH/NIDDK (1R21DK082930-01A1).

Finally, I would like to thank my husband, Alex, and our families for your unconditional support and love. Thank you for always being there.

TABLE OF CONTENTS

CHAPTER Page

CHAPTER Page

LIST OF FIGURES

FIGURE Page

FIGURE Page

FIGURE Page

LIST OF TABLES

CHAPTER I

INTRODUCTION

Motivation

Glucose is a simple sugar and one of the most important fuels for the body. In order for the energy to get into cells though, a key is needed. This key is the hormone insulin. Diabetes mellitus is a disease in which the body does not produce or properly use insulin, leading to abnormal glucose levels. The term diabetes was first used by Araetus of Cappodocia (81 – 133 AD).[1] The Greek word is comprised of *dia*, which means "through", and *betes*, meaning "to go".[2] Combined the word was used to refer to the excessive amounts of urine that were passed by those affected by the disease. *Mellitus*, Latin for "honey", was later added by Thomas Willis to describe the sweet taste of the urine of diabetics.

In type 1 diabetes, which has previously been known as insulin-dependent (IDDM) or juvenile-onset, the immune system attacks the insulin-producing beta cells in the pancreas, resulting in little to no insulin production. In order to survive, type 1 diabetics must have daily insulin administrations either by injection or a pump. In type 2 diabetes, previously known as non-insulin dependent (NIDDM) or adult-onset, diabetics have developed an insulin resistance.[3] As the cells do not use the insulin properly, the need for

---

This dissertation follows the style of Journal of Biomedical Materials Research.

insulin rises, and the pancreas gradually loses its ability to produce the hormone. Type 2 diabetes is often associated with obesity, older age, and family history and accounts for about 90 to 95% of diagnosed cases in adults.[4] Gestational diabetes is similar to type 2 diabetes in that it involves an inadequate level of insulin secretion and responsiveness, but it is first diagnosed during pregnancy. Though 90 to 95% of women revert to normal after pregnancy, maternal glucose levels must be controlled to avoid complications in both the mother and infant. In addition, women who have had gestational diabetes have a 40 to 60% chance of developing diabetes in the following 5 to 10 years.[4]

Incidence of Diabetes

Diabetes is a debilitating disease that affects over 180 million people, according to the World Health Organization, with estimates projecting to 366 million in 2030.[5,6] Figure 1.1 shows the affected populations and future projections.[7] In upper-middle income countries, diabetes-related deaths are expected to increase by over 80% between 2006 and 2015.[6] Even closer to home, the state of Texas experienced the second highest number of newly diagnosed cases (156,000) out of 33 states surveyed between 2005 and 2007.[8] The age-adjusted incidence of diabetes increased by 208% from the period of 1995-1997 to 2005-2007. Overall, diabetes is rapidly becoming more prevalent, causing major concerns in the health care industry.

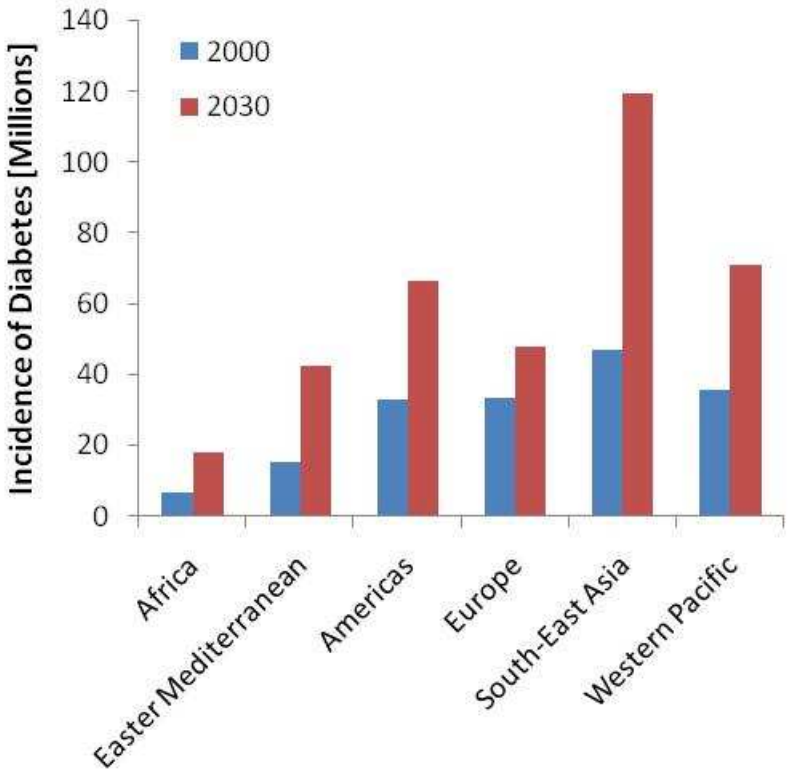

Figure 1.1. Prevalence of diabetes throughout the world in 2000 and projections for 2030

The related costs in the United States alone, were estimated to be approximately $174 billion in 2007.[4] In addition to the costs incurred by known diabetics, approximately 5.7 million people are undiagnosed.[4] Furthermore, there are 57 million people in the U.S. with prediabetes that may develop into type 2 diabetes unless serious lifestyle interventions are performed to prevent or delay onset.[9] Prediabetics can have impaired fasting glucose (IFG) in which the fasting blood sugar level is 100 to 125 mg/dL after an overnight fast and/or impaired glucose tolerance (IGT) where the blood sugar level is 140 to 199 mg/dL after a 2 hour oral glucose tolerance test.[4] The growing epidemic is so

serious that it prompted a United Nations Resolution on diabetes, which designates November 14th as World Diabetes Day in order to raise public awareness of the problem and encourages Member States to develop national policies for both the prevention and treatment of diabetes. [10,11]

Controlling Glucose Levels

Better glycemic control can lead to better health and quality of life and is associated with a significant health care cost savings.[12] While type 1 diabetes is typically treated with injections of insulin, type 2 diabetes is often controlled through diet, exercise, and oral medication. Figure 1.2 shows the breakdown of patients receiving insulin and/or oral medication.[4] In order to administer either treatment, a diabetic must know how much glucose is in their blood. Typically, a finger is pricked with a small needle called a lancet to get a drop of blood which is then tested by an enzymatic assay in a glucometer machine.

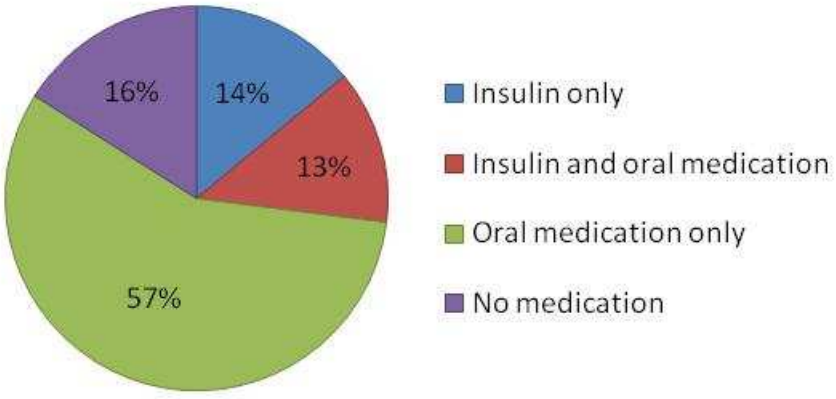

Figure 1.2. Treatment methods among adults with diagnosed diabetes in the United States, 2004-2006

Diabetes-related Complications

Maintaining glucose levels in a tight range (70-120 mg/dL) may help avoid complications such as blindness, heart disease, stroke, kidney failure, and nerve damage.[3,13] Adults with diabetes have about 2 to 4 times higher rates of death due to heart disease and 2 to 4 times higher risk of stroke.[4] Diabetes is the leading cause of new cases of blindness among adults 20 to 74 years old.[4] After only 15 years of diabetes, about 10% of people develop severe visual impairment.[6] Diabetes is the primary cause of kidney failure, accounting for 44% of new cases in 2005, and 10 to 20% of diabetics die of kidney failure.[4,6] Poorly controlled diabetes during pregnancy can cause major birth defects in 5 to 10% and spontaneous abortions in 15 to 20% of pregnancies.[4] Diabetic neuropathy causes about 60 to 70% of diabetics to have impaired sensation or pain in the feet and hands, slowed digestion of food in the stomach, carpal tunnel syndrome, erectile dysfunction, or other nerve problems.[4] Diabetes is responsible for an amputation every 30 seconds and a death every 10 seconds.[14] Regular monitoring of glucose levels is important for treating diabetes and minimizing the risk of such complications.[13]

Commercially Available Sensors for SMBG

While there are currently over 40 blood glucose meters that are commercially available for self-monitoring of blood glucose (SMBG), the majority of the market is shared between Roche Diagnostics, Johnson & Johnson's LifeScan, Abbott, and Bayer.[15] Most of these glucose sensors are based on an enzymatic assay that converts glucose in the

blood into a measurable end product, as proposed by Clark and Lyons in 1962.[16] The most commonly used enzymes contain redox groups that change redox state during the biochemical reaction, such as glucose oxidase (GOx) and glucose dehydrogenase (GDH).[15] For example, glucose oxidase can be fixed to an electrode where it will catalyze the conversion of glucose into gluconolactone and hydrogen peroxide. The hydrogen peroxide then reacts at the sensing electrode, resulting in a measurable electric current.

$$\text{glucose} + O_2 \xrightarrow{GOx} \text{gluconolactone} + H_2O_2$$

$$H_2O_2 \longrightarrow 2e^- + O_2 + 2H^+$$

Because the testing occurs *ex vivo*, results can be affected by environmental factors such as temperature, altitude, and humidity as well as internal confounders like hematocrit, uric acid, glutathione, and vitamin C.[17] Additionally, the analytical quality of many self monitored tests does not meet American Diabetes Association error standards when performed by a patient as opposed to a trained technician.[18] The ADA has stated that all SMBG systems should have a total error of less than 10%.[18] The International Organization for Standardization more specifically specifies that a glucose meter should obtain 95% of results within 5, 10, and 15 mg/dL for glucose values less than 75 mg/dL and within 5%, 10%, 15%, and 20% of the reference if the glucose value is equal to or greater than 75 mg/dL.[19]

One of the main disadvantages of current SMBG meters is that they require a blood sample. Whether obtained through finger-pricking or forearm acquisition, this can be painful, cause calluses, and could lead to other complications such as infection. The inconvenience and embarrassment may also contribute to low patient compliance. Current guidelines regarding testing frequency vary depending on the individual patient treatment regimen. For example, the ADA recommends that patients using multiple insulin injections should test a minimum of three times a day.[20] Cost may be another potentially prohibitive factor to testing. An individual disposable test strip is estimated to cost about $1, leading to an average annual expense of $1,460 for patients with type 1 diabetes.[21] This can be higher for patients using an insulin pump, who typically test more frequently.[22] Another problem with the current SMBG meters is the potential for hypoglycemia unawareness. Testing is rarely done at night when patients are vulnerable to dangerous glucose levels while sleeping. Additionally, testing is done a few times a day at best, providing only a "snapshot" of the blood glucose level.[23]

CHAPTER II

CONTINUOUS GLUCOSE SENSING

Advantages of Continuous Glucose Sensing

There are several advantages to continuous glucose monitoring that have driven research for the past 30+ years. It is estimated that a patient who closely monitors glucose levels will gain 5 more years of life, 5 more years of eyesight, 6 more years free of kidney disease, and 6 more years without amputations and nerve damage than the average patient.[24] Increased SMBG is correlated with better long term glucose levels, but for practical reasons most patients do not test their blood sugar more than 5 to 7 times a day.[25] Continuous glucose monitoring has been shown to help identify periods of significant glycemic excursion, which allowed physicians to modify recommendations for timing and dosage of insulin injections and dietary changes, resulting in improved glycemic control.[26,27] In addition to lowering the average values of HbA1c, which is a form of hemoglobin used to quantify the average plasma glucose concentration over long periods of time, continuous monitoring has also been shown to reduce the rate of severe hypoglycemia, or dangerously low blood sugar.[28] Alarms can also be incorporated into continuous glucose monitoring systems (CGMS) to warn patients when sugar levels exceed a certain range, preventing dangerous “highs” and “lows”, particularly at night when patients are unaware of their glycemic status.

In an effort to "close the loop" and develop an artificial pancreas system, current CGM systems have been paired with external insulin pumps. A recent clinical trial showed that insulin pump therapy combined with CGMS improves blood sugar levels more than conventional pump therapy.[25] The idea of connecting glucose sensing to insulin delivery was first used in 1964 with intravenous infusions of insulin and glucose.[29] A fully automated system could be achieved as shown in Figure 2.1, whereby the sensor detects the glucose concentration, relaying the information to a receiver that would determine the amount of insulin needed using a control algorithm. The information is then sent to the insulin infusion device which would distribute the appropriate amount of insulin to the body. This feedback-controlled system has the potential to eliminate the necessity of frequent patient performed blood draws and injections, while simultaneously improving glycemic control.

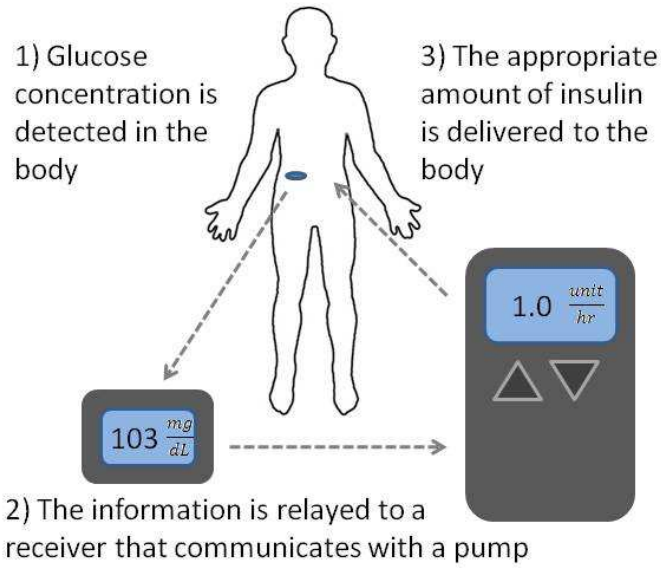

Figure 2.1. Potential closed loop system for regulating *in vivo* glucose levels

Transdermal Meters

Transdermal meters sample glucose through the intact skin by drawing the glucose out, typically using some sort of enhancement technique such as electric current (iontophoresis), acoustic energy (sonophoresis), chemicals that enhance the permeation of glucose through skin (passive diffusion), or mechanical permeation (microporation).[30]

The first commercially available non-invasive glucose sensor in the US, the GlucoWatch Biographer (originally by Cygnus, Redwood City, CA), was approved by the FDA in 2001 as an adjunct to traditional SMBG. The device extracts glucose using reverse iontophoresis. A low-level electric current is passed through the skin and uncharged glucose molecules are carried along by convective transport. The glucose concentration is then measured electrochemically using a glucose oxidation reaction. The system has shown good linearity between the recorded signal and blood glucose level, but has encountered many problems such as an average lag time behind blood glucose of 18 minutes, low sensitivity in detecting hypoglycemic values below 3.9 mmol/L, and skin reactions at the electrode sites.[31] Additionally, the GlucoWatch needs to warm up for 3 hours and then makes only up to three measurement an hour for 12 hours before needing to be recalibrated via finger-stick.[15] Animas purchased the technology in 2005 and attempted to make an improved 3rd generation GlucoWatch, but decided to cease sales of the device in 2007.

Impedance Measurements

Another watch-type glucose sensing device, the Pendra, was introduced by the Swiss company Pendragon Medical in 2000 and received CE approval for use in Europe as a supplemental device to traditional SMBG in 2003.[32] The Pendra determines glucose concentrations indirectly using impedance spectroscopy to measure sodium transport over the erythrocyte membrane, which is linked to changes in glucose. The sodium flux induces changes in impedance, which are detected and converted into a corresponding glucose value. Beyond normal physiological interference, impedance values can be influenced by additional confounders such as temperature, hematocrit, and erythrocyte sedimentation rate.[33-35] Another drawback to this system is the lengthy calibration process that lasts 2 to 3 days, after which approximately 30% of patients are deemed ineligible to use the Pendra as their skin is found to be unsuitable for these measurements.[32] During the calibration process, patients intentionally try to elevate glucose levels by at least 100 mg/dL to assess the signal sensitivity, which is contrary to normal glycemic goals.[36] Furthermore, the adhesive tape must be changed daily followed by a 1 hour equilibration time and baseline adjustment before it can be used again.[37,38] Another prohibitive aspect is cost. The first devices were distributed for an initial €1,250 followed by a leasing fee of €95 a month for at least two years.[32] A postmarket reliability study found the results of Pendra-measured glucose to differ by 52% from traditional SMBG values. Additionally, 4.3% of the error was in a “danger zone” that would fail to detect severe hyperglycemia or hypoglycemia.[39] A number of technical issues and

internal company concerns led Pendragon to cancel further marketing of the Pendra in 2004 and the company eventually filed for bankruptcy in 2005.[32]

Transcutaneous Monitors

GlucoDay is a microdialysis device marketed in Europe by A. Menarini Diagnostics. Interstitial fluid is sampled through a subcutaneous catheter and the glucose concentration is detected using glucose oxidase. Calibration by finger-stick is required every 72 hours, but the current recommendations only allow the device to be worn for 48 hours. Measurements are made every 3 minutes and the sensor has an excellent linear range extending to 27 mM (486 mg/dL), but the lag time of the sensor is about 35 minutes.[39-41] While patients reported experiencing little pain during catheter insertion, they expressed a mean discomfort of 3.6 out of 5 while wearing the device.[42] In an age of increasingly smaller "nano" personal music devices, the GlucoDay is a bulky, Walkman-sized piece of machinery that is carried around in a pouch around the waist. Currently the catheter insertion is performed by a physician and the device is not approved for autonomous use.[43] The device has the potential for real-time CGM, but as of yet, Menarini has not announced any plans to bring the GlucoDay to the U.S. market.

There are currently four CGM systems available in the United States: the DexCom Seven, the FreeStyle Navigator, the Medtronic MiniMed Guardian REAL-Time System, and the Medtronic MiniMed Paradigm REAL-Time System, which is combined with a

manually operated insulin pump. These devices are transcutaneous and can remain *in situ* between three to seven days.[44]

Table 2.1. Characteristics of commercially available CGMS

Model	Manufacturer	Measurement Frequency	Predictive Alarms	Calibration	Sensor Life
Seven	DexCom	every 5 min	No	At 2 hr x 2, then every 12 hrs	7 days
Freestyle Navigator	Abbott	every 1 min	Yes	At 10, 12, 24, 72 hr	5 days
Guardian	Medtronic MiniMed	every 5 min	Yes	At 2 h, 6 hr, then every 12 hrs	72 hrs
Paradigm	Medtronic MiniMed	every 5 min	No	At 2 h, 6 hr, then every 12 hrs	72 hrs

The subcutaneous portion of the sensor contains a glucose oxidase sensor that measures interstitial glucose in terms of electric current, continuously measuring glucose levels and sending readings via a wireless transmitter to a separate monitor. The data can be downloaded to a computer in the home or clinic and used to evaluate overall glycemic trends. The first generation of CGMS devices did not have a display for patient use, but were used only to provide information to physicians. The current systems generate real-time measurements in the interstitial fluid, which can lag behind blood by up to 10-15 minutes.[45] This must be considered when a glycemic fluctuation is noticed and it is recommended that a finger-stick be performed prior to starting treatment such as an

insulin bolus. Additional finger-stick testing must be done to calibrate the systems upon initial setup and for recurring alignment as shown in Table 2.1.[39] The overall percentage of error averages around 15% for each of these systems.[46] Clinical studies concluded that the largest source of error is the calibration process.[47] These CGM systems have shown a lot of promise in terms of helping patients to achieve tighter glycemic control and minimizing hypoglycemic events, but there is still much to be done to increase sensor longevity and overcome some of the other barriers mentioned here.[26-28]

Optical Methods

Optical glucose detection techniques are advantageous because they allow for the possibility of non-invasive or minimally-invasive sensing. A significant amount of research has been done as evidenced by the 3990 non-invasive/noninvasive glucose patents issued by the USPTO since 1976.[48] A wide range of methods have been explored, including infrared absorption, near-infrared scattering, Raman spectroscopy, fluorescence spectroscopy, kromoscopy, thermal gradient spectroscopy, polarimetry, optoacoustic techniques, optothermal systems, and optical coherence tomography, but as of yet, none of these are commercially available.[49,50]

One method to achieve continuous measurement is through the use of a fluorescence-based glucose sensitive sensor that could be implanted intradermally. Once implanted, the corresponding optical signal would be monitored non-invasively with an external portable device. A system such as this would eliminate the potential for infection caused

by the transcutaneous nature of the current CGMS devices, while increasing accuracy over transdermal devices as the glucose concentration would be directly measured in the interstitial fluid. Fluorescence is the process by which a molecule in an excited state releases energy in the form of photons, as shown in Figure 2.2. Incoming light is absorbed by a fluorescent molecule in the ground state, S_0, raising it to an excited energy state, S_1. The molecule relaxes to a lower vibrational state through internal conversion (IC). Energy can then be released through spontaneous emission of a lower energy (longer wavelength) photon as in fluorescence, or through a nonradiative pathway such as quenching, scattering, or releasing heat, returning the molecule to the ground state.[51]

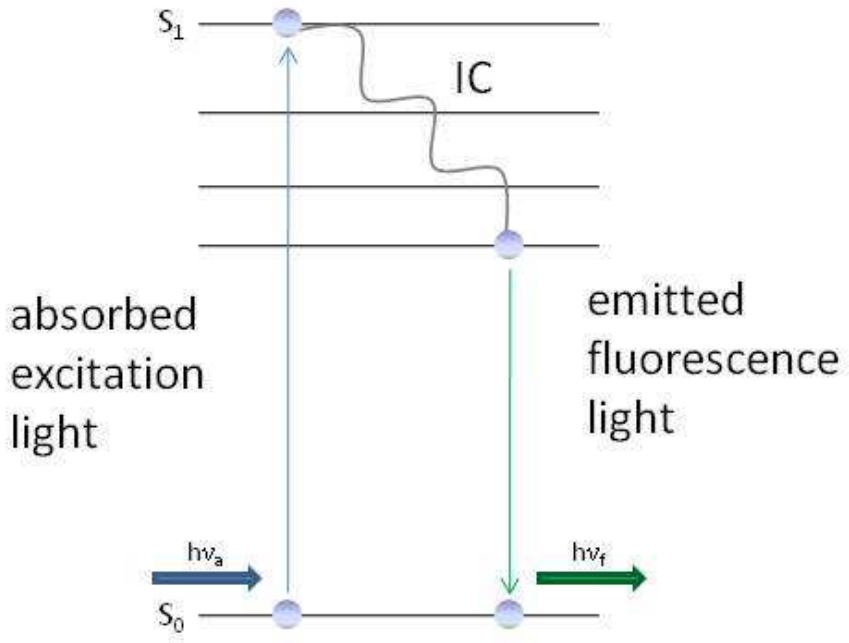

Figure 2.2. Jablonski energy diagram displaying the process of fluorescence

Some of the early work using fluorescence principles for glucose sensing involved fluorescence resonance energy transfer (FRET). FRET is the transfer of excited-state energy from a donor molecule (D) to an acceptor molecule (A) without the emission of a photon. The emission of the donor molecule is at shorter wavelengths and overlaps with the acceptor's absorption spectrum. The energy transfer is a result of dipole-dipole interactions between D and A, which lowers the fluorescence of D when both dyes are between 20 and 70 Å apart.[52] Figure 2.3 demonstrates this principle.

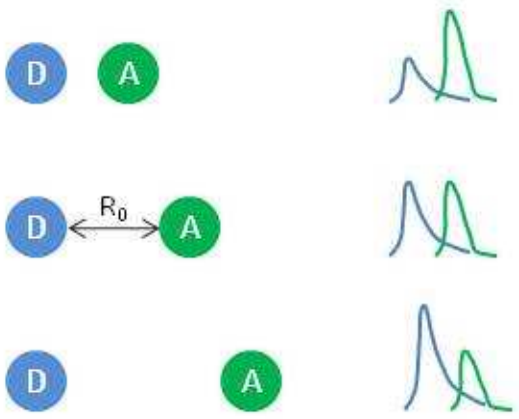

Figure 2.3. Relationship between donor-to-acceptor distance and fluorescence spectra intensity

When D and A are very close, energy transfer occurs, resulting in a smaller donor emission spectra intensity shown in blue. As the distance between D and A increases beyond approximately 70 Å, the energy transfer does not tend to occur, and therefore, the intensity of the donor emission spectra will increase.

The rate of energy transfer depends upon the extent of spectral overlap of the emission spectrum of the donor with the absorption spectrum of the acceptor, the quantum yield of the donor, the relative orientation of the donor and acceptor transition dipoles, and the distance between the donor and acceptor molecules.[51] It can be calculated from the following:

$$k_T = \frac{1}{\tau_D}\left(\frac{R_0}{r}\right)^6$$

where k_T is the rate of energy transfer from donor to acceptor, τ_D is the decay time of the donor in the absence of acceptor, R_0 is the Förster distance at which energy transfer is 50% efficient, and r is the donor-to-acceptor distance. The efficiency of energy transfer (E) is the fraction of photons absorbed by D that are transferred to A.[51]

$$E = \frac{k_T}{\tau_D^{-1} + k_T} = \frac{R_0^6}{R_0^6 + r^6} = \frac{1}{1 + \left(r/R_0\right)^6}$$

This can be seen in figure 2.4. From this diagram, it is evident that for r-values less than R_0, the energy transfer efficiency rises rapidly towards 100%.

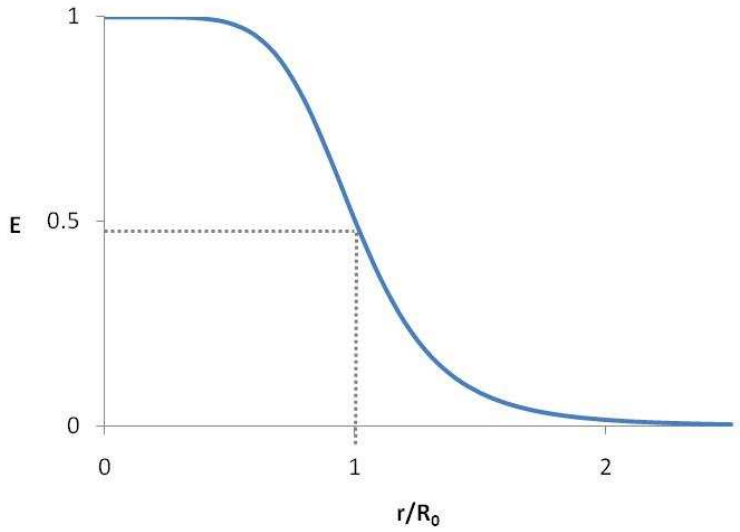

Figure 2.4. Dependence of the energy transfer efficiency on the ratio of D-to-A distance to the Förster distance

The donor-to-acceptor distance is important as the rate of energy transfer is inversely proportion to r^6. This principle has been studied extensively for glucose sensing. If the chemistry can be arranged so that the addition of glucose to the system causes an increase in *r*, then the fluorescence intensity will increase proportionally, as well.

One way to do this is by using a protein called Concanavalin A. Con A is a lectin isolated from the jack bean plant, *Canavalia ensiformis*.[53] At physiological pH, it tends to exist in tetrahedral form with one saccharide binding site in each subunit, as depicted by the red molecules in Figure 2.5.[54] If the pH is lowered to less than 5.6 or the temperature is less than 4 °C, Con A will take on a dimeric form.[55] Con A also contains binding sites for specific metals. The first site, S_1, can bind a transition metal such as

Mn^{2+}, Ni^{2+}, Co^{2+}, Zn^{2+}, or Cd^{2+}. The second site, S_2, tends to bind Ca^{2+} or Cd^{2+}. The most typically bound ions are manganese (shown in teal) and calcium (blue).

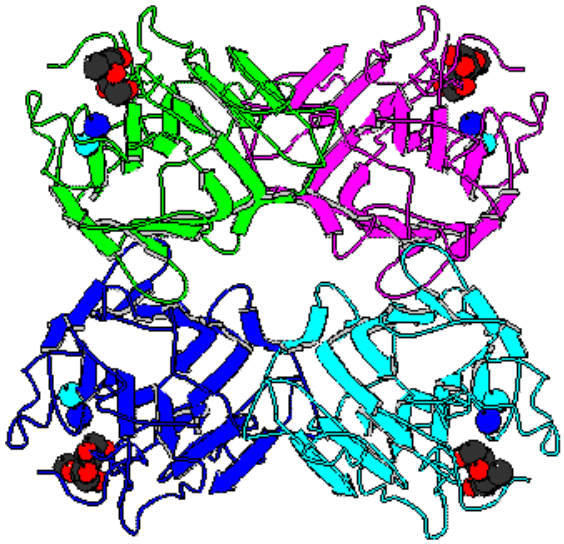

Figure 2.5. Concanavalin A tetramer

S_1 binding must take place before S_2 binding can occur and both sites must be occupied for the saccharide binding site to be active.[55] The sugar binding site is approximately 350-600 pm wide, 750 pm high, and 1.8 nm deep.[55] It has a particular affinity for saccharides containing α-D-glucose or α-D-mannose residues.[56] Therefore, Con A has been a popular topic of research for glucose sensing to treat diabetes.

Some of the earliest work in this area was done by Schultz *et al.*[57] They used Concanavalin A as a selective bioreceptor and took advantage of the competitive binding

between FITC-labeled dextran and glucose. The Con A was immobilized on the inner membrane of a hollow dialysis fiber. The large size of the dextran prevented it from leaving the dialysis fiber, while the much smaller glucose molecules were free to diffuse in and out, displacing dextran as they became bound to the Con A. Because the dextran was labeled with FITC, it fluoresced as the free molecules were excited by an optical fiber. The measured fluorescence intensity was proportional to the amount of glucose attached to the Con A. The rate of response of this sensor to changes in glucose concentration is based on the rate of glucose diffusion through the dialysis fiber wall, the competitive displacement of dextran by glucose, and the rate of diffusion of all of the components in solution. One major problem with this early sensor is that the Con A had to be immobilized to the wall of the hollow fiber, which is not easily reproducible. The optical fiber and the dialysis fiber must also be carefully aligned in order to maintain the spatial difference in the bound and free dextran and calibration must be performed using external standards because of the lack of an internal reference.

One of the first improvements on this sensor was to eliminate the immobilization of Con A. Meadows and Schultz used FITC-labeled dextran again and added Rhodamine-labeled Con A. The labels absorb and fluoresce in the visible region and were useful in tracing the following reactions[58]:

$$\underset{\text{(competing analyte)}}{\text{FITC}-\text{dextran}} + \underset{\text{(receptor)}}{\text{Rh}-\text{Con A}} \leftrightarrow \underset{\text{(competing analyte receptor)}}{\text{FITC}-\text{dextran: Rh}-\text{Con A}}$$

$$\underset{\text{(analyte)}}{\text{Glucose}} + \underset{\text{(receptor)}}{\text{Rh}-\text{Con A}} \leftrightarrow \underset{\text{(analyte receptor)}}{\text{Glucose: Rh}-\text{Con A}}$$

When the dextran is bound to the Con A, the labels are less than 50 Å apart, which is close enough to cause significant quenching. As glucose is added, it binds to the Con A, freeing dextran. The distance between the FITC and Rh labels is increased, lowering the quenching and increasing the signal intensity. This design is a significant improvement over the original sensor. The Con A does not need to be immobilized, eliminating the lack of immobilization reproducibility and allowing more leeway in the alignment of the optical and dialysis fibers. Because all of the reaction components are contained in a homogeneous solution, the size of the assay can be reduced from 1-10 mL down to around 1 μL. Also, the Rhodamine fluorescence signal tends to be unaffected by the energy transfer and is therefore useful as an internal reference for calibration.

The next improvement on this system involved changing the receptor label from Rhodamine to tetramethylrhodamine isothiocyanate (TRITC).[59] The new label was chosen because of the large spectral overlap between the emission spectra of FITC and the absorbance spectra of TRITC. The FITC/Rh overlap spans from approximately 515 to 550 nm while the FITC/TRITC overlap reaches from about 480 to 600 nm, causing higher energy transfer efficiency. In addition to the increased energy transfer efficiency, the dynamic range of the TRITC-Con A conjugates was improved due to higher dye to protein ratios.

These sensors are all based on hollow-fiber systems in which an optical fiber is inserted into one end of the membrane. If they were to be used *in vivo*, there would be an

increased risk of infection around the skin that the fiber penetrates. Ballerstadt and Schultz designed a sensor that is totally implantable.[60] It is comprised of a semipermeable membrane containing porous beads with labeled Con A. It is placed within 0.5 mm of the skin surface so that light can easily travel to and from the sensor. Because some light will be lost due to scattering and absorption of the tissue, the sensor must demonstrate a significant fluorescence response to glucose. The sensor uses porous Sephadex beads that contain glucose residues. Alexa-488 labeled Con A binds to the residues inside the beads and is thereby shielded from light because the absorption spectrum of the bead color overlaps with the excitation and emission spectra of the label. When glucose is added to the solution, the Con A diffuses out of the beads to bind with the glucose. It can then be exposed to light, resulting in an increase in fluorescence intensity. This sensor has several advantages. It is small enough to be implantable (0.5 x 0.2 mm). It also has a response time of only 4 to 5 minutes. Most importantly, though, it shows a strong dynamic signal change for glucose concentrations in the range of 0 to 30 mM. This was achieved because the Sephadex beads provided a large number of glucose residues for Con A binding and the dye on the beads prevented excitation light from reaching the bound Con A.

Another alternative to the hollow fiber sensor was suggested by Russell and Pishko.[61] They pointed out that the majority of past research was limited to aqueous solutions and did not address the issue of assay chemistry encapsulation. They designed a system using a PEG hydrogel to incorporate chemically immobilized pendant TRITC-Con A

and physically immobilized FITC-dextran. PEG, or poly(ethylene glycol), is biocompatible and may improve the stability and solubility of many bound proteins.[61] The sensing was based on FRET in the same manner as the previous aqueous systems. The sensors were optimized by adjusting the Con A to dextran ratio to achieve maximum glucose sensitivity and the response was found to be linear up to 600 mg/dL, which is reasonable for physiological use. The measured response time was between 10 and 12 minutes, but the limiting factor was diffusion time. This time could potentially be lowered by creating smaller spheres, thereby reducing the diffusion distance. If contained in a capsule such as a diffusion membrane, the tiny hydrogel spheres have the potential for transdermal injection, creating a minimally-invasive “smart tattoo” for glucose sensing.

In order to increase the dynamic response of the competitive binding assay, the dextran molecule was replaced with a spherical dendrimer molecule.[62,63] Dendrimers are repeatedly branched structures consisting of a core molecule surrounded by consecutive branching layers. In this embodiment, a fourth-generation polyamidoamine (PAMAM) glycodendrimer was used as the competing ligand, as shown in Figure 2.6. In the absence of glucose, the Con A tetramers are bound to the glycodendrimer molecules. As glucose is added to the system, it binds to the receptors on the Con A, competitively displacing the dendrimers, resulting in an increase in the intensity of the dye label affixed to the Con A as the dye is no longer quenched. The spherical shape of the dendrimer only allows a single bond to be formed with each Con A tetramer, eliminating

the potential for incomplete dissociation. This assay is fully reversible and has a larger dynamic response to physiological concentrations than the previous dextran-based assay. This assay could also be encapsulated in order to introduce it as a semi-invasive sensing modality in the body.

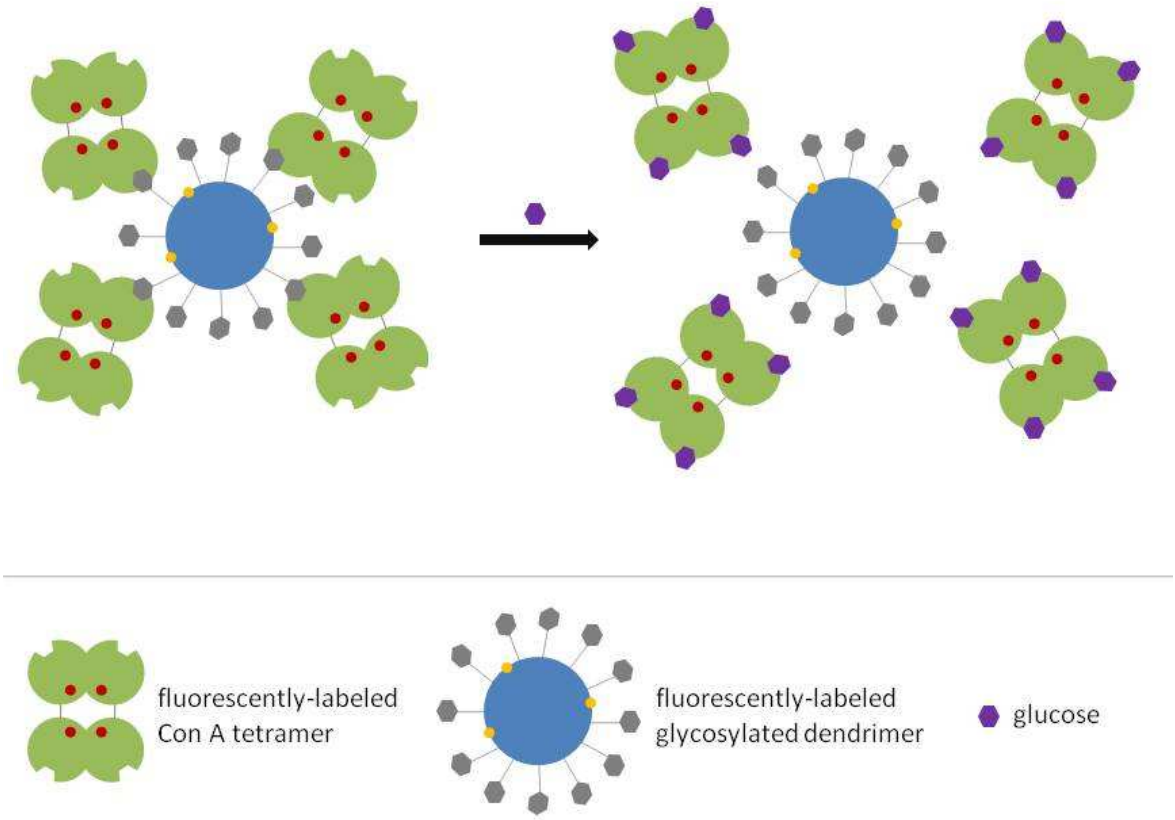

Figure 2.6. Schematic showing the Con A-glycodendrimer assay system

The fluorescence-based affinity sensor approach has several advantages. First of all, it is minimally-invasive and does not require a blood sample for measurement. The fluorescence response is determined by the competitive equilibrium between glucose and a ligand and not the rate of consumption as in enzyme-based sensors. Therefore, kinetic factors such as membrane permeability and fouling have less impact. High selectivity and sensitivity can be obtained by choosing the optimal binding protein and competitive ligand. The potential system is very small, allowing the response time to be on the order of minutes.[57] Con A also has several advantages for glucose sensing. It has a reversible binding mechanism, so it does not use up glucose or other reagents. It is independent of oxygen concentrations and there are not many competing glucose-like molecules in interstitial fluid, so the sensing will not be inadvertently hindered. Con A is also inherently stable.[64] Fluorescence-based sensing is fast, reagentless, minimally-invasive, and tends to be highly specific.[65] Though there are not currently any optically-based sensors on the market for glucose, the advantages make it a likely possibility for the future.

Summary

Continuous glucose monitoring has been shown to have many benefits, including tighter glycemic control and a reduction in the incidence of hypoglycemic events. Long-term tracking can be used by physicians to advise patients on dietary and treatment recommendations, as well. Transdermal meters, such as the GlucoWatch, draw glucose through the skin to measure concentration. While this system is advantageous because it

avoids puncturing the skin, the GlucoWatch suffered from several technological issues and was withdrawn from the market in 2007. Another noninvasive device, the Pendra, uses impedance to determine glucose levels. Though it received its CE mark and was being distributed in Europe, the Pendra had a number of drawbacks including the incompatibility of the system with the skin of about 30% of potential users. Additionally, the device experienced significant error issues, leading Pendragon to cease sales in 2004. GlucoDay is a microdialysis device that samples interstitial fluid through a subcutaneous catheter and detects glucose concentration using a glucose oxidase reaction. The linear range is excellent, but the device experiences an extensive lag time and patients experienced high levels of discomfort during use. Furthermore, the device is only approved for 48 hour clinical use in Europe. In the US, there are currently four CGM systems that continuously measure glucose using a transcutaneous glucose oxidase sensor including the DexCom Seven, the FreeStyle Navigator, the Medtronic MiniMed Guardian, and the Medtronic MiniMed Paradigm. These systems have shown a lot of promise in terms of helping patients achieve better glycemic control, but the sensor lifetime is relatively short and transcutaneous devices introduce the possibility of infection. Optical methods are advantageous because they allow for the opportunity of noninvasive or minimally invasive sensing. Fluorescence-based sensing, in particular, is fast, reagentless, and tends to be highly specific. Though there are not currently any optically-based glucose sensing devices on the market, they have the potential to improve continuous glucose monitoring by offering a sensitive, stable response for long-term glucose detection.

CHAPTER III

MICROPORATION FOR ANALYTE DETECTION*

Introduction

Polymer hydrogels have been used to encapsulate fluorescently labeled molecules in order to sense a variety of analytes.[61,66-71] Poly(ethylene glycol) (PEG) is one such polymer that is widely used for biosensing because of its inherent biocompatibility.[72-75] PEG hydrogels are created via cross-linking of the polymer chains, creating a mesh that retains the larger sensing molecules, while allowing for efficient diffusion of small analytes. The mesh size of pure poly(ethylene glycol) diacrylate (PEG-DA) has been reported to be between 8.6 and 10.8 Å.[76-78] The mesh size of the hydrogels can be increased by introducing aqueous solution to the precursor solution, reducing the potential for cross-linking. The ratio of aqueous solution to PEG-DA has been shown to alter the mesh size considerably.[77] Furthermore, the addition of aqueous solution alters the mechanical properties of the polymer as increased hydration leads to decreased strength. The aqueous gels also require continuous hydration after formation of the hydrogel to prevent drying. This increase in mesh size does allow for increased diffusion of small analytes through the hydrogel which could speed up sensor response time.

---

* Part of the data reported in this chapter is reprinted with kind permission from Spring Science + Business Media: Journal of Fluorescence, Microporated PEG Spheres for Fluorescent Analyte Detection, 17, 2007, 57-63, Rounds RM, Ibey BL, Beier HT, Pishko MV, Coté GL.

However, in applications focusing on entrapping larger assay molecules within the hydrogel matrix, increased leaching typically results, thus limiting the functional life span of the sensor.

For assays that detect a spatial displacement of molecules that bind to the sensing element inducing a change in fluorescence through a fluorescence resonance energy transfer (FRET) reaction or steric quenching, the current hydrogels do not allow for sufficient mobility of the components without increasing the hydrogel mesh size, which can lead to increased leaching. For example, several approaches for fluorescent glucose sensing function successfully in solution, but lose activity upon hydrogel encapsulation because of the physical inability of the assay chemistry to completely dissociate and re-associate within the confines of the hydrogel network.[61,62] One such sensor is based on a FRET reaction that occurs between fluorescein isothiocyanate (FITC)-labeled dextran and tetramethylrhodamine isothiocyanate (TRITC)-labeled concanavalin A (Con A) that are within close proximity, as the absorption spectra of TRITC heavily overlaps the emission spectrum of FITC.[57-59] Con A, a lectin, or highly specific sugar-binding protein, derived from the Jack bean plant, has an inherent affinity for saccharides such as dextran and glucose.[53,56] The sensor is created by allowing labeled dextran to bind with the labeled Con A, bringing the independent fluorophores within 50 Å, close enough to cause significant quenching of the FITC signal.[59] As glucose is added to the solution, some of the dextran molecules are displaced, increasing the distance between the fluorophores, thereby lowering the quenching and increasing the signal intensity. This

process has been shown to be reversible, meaning that as less glucose becomes present in the system, the dextran molecule will resume conjugation with the Con A protein and the FITC fluorescence will again be quenched. In order to contain this chemical assay in a protected environment in which it could eventually be implanted into the human body, PEG encapsulation has been investigated.[61,79] Pure 100% PEG was disregarded because of the limited motility it offered to the entrapped molecules. Higher hydration ratios have been explored, but they resulted in leaching of the sensor chemistry as the increased mesh size could not contain the assay for long periods of time. In order to overcome this, a polymer ester complex (poly(ethylene glycol)-NHS) was used to cross-link the sensing elements to the backbone of the polymer matrix while still allowing freedom to bind and unbind. This procedure showed potential, but resulted in a large reduction in the response of the sensor due to the decreased motility offered by the tethering ester complex.[61]

Previous Methods

Several previous attempts to improve sensor response have been made using various hollow embodiments. Ballerstadt and Schultz created a fluorescence affinity hollow fiber sensor based on the competitive binding of fluorophore-labeled Con A to glucose residues inside Sephadex beads.[60,64] As glucose diffuses into the sensor, the Con A molecules are displaced from the beads, and being no longer shielded from the excitation light, display an increase in fluorescence intensity. The main problem with this sensor was leakage of the Con A through the sealant/membrane interface, reducing sensor

lifetime and exposing the surrounding tissues to the assay components. Barone, Parker, and Strano proposed a single-walled carbon nanotube-based (SWNT) optical sensor that is coated in a hydrogel matrix to improve biocompatibility and prevent leakage.[80] The SWNTs fluoresce from 900 to 1600 nm and are coated with a glucose analogue such as dextran. A glucose-specific protein like Con A binds to the dextran coated walls, attenuating the fluorescence signal, until glucose is introduced, competitively binding and freeing the Con A. This is potentially advantageous because SWNTs are photobleaching-resistant, but results so far have been limited to theoretical modeling. Chinnayelka and McShane have created microcapsules containing a competitive binding assay by using a layer-by-layer fabrication technique.[81,82] Initially, dissolvable resin microparticles were coated with FITC-dextran and TRITC-Con A layers and an outer polymer layer.[81] Then the core was dissolved to produce a hollow microcapsule lined with immobilized Con A and dextran. This approach had a limited response due to the low assay concentration within the walls and a significant drop in pH was used to dissolve the inner core that could be harmful to many sensing assays. This system was improved upon by first creating hollow spheres and then filling them with a competitive binding assay that was free to move within the microcapsules.[82] This method is promising, but the loading of the microcapsules is diffusion-limited and requires excessive amounts of expensive assay components to drive the particles into the capsules.

Methods of Poration

Our group has devised a simple approach of porating PEG microspheres in order to increase assay motility while simultaneously preventing assay leaching. A variety of methods exist for creating porous hydrogels, including the porosigen technique, phase separation technique, foaming technique, and cross-linking of individual hydrogel particles. [83] The porosigen or porogen technique is particularly useful for our applications as it can be used in many different polymers, is capable of creating a variety of pore sizes, and can create individual cavities as opposed to channels that open to the surface, which would allow the assay the potential for escape. In order to create these cavities, a water-soluble porogen material, such as sucrose, is dispersed throughout the hydrogel precursor solution. After polymerization, the porogen is dissolved and dispersed, leaving cavities in the hydrogel matrix that are dependent on the size of the initial sucrose crystals.[84] Similar processes have been used previously for drug delivery and tissue engineering, but have been focused primarily on increasing transport rates rather than retaining molecules.[85,86] Applied to sensing, this process of poration creates small cavities within the hydrogel that contain the assay component in aqueous solution. The cavities allow for a response similar to that in pure aqueous solution by providing more room for increased assay component motility, while simultaneously reducing leaching through the fine mesh of the 100% PEG hydrogel.

Microsphere Fabrication

Three hydrogel compositions were created for comparison: 100% PEG, 50% aqueous PEG, and microporated 100% PEG. The 100% pure PEG hydrogel solutions were composed of liquid PEG-DA, while the 50% aqueous hydrogels were made with 50% PEG-DA and 50% water. A pH-sensitive assay of 10 mg/mL FITC-dextran (MW 10,000, 1% v/v) was added to test the sensing capabilities of each composition. A photoinitiator, Darocur, was added to promote cross-linking during polymerization (1% v/v). Spherical particles were created using an emulsion technique and cured via a 2.0 second UV exposure, as shown in Figure 3.1 (300 mW/cm^2, λ_{peak} = 365 nm, EFOS Ultracure 100SS Plus).

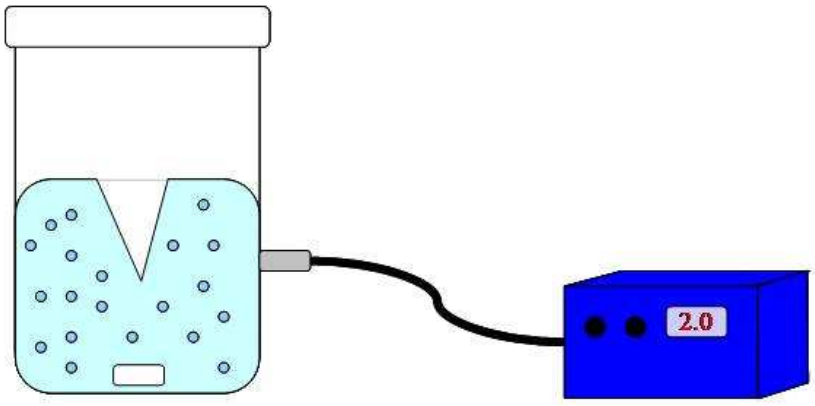

Figure 3.1. Sphere manufacture setup

In order to test the glucose sensing capabilities of the hydrogel compositions, a previously devised FITC-dextran/TRITC-Con A assay was incorporated.[58,59] An

additional composition was also created with the TRITC-Con A chemically immobilized through linkage to PEG-NHS, as done in previous work.[61]

To induce microporation within the hydrogels, a powdered combination of mannitol and fluorophore was added to the pure PEG precursor solution. The powders were formed through lyophilization of 100 mg of mannitol, 100 μL of fluorophore assay solution and 900 μL of 0.1 M PBS. Large aggregations of the powder were separated by sonicating the PEG solution for 15 minutes prior to use. After polymerization, the spheres were soaked in PBS to dissolve the mannitol porogen. The porogen was then removed by washing, leaving pockets in the hydrogel containing the sensing elements in aqueous solution, as shown in Figure 3.2.

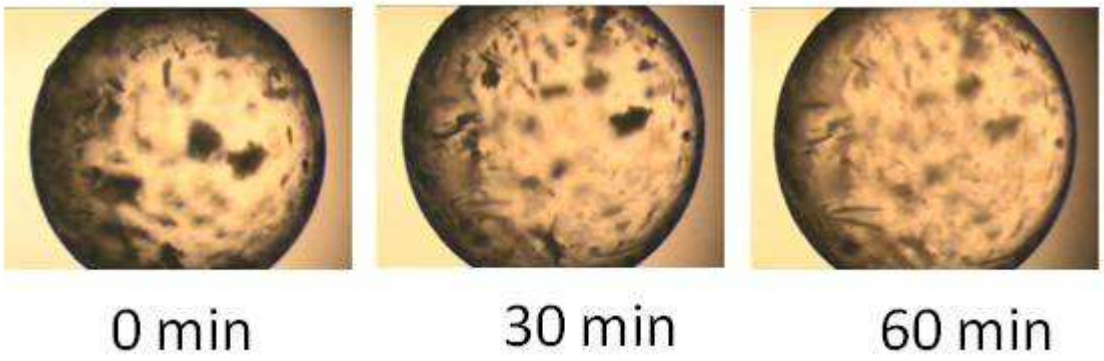

Figure 3.2. Mannitol dissolving from a sphere over time, leaving cavities filled with a glucose sensitive assay in solution

Detection and Imaging

A fluorescence detection system from Photon Technologies Inc. consisting of a mercury arc lamp, an excitation monochrometer, a sample chamber, an emission monochrometer, and a PMT was used to collect fluorescence at 90° (PTI, Lawrenceville, NJ). The spheres were placed in a microcuvette (Ocean Optics, Dunedin, FL) with 0.1 M PBS and excited with 480 nm light. For pH sensing, spectra were acquired from 500 to 550 nm and for glucose sensing, spectra were taken from 500 to 600 nm to include the FITC peak around 520 nm and the TRITC peak at approximately 580 nm. Changes in pH were induced using 1 M HCl and verified using a pH meter (420 A+, Orion; electrode 5990-30, Cole-Parmer, Vernon Hills, IL).

For sphere characterization, fluorescent images were acquired using an inverted microscope (Nikon CFI60, East Rutherford, NJ) containing two emission filters and differential interface contrast (DIC) optics (Chroma DIC, FITC, Filter Sets, Rockingham, VT). Fluorescent and DIC images were obtained using standard light microscopy (MetaVue Software, Sunnyvale, CA) and a CCD camera (Roper Scientific Photometrics Coolsnap HQ, Duluth, GA) with a 100 ms integration time. Confocal microscopy was used to determine the degree of poration using 2D fluorescent images at the point of maximum diameter of the sphere. A program was generated using the image processing toolbox with Matlab to calculate the fraction of fluorescent pixels to background pixels in order to estimate the total percent poration.

Sphere Characterization

In order to determine the feasibility of our new microporated sphere moiety, FITC fluorophores were encapsulated in a PEG-DA hydrogel. FITC undergoes a change in fluorescence intensity in the presence of H^+ ions and was therefore used to detect changes in pH. The distribution of sphere diameter for a set of 60 spheres made in 3 separate batches can be seen in Figure 3.3. The average sphere diameter was found to be about 370 μm, but the distribution is positively skewed due to the presence of a few larger spheres. It is possible that there could have been a few corresponding smaller spheres, but at sizes under 100 μm, the spheres tend to float and could be lost during the washing process. The optimal sphere size has been previously determined to be 100 μm based on photon flux and fluorescence intensity, but may be larger due to the additional light scattering caused by the cavities.[87]

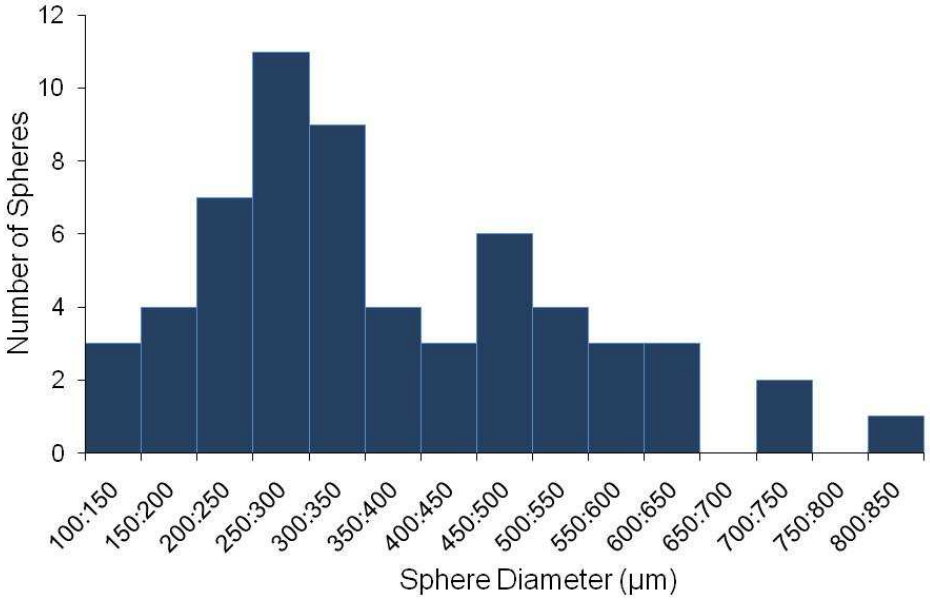

Figure 3.3. Sphere diameter distribution of 60 spheres sampled from 3 batches

Fluorescent images, generated using confocal microscopy, were taken of 52 individual microspheres to determine the extent of poration. The number of fluorescent pixels, given a threshold, was counted and divided by the total sphere pixel area to yield a percent poration for each sphere that is shown in Figure 3.4.

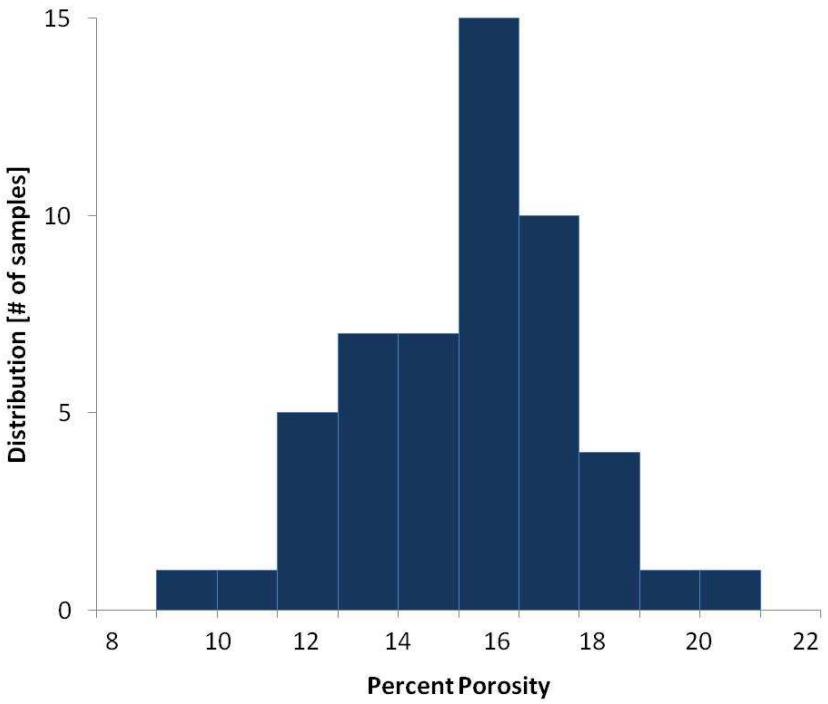

Figure 3.4. The distribution of sphere poration

The percent pore volume was estimated using image analysis and found to be about 15.12% with a standard deviation of 2.24%. Figure 3.5 shows the location of the micropores within the sphere in A and the corresponding entrapped fluorophore in B.

The fluorophore is primarily contained within the cavities of the microporated spheres, which allows for easy detection, but makes the sensors less prone to surface leaching.

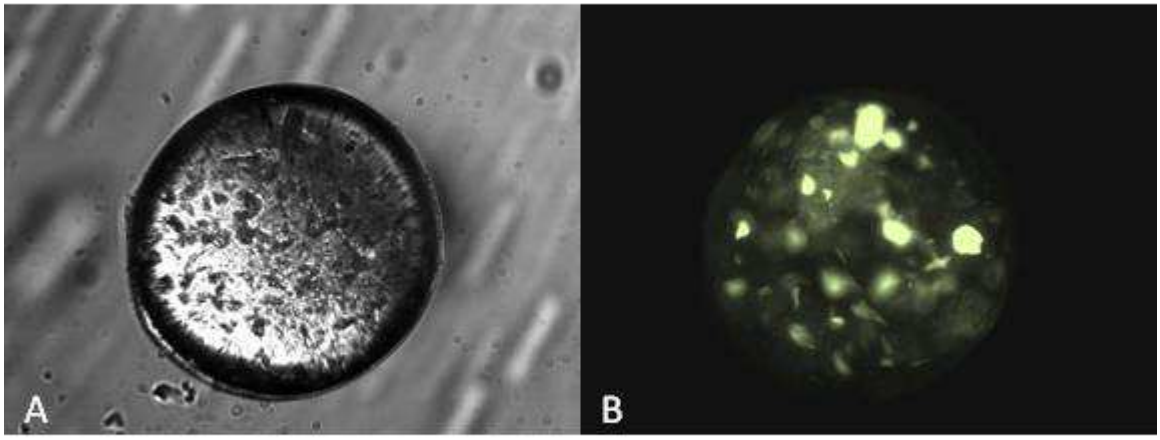

Figure 3.5. A sphere of approximately 400 μm diameter with micropores (A) and fluorophore contained within the cavities distributed throughout the sphere (B)

Sensor Response Time

As the cross-linking density increases, the diffusion coefficient through a hydrogel decreases.[88] Therefore, analytes should diffuse more quickly through the 50% PEG than through the 100% PEG, and much faster in free solution where there are few barriers. The microporated spheres were designed to decrease the time response by alternating areas of dense polymer and pockets of solution. Combining the two environments to create a pure PEG sphere with 15% poration, should result in a noticeable decrease in the transport time of small analytes.

Analyte diffusion through the polymer can be described by Fick's law of diffusion:

$$j_{A,x} = -D_{AB} \frac{dc_A}{dx}$$

where $j_{A,x}$ is the diffusive flux in kg/m^{2}s of analyte *A* at point *x*, c_A is the concentration of *A* in kg/m^3, *x* is the distance in m, and D_{AB} is the diffusivity of *A* in the polymer matrix *B* in m^2/s.[89,90] Theoretically, the sensor should respond as soon as the analyte has reached the first fluorophore-filled cavity and continue to increase in intensity as the analyte travels towards the center of the sphere, as shown in Figure 3.6.

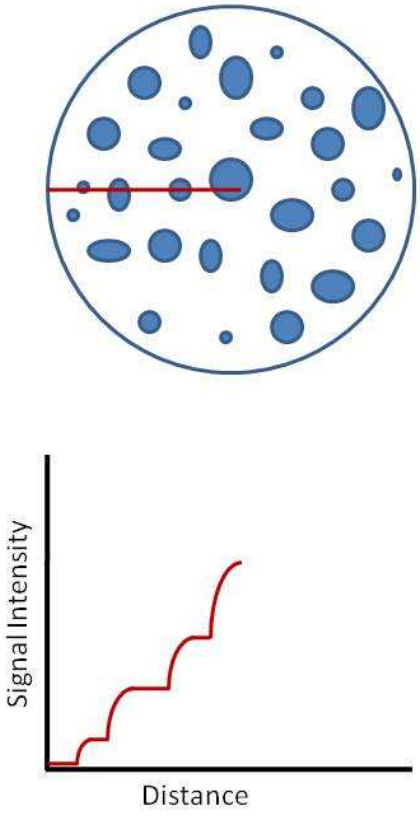

Figure 3.6. Diagram of a sphere showing a potential 1D path of analyte transport and the corresponding signal intensity

Glucose, for example has a diffusivity of approximately 6.8 x 10^{-6} cm^2/s in aqueous solution, while tetramethylrhodamine, a fluorescent tracer on the same order of molecular weight as glucose has a diffusivity of about 2.99 x 10^{-9} cm^2/s in PEG-DA.[76] For 1-D diffusion, the total time can be found with respect to the mean-square displacement $<x^2>$ and diffusivity, D.[89]

$$t = \frac{< x^2 >}{2D}$$

As shown in Figure 3.7, for a sphere of diameter 370 µm, it should take about 25 seconds to reach the center of the sensor in solution, while travelling through pure PEG would take significantly longer.

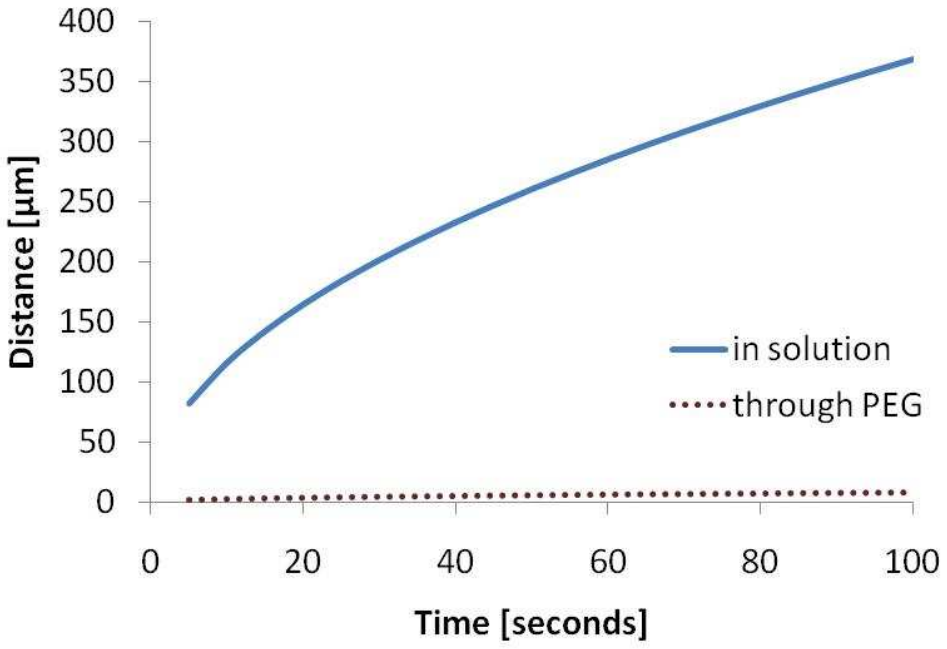

Figure 3.7. Approximate distance traveled by glucose over time in solution and through pure PEG

The time response of the sensors was measured by inducing a change in pH and measuring the resulting signal over time. A steady baseline intensity was established and then 5 µl of HCl was added. As shown in Figure 3.8, the assay responded immediately in free solution and was quick enough to capture the initial buffering activity. The time response of the solid PEG spheres is much slower, but microporation improves the reaction time, nearly matching that of the 50% PEG hydrogel. This could be further improved by reducing the sphere size so there is less distance for the analyte to travel and increasing the percentage of pore volume within the microporated spheres.

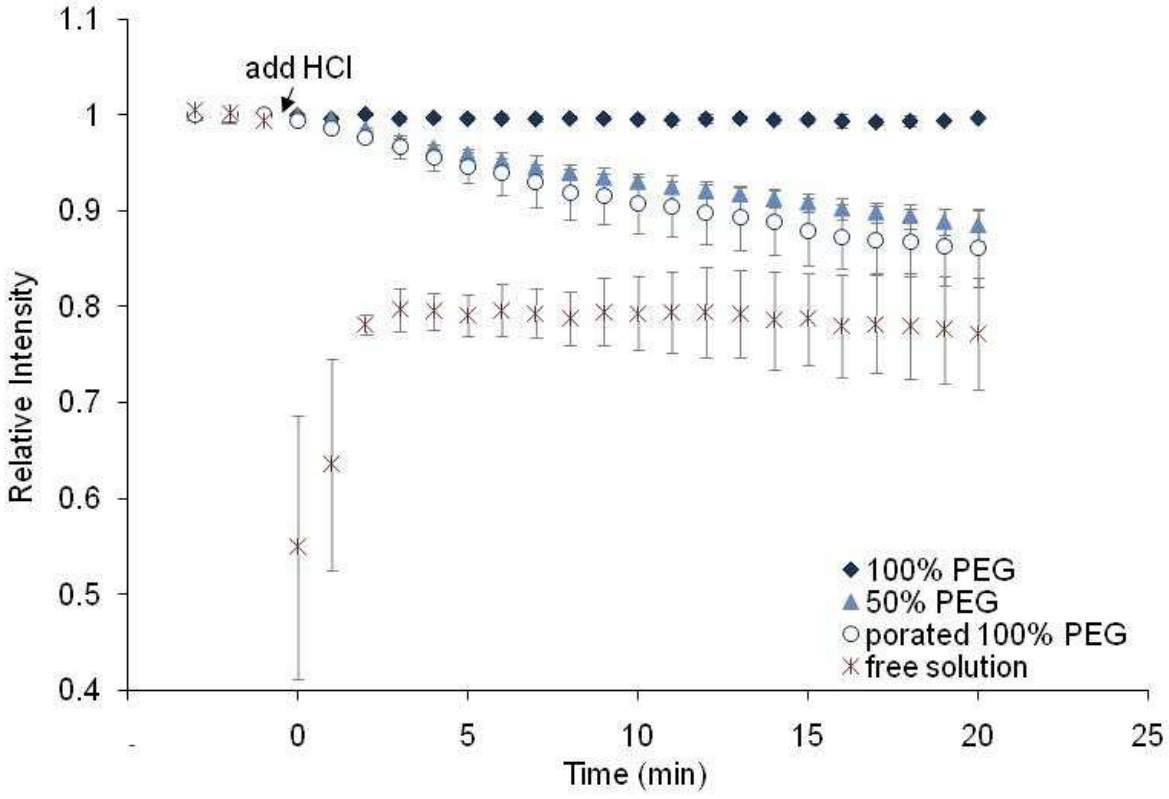

Figure 3.8. Sensor time response to a pH change induced by 5 µL of HCl in the three sphere sets versus free FITC-dextran in solution

Sensor Stability

Sensor stability was monitored using spectra taken daily for a period of one month. Prior to measurement, the buffer solution surrounding the spheres was removed and fresh PBS was added so that any fluorophore that was initially on the sphere surface, but then fell into solution would be excluded from the intensity readings. Intensities for each sphere composition were normalized for comparison and Shewhart control charts were created using JMP, a statistical software package, as shown in Figure 3.9 (Individual Measurement Chart, JMP 6, SAS Institute, Cary, NC).[91,92]

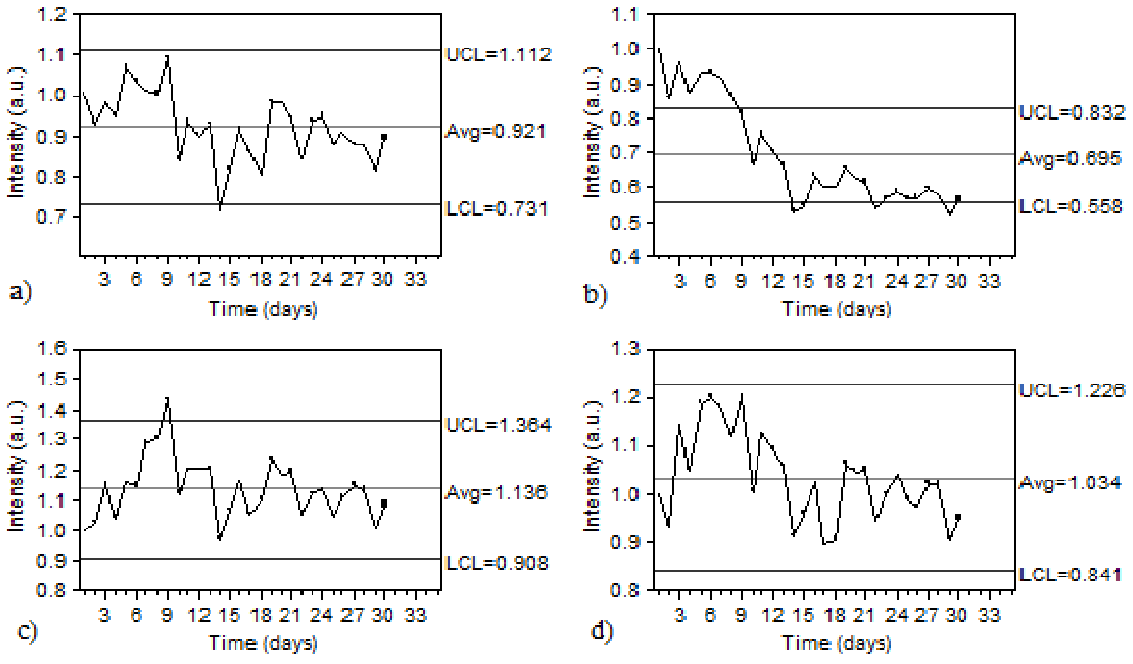

Figure 3.9. Control charts for sensor stability over one month showing the upper (UCL) and lower control limits (LCL) for (a) 100% PEG, (b) 50% PEG, (c) porated 100% PEG, and (d) free solution. Only the 50% PEG experienced a statistically significant decrease in intensity due to fluorophore leaching

The upper (UCL) and lower control limits (LCL) are defined as:

$$UCL = \overline{X} + k\sigma$$
$$LCL = \overline{X} - k\sigma$$

where $\overline{X}$ is the mean of the individual measurements, *k* is a multiple of the standard error set at 3, and σ is the standard deviation.[91] The 100% PEG spheres, shown in part a, remained relatively stable as the fine mesh size limits fluorophore leaching and promotes sensor stability over time. The 50% PEG spheres, on the other hand, showed a large decrease in intensity in part b, which is attributed to significant fluorophore leaching. The porated PEG spheres, shown in part c, performed well, remaining relatively steady throughout the month as the dense polymer matrix retained the majority of the sensing molecules. The free FITC in solution, though stable, shows slight day to day variability in part d, potentially due to a combination of source variability, temperature fluctuation, photobleaching, and changes in sphere packing. System noise is similarly evident in each of the sphere sets, but the overall statistical trends are notable.

Assay Motility

Sensor motility was assessed using a glucose sensitive assay that is based on a binding reaction with FITC-dextran and TRITC-Con A. A 1000 mg/dL glucose change was induced and the resulting change in fluorescence intensity was measured, as shown in Figure 3.10. The response was minimal in the 100% PEG spheres and the 50% PEG spheres, most likely because of the immobilization of the assay components within the

PEG mesh, allowing little room for unbinding to occur. The PEG-NHS spheres used in previous research have a portion of the sensor chemistry bound directly to the polymer backbone in attempt to minimize leaching, which also appeared to reduce the sensor activity in combination with the limiting mesh size.[61] The response in the microporated spheres was, however, much faster than that of the other sphere sets. It was also only slightly slower than the response in solution and comparable in relative intensity.

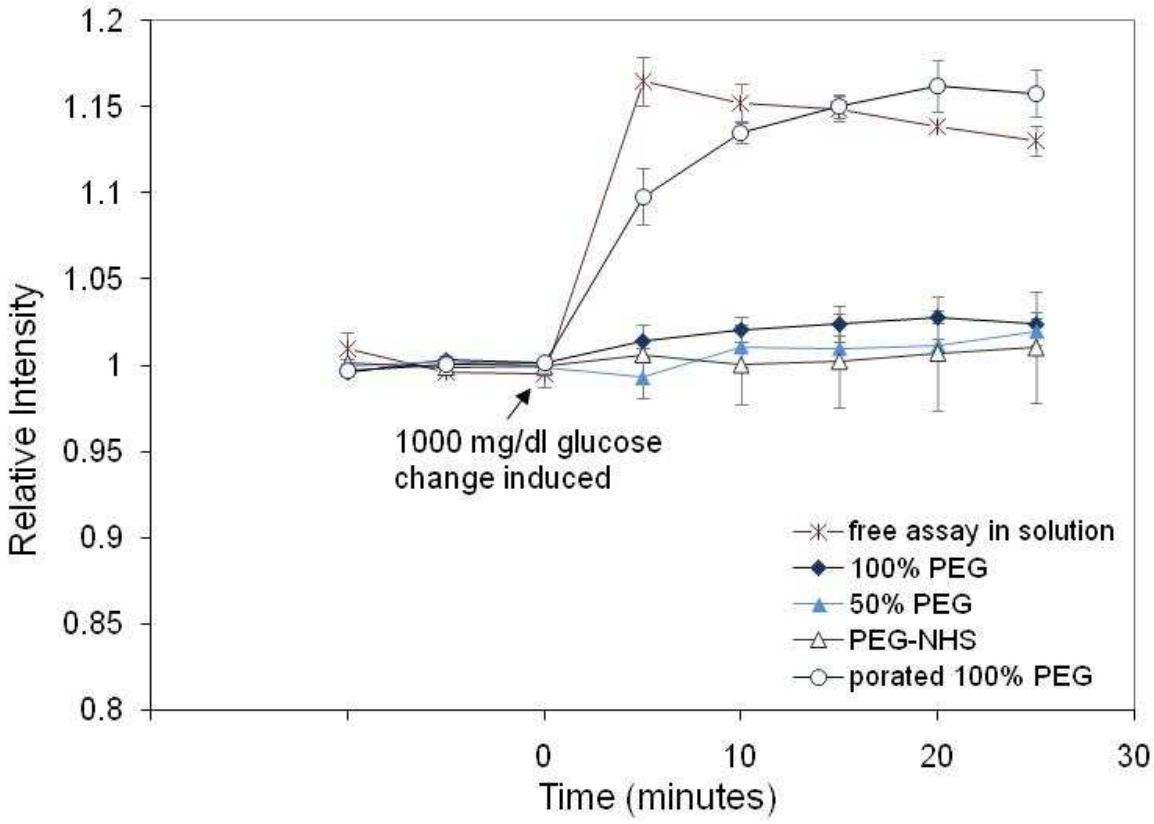

Figure 3.10. Sensor response to 1000 mg/dL glucose change

Conclusions

An ideal hydrogel encapsulation would retain sensing elements while allowing for efficient diffusion of the analyte of interest. Microporation of poly(ethylene glycol) spheres creates cavities where analytes may quickly diffuse and interact with the sensing elements. Pure 100% PEG spheres have a very slow response time, which is significantly improved by microporation, nearly matching the response rate of 50% PEG hydrogels. Loose mesh sizes promote fast analyte transfer, but also tend to allow the assay chemistry to leach out into solution, reducing the functional sensor lifetime. Microporation allows for the use of a fine mesh size to minimize leaching without limiting molecule mobility. Over a one month period, the microporated spheres maintained relatively consistent intensity levels, while the 50% PEG spheres experienced a significant decrease in fluorescence over time. Additionally, the microporated PEG provided adequate space for increased assay motility, allowing a binding reaction with FITC-dextran and TRITC-Con A to occur nearly unhindered while the other sphere compositions displayed minimal responses due to their restrictive mesh sizes. Microporation of PEG hydrogel spheres creates cavities of aqueous solution in which the assay chemistry is free to react with small analytes, while limiting leaching, promoting both functionality and stability of the encapsulated sensors.

CHAPTER IV

MINIMIZING THE HOST RESPONSE*

Host Response to Implant

The host response to the injury incurred upon device implantation depends on many factors including the extent of injury, the loss of basement membrane structures, blood-material interactions, provisional matrix formation, the extent of cellular necrosis, and the degree of the inflammatory response, as well as the size, shape, and chemical and physical properties of the implant material. The general sequence of events following the implantation is shown in Figure 4.1. The initial inflammatory response is triggered by injury to vascularized connective tissue which leads to immediate development of the provisional matrix consisting of fibrin, activated platelets, inflammatory cells, and endothelial cells. This serves to seal the wound and initiate further repair. Acute inflammation involves the exudation of fluid and plasma proteins and the emigration of leukocytes, and can last for minutes to hours to days, depending on the extent of the injury. Polymorphonuclear leukocytes, or neutrophils, are the first cells to appear, attempting phagocytosis, the engulfing and degradation of solid particles. Monocytes migrate to the wound where they differentiate into macrophages. The macrophages clean up the wound site, removing foreign material, bacteria, and dead cells, and recruit cells

---

* Part of the data reported in this chapter is reprinted with permission from Gant RM, Hou Y, Grunlan M, Coté GL. Development of a self-cleaning sensor membrane for implantable biosensors. Journal of Biomedical Materials Research Part A 2009; 90A(3): 695-701, by Wiley.

such as fibroblasts and endothelial cells. Due to the relative size disparity between the cells and the implant, phagocytosis is usually unsuccessful, resulting in frustrated phagocytosis and the release of lysozymes and oxidative products. The following chronic inflammation is typically short, lasting hours to days, and is confined to the implant site. This stage is less histologically uniform than acute inflammation and is generally characterized by the proliferation of blood vessels and connective tissue along with the presence of macrophages, monocytes, and lymphocytes, which release substances that cause the migration and proliferation of the fibroblasts.

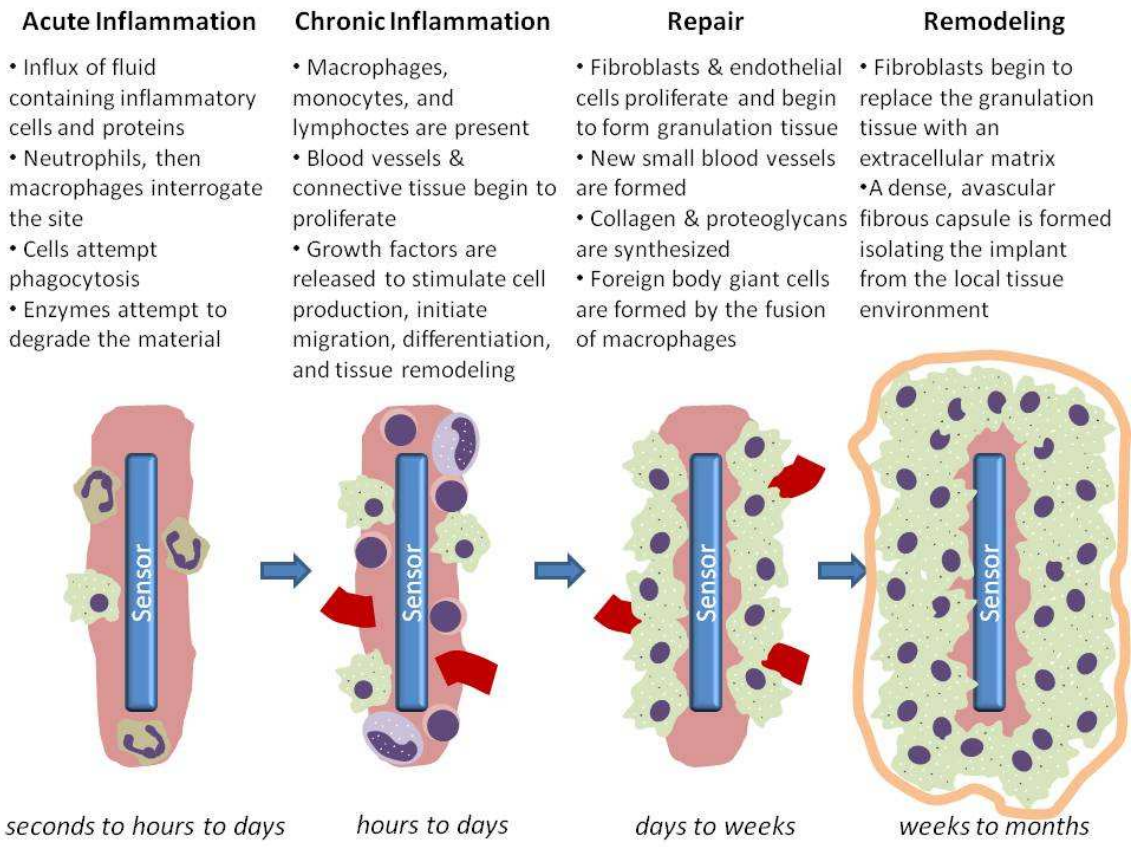

Figure 4.1. Physiological responses to an implanted biosensor leading to the formation of a fibrous capsule

Within a day of implantation, healing is activated by the products secreted by macrophages, including neutral proteases, chemotactic factors, arachidonic acid metabolites, reactive oxygen metabolites, complement components, coagulation factors, growth-promoting factors, and cytokines. Fibroblasts and vascular endothelial cells proliferate and begin to form granulation tissue several days after implantation at the start of the repair phase. New blood vessels are formed and fibroblasts synthesize collagen and proteoglycans. Macrophages fuse to form foreign-body giant cells in an attempt to phagocytose the implant while myofibroblasts begin the process of contraction, drawing the edges of the wound together. During the foreign body reaction, relatively smooth surfaces elicit a layer one to two cells in thickness, while rougher surfaces have more complex responses. Though the cells may remain on the surface of the implant indefinitely, it is not known if they remain activated or become quiescent. The final stage of the wound healing response after implantation of a biomaterial is typically fibrosis or fibrous encapsulation. As the surrounding tissue heals, regenerating, remodeling and replacing the injured tissue, connective tissue continues to proliferate, forming an avascular fibrous capsule. Spindle-shaped fibroblasts and a small number of macrophages are usually associated with the capsule, which is formed primarily of collagen and can range in size from about 0.05 to 1.5 mm. The fibrous encapsulation is influenced by many factors, including structure and morphology of the material, size of the implant, implantation site, and material biodegradability.[93-102]

Biocompatibility

The widely accepted definition of biocompatibility is “the ability of a material to perform with an appropriate host response in a specific application”, which was decided upon at a consensus conference of the European Society for Biomaterials.[103] It has been suggested that though this definition is functional, it offers no insight as to extent of biocompatibility or a basis on which to improve the biocompatibility of a material.[94,104] Currently, there is no list of materials considered safe or unsafe. Instead, each potential material must be evaluated for its specific purpose in a specific location. In addition to the effects from the implant on the host tissues, the effects of the host on the implanted device, or sensocompatibility, must also be considered to minimize medical complications and device failure.[105]

Biofouling and the scar-like, avascular fibrous encapsulation that eventually surrounds implanted sensors can reduce analyte diffusion and perfusion, causing a decrease in sensor response. Rebrin *et al.* show the decay of glucose sensor response as a function of implantation time in subcutaneous tissue.[106] The signal loss is extensive, in some cases dropping to nearly 20% of the original intensity over a period of several hours. Sharkawy *et al.* show that the fibrous capsule surrounding a subcutaneously implanted sensor imposes a significant diffusion barrier to glucose, halving the diffusion rate and increasing the lag time of the sensor by as much as threefold.[107] A diffusion barrier is imposed by the dense fibrous tissue while a perfusion barrier exists due to the capsule avascularity. Dungel *et al*. demonstrate the loss of sensor function without functional

blood vessel access.[108] In addition, local analyte levels could be altered by the metabolic changes in the surrounding cells as wounded tissue causes cells to function in a hypermetabolic state.[109] Biofouling and fibrous encapsulation can also cause problems in optical biosensors by reducing the signal via additional light scatter and absorption.

Many methods have been suggested to combat biofouling, including hydrogel overlays, phospholipid-based mimicry, flow-based systems, Nafion membranes, surfactant modification, naturally derived membrane materials, covalently modified membranes, diamond-like carbon coatings, and topology treatments.[110] None of these strategies can completely eliminate biofouling, nor do any of these approaches appear to stand out as most effective.

Smart Materials

Smart materials undergo rapid, reversible conformational or phase transitions triggered by small changes in the local environment. Stimuli include temperature, pH, light, electric field, stress, pressure, metal ions, glucose or other biochemical stimuli.[111-113] Hydrogels are three-dimensional networks of hydrophilic polymers that do not dissolve, but swell in water and were the first biomaterials designed for use in the human body.[112] The amount of water uptake depends on the polymer structure and type and degree of cross-linking.

Thermosensitive hydrogels exhibit a phase transition, existing in a swollen hydrophilic state at temperatures below the volume phase transition temperature (VPTT) due to hydrogen bonding with water molecules, and contracting into a collapsed hydrophobic state as the temperature is raised above the VPTT, as shown in Figure 4.2. Above the VPTT, the efficiency of the hydrogen bonding becomes insufficient to maintain the structure in solution, as the hydrophobic interactions between the polymer molecules become more favorable than the interactions between the polymer and water.[114]

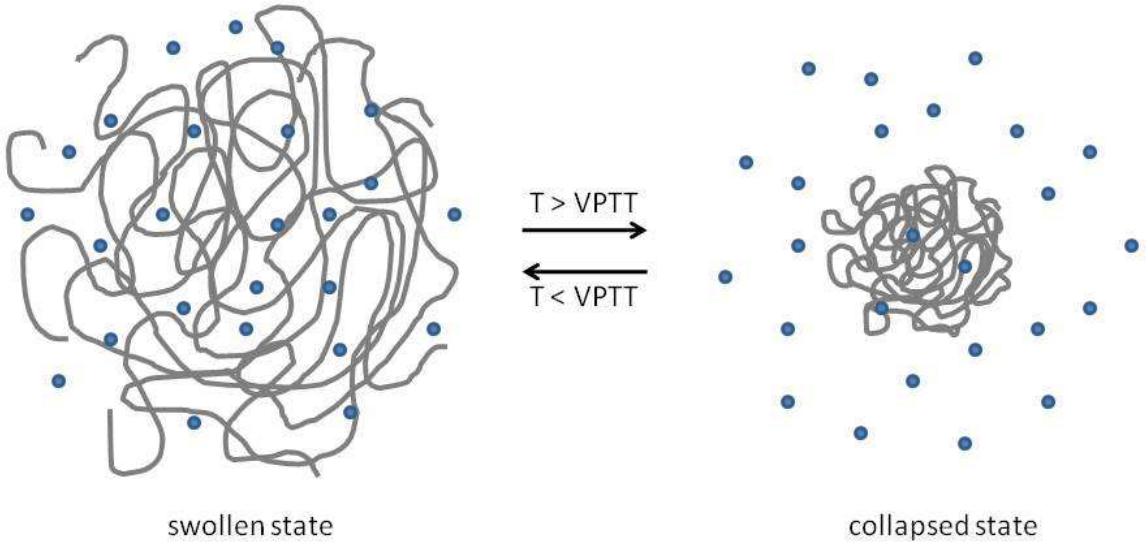

Figure 4.2. Schematic of thermosensitive hydrogel response: At temperatures below the VPTT, the gel exists in a swollen, hydrated state, while increasing the temperature above the VPTT causes the gel to expel water, resulting in structural collapse

The study of thermoresponsive gels was first reported in 1978 when Tanaka examined the dynamics underlying the collapse of the polymer network in polyacrylamide gels.[115]

Since then, the dramatic phase transition has been used in a variety of ways including as motors/actuators[116,117], in drug delivery[118-121], gene delivery[122], and for cell release in tissue engineering and artificial organ development[123-125]. For example, Shimizu *et al.* cultured cells on a thermoresponsive surface and were able to release the confluent cells as an entire sheet of cardiac tissue.[126] Stimuli-responsive polymers have also been used for culturing cells that are too sensitive to be enzymatically detached from the culture dish.[123]

The most extensively studied synthetic responsive polymer is poly(*N*-isopropylacrylamide) (PNIPAAm) because of the relatively sharp transition near body temperature.[127-129] In 1968, Heskins and Guillet first reported that PNIPAAm precipitates from aqueous solution at about 31 °C, depending on polymer concentration.[130] The enthalpy of phase transition for PNIPAAm is about 6.3 kJ/mol.[128] This is similar to H-bond energy, but hydrogen bonding is unlikely to be the only factor. In addition to polymer-water hydrogen bonding, polymer-polymer hydrophobic reactions are also likely to be involved.

Self-cleaning Sensor Membrane

A “self-cleaning” hydrogel has been developed with temperature-dependent hydrophobicity that could limit protein and cellular adhesion. Thermoresponsive hydrogels are advantageous for *in vivo* use as they undergo a sharp volume change over a short range of temperature. Furthermore, the high water content of the hydrogels

makes them relatively flexible, minimizing the local tissue irritation that could occur with a stiffer material. However, the highly swollen nature of the polymers also contributes to poor mechanical integrity.[119,131,132] The mechanical properties may be improved by copolymerization with another monomer, but this can alter the transition temperature, which would not be ideal for *in vivo* use.[133] Nanocomposite hydrogels have been prepared by introducing polysiloxane colloidal nanoparticles into PNIPAAm hydrogel matrices. This addition does not significantly alter the phase transition temperature, but does increase the mechanical strength of the hydrogels, increasing the potential for *in vivo* success.[134] This nanocomposite PNIPAAm material is described for the ultimate application as a "self-cleaning" sensor membrane for an implantable optical sensor targeting glucose as the analyte of interest. Figure 4.3 demonstrates the anti-fouling properties of the material as it is activated by thermal fluctuations. At room temperature, the hydrogels are hydrophilic and swollen with water. As the temperature is increased above the VPTT, the gels become more hydrophobic and expel water, resulting in a collapsed structure. Theoretically, the combination of the mechanical stretching forces from the swelling and deswelling behavior along with the change in hydrophobicity may prevent proteins and cells from adhering to the surface of the material.

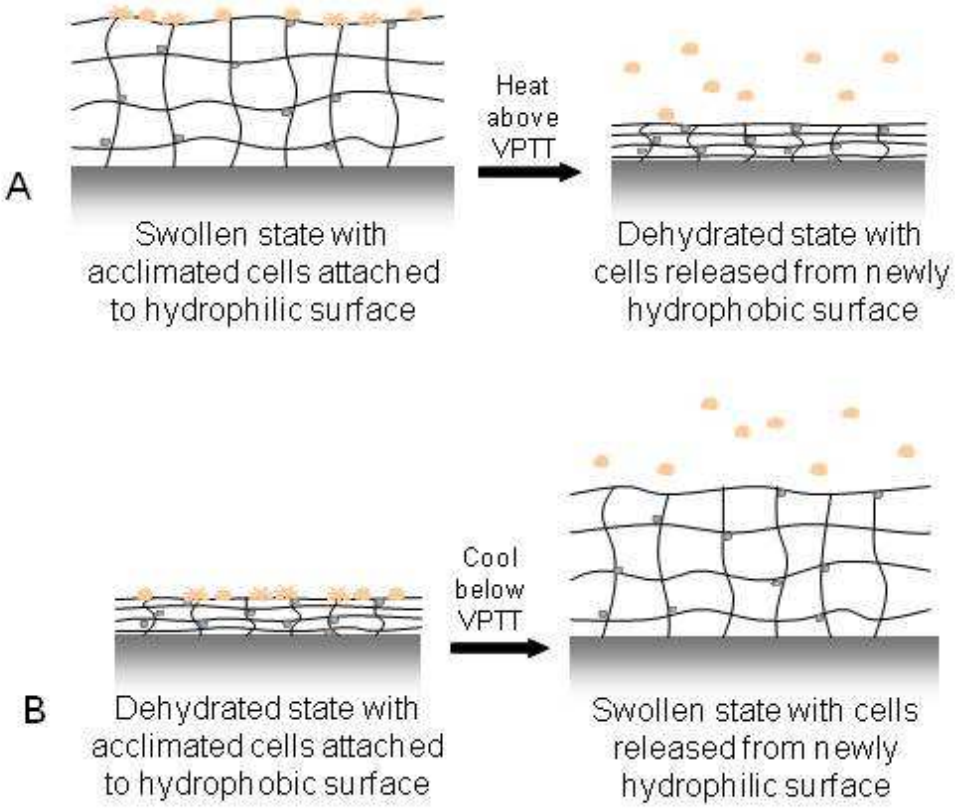

Figure 4.3. Swelling and deswelling behavior of the self-cleaning membrane on a sensor surface

Three PNIPAAm-based hydrogels, A, B, and C, were prepared along with a PEG hydrogel control, D, to assess the potential of the materials for use as a self-cleaning membrane for implantable biosensors. The composition of each precursor solution is shown in Table 4.1. The solutions were purged with nitrogen for 10 minutes and injected into a glass mold, which was then sealed and submerged into an ice water bath (~7 °C). The solutions were photopolymerized via 10 minute exposure to UV light (9 mW/cm^2, λ_{peak} = 365 nm, UVP UV-Transilluminator). The hydrogels were thoroughly rinsed with

DI water and soaked for at least 24 hours to remove impurities and allow time for adequate hydration. A pure PNIPAAm hydrogel, A, was used as a comparison for the properties of the nanocomposite hydrogel, B. The pure PNIPAAm hydrogels are limited by diminished strength when they are in a highly hydrated state.[119,132] In order to overcome this, nanocomposite hydrogels were prepared with polysiloxane colloidal nanoparticles. Higher mechanical strength is achieved with increasing nanoparticle concentrations, but there is a tradeoff with optical transparency.[134] The concentration of 1 wt% was chosen to incorporate into the PNIPAAm hydrogels as this allows sufficient light propagation for biosensing purposes while improving strength. In addition, the PNIPAAm-based hydrogels were photopolymerized at ~7 °C as polymerization at temperatures below the lower critical solution temperature (LCST) has been shown to produce gels with homogeneous morphology, resulting in optically clear hydrogels with improved mechanical integrity.[135] Poration was achieved in composition C by adding 20% PEG (MW 1000) to the precursor solution. After photopolymerization, the porogen was removed by extended soaking for at least 72 hours in DI water. A poly(ethylene glycol) diacrylate solution was prepared in composition D as a non-thermoresponsive control.[61,136] Aqueous PEG hydrogels were made with 60% v/v poly(ethylene glycol) diacrylate (MW 575) and 1% v/v Darocur 1173 photoinitiator and photopolymerized at room temperature for 3 seconds.

Table 4.1. Composition of the hydrogel materials

Hydrogel	Aqueous Precursor Solution
(A) PNIPAAm	NIPAAm monomer (12.5 wt%)
	BIS cross-linker (2 wt%)
	Irgacure photoinitiator (1 wt%)
(B) Nanocomposite PNIPAAm	NIPAAm monomer (12.5 wt%)
	BIS cross-linker (2 wt%)
	Irgacure photoinitiator (1 wt%)
	Polysiloxane colloidal nanoparticles (1 wt%)
(C) Porated nanocomposite PNIPAAm	NIPAAm monomer (12.5 wt%)
	BIS cross-linker (2 wt%)
	Irgacure photoinitiator (1 wt%)
	Polysiloxane colloidal nanoparticles (1 wt%)
	Leachable PEG, MW 1000 (20 wt%)
(D) PEG	PEG-DA, MW 575 (60% v/v)
	Darocur photoinitiator (1% v/v)

Temperature-dependent Equilibrium Swelling

The temperature-dependent equilibrium swelling behavior of each of the materials was measured from 10 to 50°C. Polymer slabs (1 cm x 1 cm x 500 μm) were submerged in DI water of a specific temperature for 24 hours and then the wet weight (w_{wet}) was measured. The dry weight (w_{dry}) was determined by drying the polymer slabs in an oven at 40°C for 24 hours before measurement. The swelling ratio is defined as:

$$SR = \frac{w_{wet} - w_{dry}}{w_{dry}}$$

Figure 4.4 shows that the PNIPAAm materials, A, B, and C, are significantly more hydrated at lower temperatures and contain much less water at temperatures above the VPTT. In contrast, the PEG hydrogel, D, served as a control, remaining at a constant level of hydration over the entire range of temperatures studied. As previously shown, the addition of the polysiloxane nanoparticles does not alter the VPTT as it would if NIPAAm was copolymerized with a second monomer.[133,134,137]

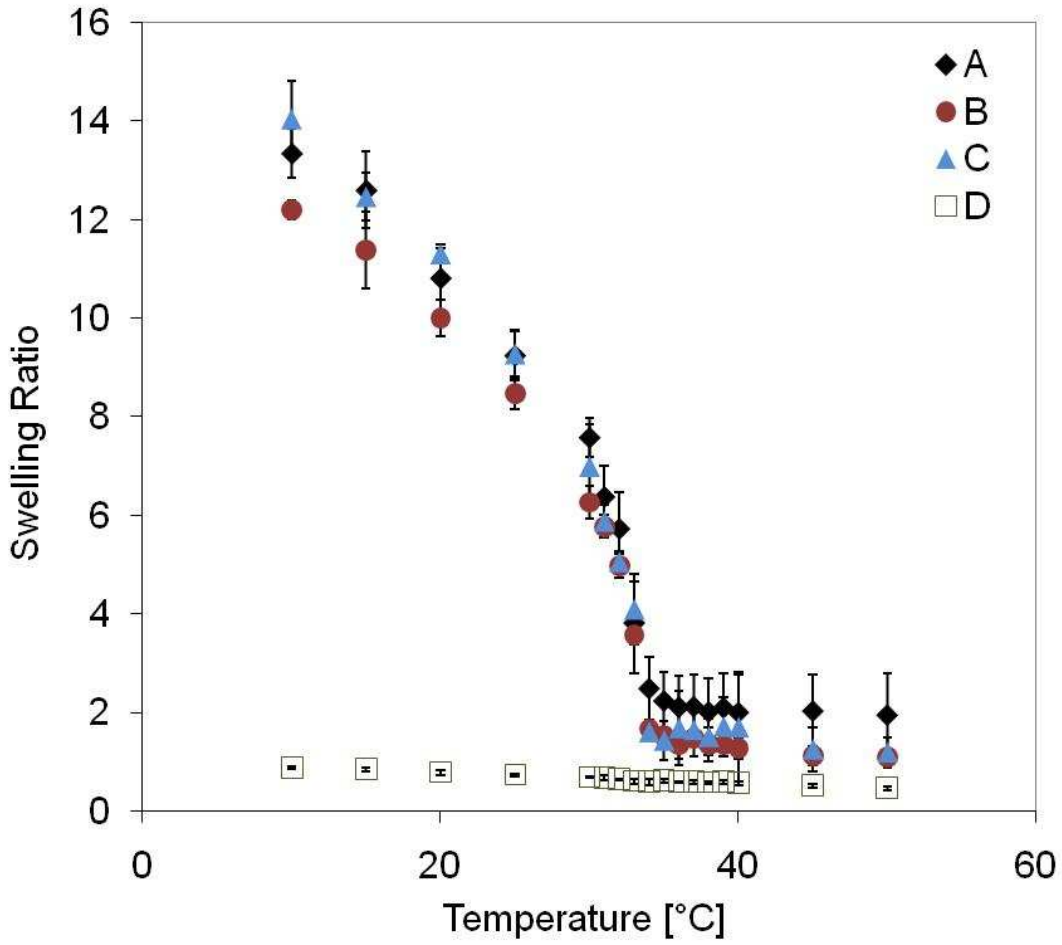

Figure 4.4. Volume equilibrium swelling ratios as a function of temperature for (A) pure PNIPAAm, (B) PNIPAAm with nanoparticles, (C) porated PNIPAAm with nanoparticles, and (D) 60% PEG

Swelling and Deswelling Kinetics

The swelling and deswelling kinetics were studied by measuring the amount of time it took for materials to transition when the temperature was varied between 25 and 37 °C. The hydrogels were maintained at 37 °C for 24 hours and introduced to 25 °C solution. The wet weight of each material was then measured every 5 minutes for 1 hour. The solution was maintained at 25 °C for the following 24 hours to allow time for the material to fully equilibrate before it was measured again. The temperature was raised to 37 °C again and measurements were made for 1 hour, followed by the measurement of the fully transitioned hydrogel after an additional 24 hours.

The polymers reach 90% hydration in ~25 to 30 minutes, as shown in Figure 4.5. After the temperature is increased, the hydrogels exhibit an initial rapid shrinking, followed by slower deswelling. This slower deswelling rate may be due to the restriction of water expulsion from the center of the hydrogels caused by the immediate surface shrinking.[119] The swelling and deswelling processes are diffusion-dependent. Hence, the swelling time is proportional to the square of the size of the material and the diffusion coefficient.[138] In order to minimize the time of swelling, the smallest dimension, or thickness, could be minimized.

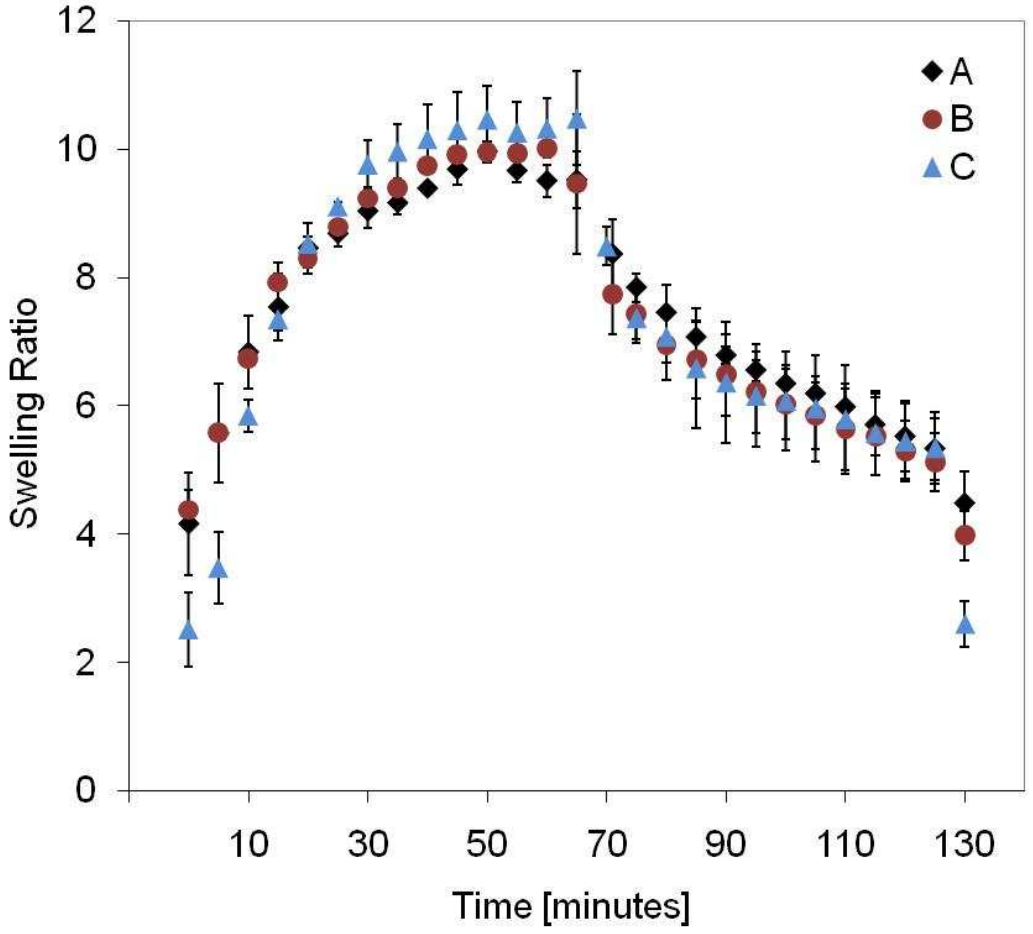

Figure 4.5. Phase transition time plot showing material swelling upon cooling to 25 °C, followed by deswelling when the temperature was raised to 37 °C for (A) pure PNIPAAm, (B) PNIPAAm with nanoparticles, and (C) porated PNIPAAm with nanoparticles

Glucose Diffusion

A diffusion study was performed to analyze the transport of small analytes through each material using glucose as an example analyte as it is a molecule of much interest for implantable sensor development. Each 500 μm thick hydrogel slab was tested in a side-by-side diffusion cell (PermeGear, Bethlehem, PA) with glucose solution in the donor

chamber and deionized water in the receptor chamber, as shown in Figure 4.6. The solutions were stirred to sustain constant concentrations throughout the chambers and a water jacket was used to maintain a consistent temperature in the system. Samples were taken every 10 minutes from the receptor chamber. The glucose concentration was measured using a glucose (HK) assay and the absorbance at 340 nm was determined with a spectrophotometer (USB 2000, Ocean Optics, Dunedin, FL).

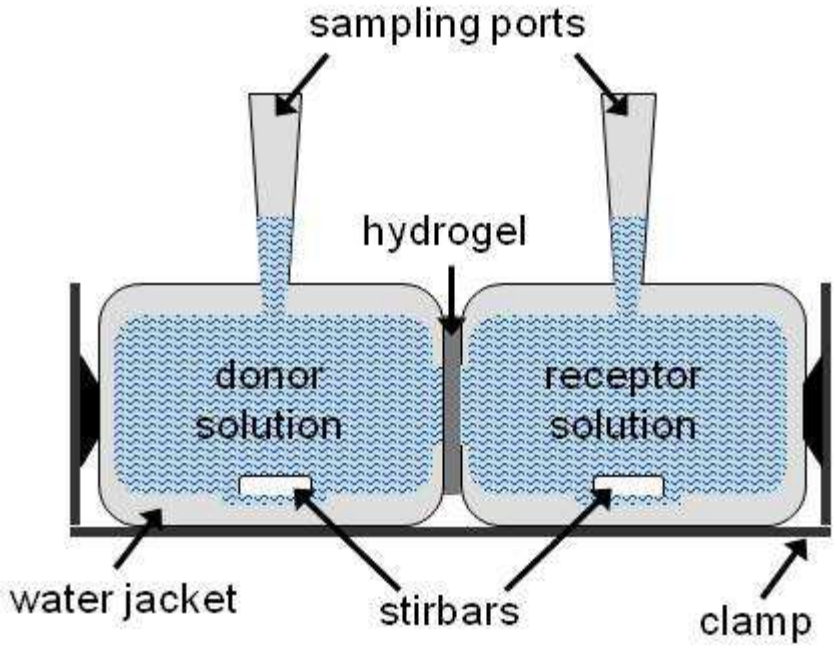

Figure 4.6. Side-bi-side diffusion cell setup for measuring analyte transport through the polymer materials

Analysis using Fick's second law of diffusion was performed to calculate the diffusion coefficients.

$$\frac{\partial c}{\partial t} = D\frac{\partial^2 c}{\partial x^2}$$

where c is the concentration in the hydrogel, t is time, D is the diffusion coefficient, and x is distance.[22-24] This assumes that the chambers are thoroughly mixed and the component concentrations are the same at the gel surface and in the bulk fluid. This can be solved to:

$$Q_t = \frac{ADC_1}{l}\left(t - \frac{l^2}{6D}\right)$$

where Q_t is the total amount of solute transferred through the hydrogel until time t, A is hydrogel area, C_1 is the solute concentration in the donor chamber, and l is hydrogel thickness. The lag time method has been previously used to calculate the diffusion coefficient using the intercept of the linear part of the curve obtained by plotting Q vs. time.[23] Zhang and Furusaki, however, have shown that using the slope leads to a much closer estimation of diffusivity and thus this was used for these calculations.[25]

PEG-based polymers have been previously shown to not significantly limit the transport of glucose to an encapsulated sensor[26], so if the nanocomposite hydrogels, samples B and C, exhibit similar glucose diffusion rates as the PEG hydrogel, sample D, then they should be considered acceptable. Table 4.2 shows that the diffusion rates in the pure PNIPAAm hydrogel, A, and the nanocomposite hydrogel, B, decrease significantly when the temperature was raised to 37 °C because of the inherent material

hydrophobicity and tight mesh size that occur above the VPTT. To overcome this potential problem, a porated nanocomposite hydrogel, C, was created. The poration caused a significant increase in the diffusion rate, particularly above the VPTT. The improvement may be due to the ability of glucose to travel more quickly through the pores, as opposed to becoming entrapped within the collapsed hydrogel matrix.

Table 4.2. Estimated average diffusion rates at temperatures below and above the volume phase transition temperature [cm^2/s]

Material	$D_{25\ °C}$	$D_{37\ °C}$
(A) PNIPAAm	$0.849 \pm 0.24 \times 10^{-6}$	$0.0637 \pm 0.04 \times 10^{-6}$
(B) Nanocomposite PNIPAAm	$1.02 \pm 0.33 \times 10^{-6}$	$0.0743 \pm 0.01 \times 10^{-6}$
(C) Porated Nanocomposite PNIPAAm	$1.97 \pm 0.29 \times 10^{-6}$	$4.25 \pm 0.97 \times 10^{-6}$
(D) PEG	$1.10 \pm 0.23 \times 10^{-6}$	$1.75 \pm 0.32 \times 10^{-6}$

Cell Release

To determine if the swelling/deswelling behavior affects the cellular adhesion, *in vitro* studies were performed. Each of the hydrogels and a polystyrene control were UV sterilized and inoculated with GFP-H2B 3T3 mouse fibroblast cells. Fibroblasts are responsible for the establishment, maintenance and repair of the extracellular matrix.[93] In addition, fibrous tissue capsules are typically composed of collagen and fibroblasts. This particular cell line was chosen to mimic a potential implant environment and because GFP-labeled chromatin is easy to image. The cells were maintained in DMEM with 10% fetal calf serum and antibiotics in an incubator at 37 °C and 5% CO_2. The inoculated

hydrogels were incubated overnight to allow the cells to attempt to adhere to the material surfaces. The samples were then imaged every 20 minutes and the number of cells remaining adhered to the surfaces were counted (Nikon Eclipse TE 2000-S). The temperature was varied between 37 °C and 25 °C every hour throughout the imaging process.

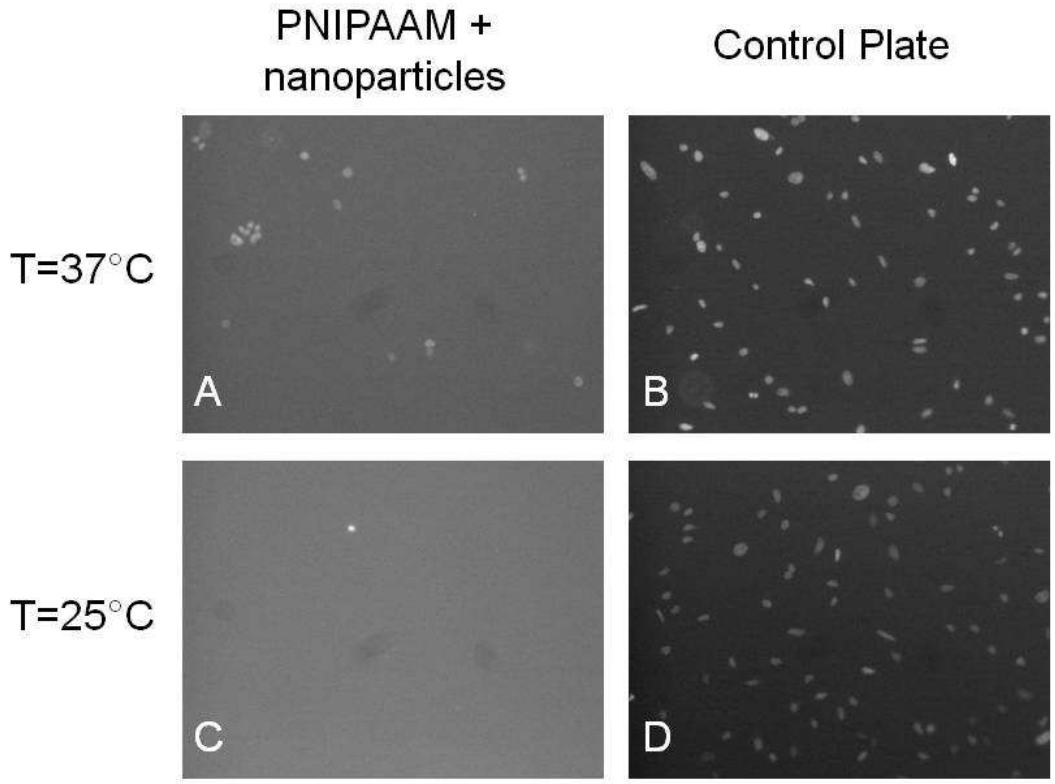

Figure 4.7. Comparison of attached cells: (A) Modified PNIPAAm nanocomposite hydrogel at initial 37 °C, (B) Polystyrene control plate at initial 37 °C, Modified PNIPAAm nanocomposite hydrogel after the temperature was lowered to 25 °C, and (D) Control at 25 °C

Several steps are typically involved in the adhesion of cells to a substrate including attachment of cells to a surface, reorganization of cytoskeletal components, formation of adhesion plaques, and deposition of an organized extracellular matrix.[97] Fluorescence images of the adherent cells are shown in Figure 4.7. Brightfield validation showing the cell morphology with the fibroblasts attached to the material surface is shown in Figure 4.8. The polystyrene control material maintained a high level of cell adhesion over the course of the experiment while the nanocomposite PNIPAAm material underwent a significant decrease in the number of attached cells when the temperature was lowered below the VPTT.

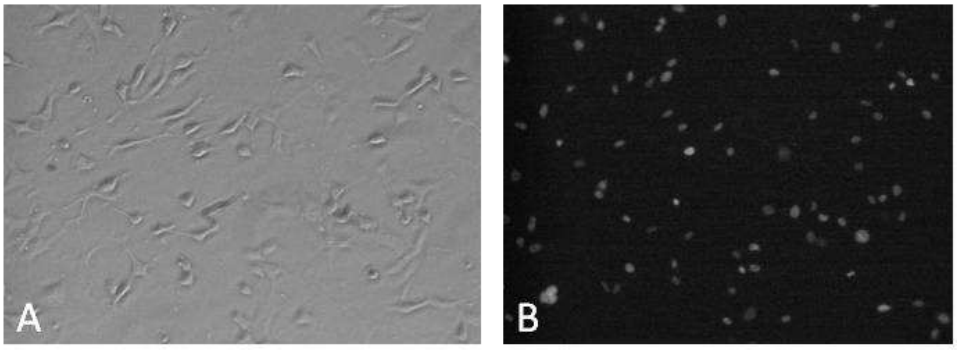

Figure 4.8. Brightfield validation of a control sample at 37 °C showing the cell morphology of the fibroblasts attached to the material surface (A) compared to the fluorescence image of the labeled nuclei (B)

Figure 4.9 shows the relative number of cells that remained adhered to each material throughout the thermal cycling process with the initial cell count being used to normalize

the following data. While the polystyrene control remained relatively constant over the duration of the experiment, the thermoresponsive hydrogels, A, B, and C, displayed a significant decrease in cell adhesion after the initial temperature fluctuation and never experienced further re-fouling. The PEG hydrogel, D, exhibited an initial decrease in the number of attached cells, likely due to its inherent anti-fouling capabilities. The relatively higher number of cells adhered to the PEG surfaces compared to those attached to the NIPAAm surfaces was due to the lower initial number of cells on the PEG, which was then used for normalization. PEG-coated materials have been shown to resist cellular adhesion for up to two weeks *in vitro*, but have been less successful during *in vivo* studies.[139] PEG-coated implants were engulfed by fibrous encapsulation four weeks after being subcutaneously implanted in mouse tissue, which limits its potential for *in vivo* sensing.[140]

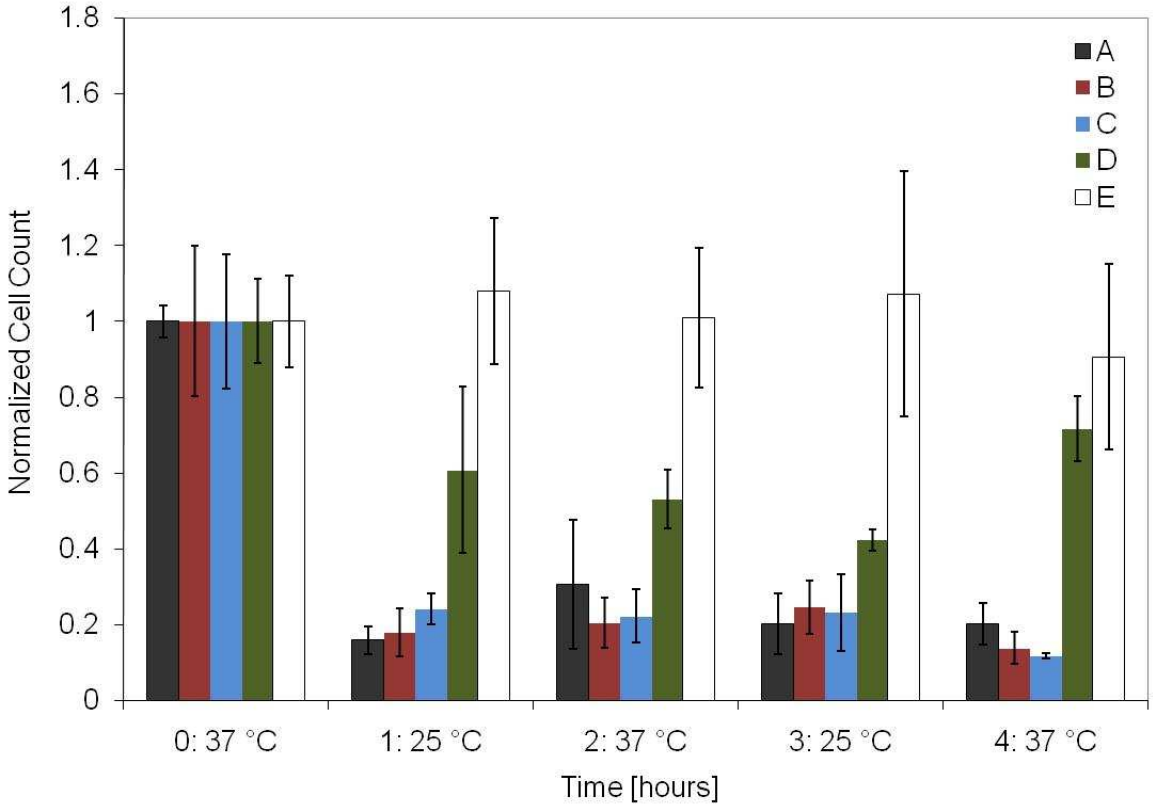

Figure 4.9. Detachment of cells in response to temperature variation for (A) pure PNIPAAm, (B) PNIPAAm with nanoparticles, (C) porated PNIPAAm with nanoparticles, (D) 60% PEG, and (E) polystyrene control plate

Cell spreading on a receptor-mediated surface depends on a delicate interplay of surface forces, including van der Waals interactions, electrostatic forces, cell membrane elasticity, steric interactions, and receptor-ligand binding interactions. The cell responds to the restraints imposed by the surface and makes the decision to recoil or adhere to the surface.[141]

Conclusions

In order for an implanted biosensor to be successful *in vivo*, it should exhibit long term stability and functionality. Therefore, the host response along with potential fibrous encapsulation should be minimized. Novel thermoresponsive PNIPAAm nanocomposite hydrogels have been created as possible self-cleaning membranes for implantable sensors. The volume phase transition of the gels occurred just below body temperature at about 33-34 °C, which is biologically relevant. The diffusion of glucose was similar to that in a PEG hydrogel below the VPTT, but significantly decreased at temperatures above the VPTT. Poration of the nanocomposite hydrogel dramatically improved glucose diffusion at temperatures above the VPTT by minimizing the distance that analytes must travel through the solid hydrogel network. An *in vitro* feasibility study showed that the nanocomposite hydrogels released approximately 70-80% of the initially attached fibroblast cells when the temperature was decreased below the VPTT and never experienced any significant reattachment during subsequent heating and cooling cycles. These results suggest that nanocomposite PNIPAAm hydrogels have the potential to be used as self-cleaning membranes for implantable biosensors. Long term studies are necessary to determine if these thermoresponsive nanocomposite hydrogels are capable of extending sensor longevity by preventing significant capsule formation *in vivo*, but its active anti-fouling properties make it a likely possibility.

CHAPTER V

TAILORING THE VPTT

Introduction

Following the implantation of a biosensor, the host experiences an immune response that results in the adhesion of proteins and cells and eventual fibrous encapsulation that will limit analyte diffusion and impair sensor performance. A thermoresponsive nanocomposite hydrogel based on poly(*N*-isopropylacrylamide) (PNIPAAm) has been developed for use as a self-cleaning sensor membrane to minimize the effects of the host response. In the previous chapter, it was demonstrated that these hydrogels can release adhered cells upon thermal cycling. However, the volume phase transition temperature (VPTT) for the hydrogels is below body temperature, resulting in a gel that is in a collapsed state *in vivo*, which would ultimately limit diffusion of the target analyte (e.g. glucose) to the encapsulated sensor. To overcome this diffusion obstacle, the hydrogel could be modified by tailoring the monomer ratio and introducing a copolymer to raise the temperature at which the maximum transition occurs. In addition to raising the VPTT to improve analyte transport efficiency, the material must be designed for optimal removal of adhered proteins and cells to control biofouling, while maintaining adequate mechanical strength for use in the body.

Normal Body Temperature and Thermoregulation

The normal body temperature of a human depends on many factors such as gender, race, activity level, fluid consumption, and time of day. The average core body temperature for healthy adult humans at rest in thermoneutral conditions (when the body temperature is controlled without shivering or sweating) is about 36.8 ± 0.4 °C.[142,143] This internal body temperature is maintained within approximately 2 °C despite large variations in ambient temperature. Hardy *et al*. showed that when temperatures were varied from 22 to 35 °C, subject core temperatures were relatively stable, while skin temperatures changed dramatically, especially at lower ambient temperatures.[144] The rate at which heat is transferred from the surface of the skin to the environment depends on the temperature difference between the two and thermal conductivity of the surrounding medium.[142]

At lower ambient temperatures, the peripheral blood flow is reduced and skin temperatures are lowered as the body undergoes vasoconstriction to preserve the core temperature. If this conservation is not sufficient to maintain the necessary core temperature, shivering will ensue. Alternately, when the internal temperature becomes too warm, increased cutaneous blood flow and sweating may occur to dissipate the heat. In addition, humans take behavioral measures to adjust for uncomfortable temperatures. The comfort zone, shown in Figure 5.1 (adapted from Datta), depends on several factors such as air temperature, surrounding surface temperature, relative humidity, and air

movement.[89] Outside of this comfort range, humans tend to adjust through modifications such as clothing and shelter.

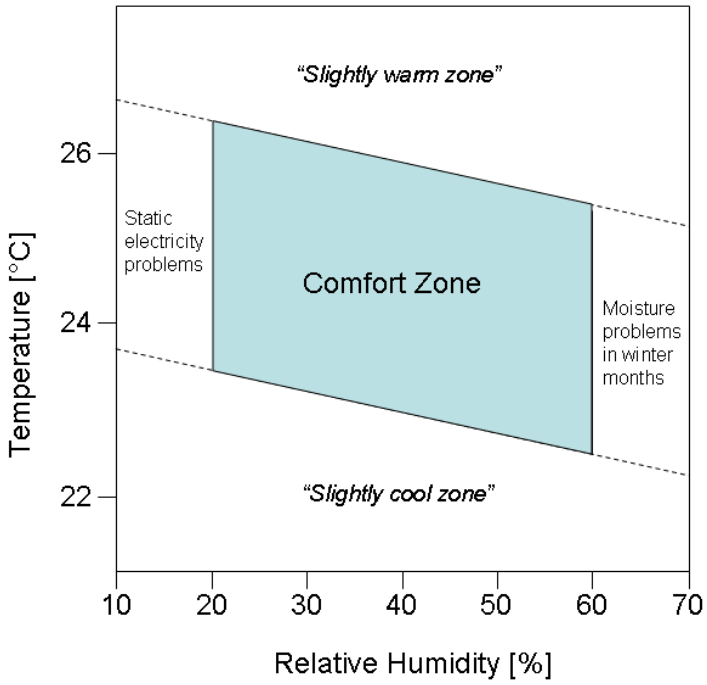

Figure 5.1. The effects of temperature and relative humidity on human comfort

Site Specific Conditions

Temperature variation occurs throughout the body because of differing geometry and material inhomogeneity.[145] An implanted optical sensor would optimally be located close to the surface of the tissue in order to minimize the signal pathlength. Therefore it is likely to be strongly influenced by the environmental temperature, as more superficial tissues are more affected by imposed thermal stresses than deeper tissues.[146] For this

particular application, the sensor is designed to be implanted in the subcutaneous tissue on the underside of the forearm for ease of accessibility and skin transparency. The inner temperature of the forearm has been determined to be 35.5 °C, but this maximum temperature was measured at a depth of 4 cm, near the center of the arm.[145] At an ambient temperature of 23 °C, the forearm surface temperature has been found to range from 29.4 °C on the lateral side to 31.4 °C on the ventral surface.[147] If implanted just under the surface of the skin, the average normal temperature of the sensor would probably be several degrees below 35.5 °C. Thus, body temperature at the implant site is considered to be approximately 35 °C in this work.

Choice of Volume Phase Transition Temperature

In order to induce the "self-cleaning" mechanism of the hydrogel sensor membrane, the temperature must be cycled around the VPTT. Because diffusion is limited at temperatures above the VPTT, the final hydrogel formulation was designed such that the VPTT is just above body temperature. Thus, under normal conditions, the hydrogel exists in a swollen state that allows adequate diffusion of the target analyte to the sensor. The "self-cleaning" is activated when the local temperature is raised just above the VPTT. This temperature must be tightly controlled as a critical thermal maximum exists from about 41.6 to 42 °C, beyond which near-lethal or lethal injury may occur.[148] The choice of temperature range was made to allow for adequate diffusion without incurring thermal damage.

Potential Thermal Limitations

As previously stated, the local forearm temperature under thermoneutral conditions is typically maintained several degrees below the core temperature. At environmental temperatures approaching body temperature, however, the thermal gradient between the core and surface temperatures is minimal, as vasodilation ensues to dissipate heat through the skin.[149] This condition is unlikely to affect the functionality of the sensor system as ambient temperatures far outside of the thermal comfort range are typically avoided or at very least, minimized. Many communities have public health warnings and response systems that are activated in the event of critical weather situations. For example, if temperatures are forecasted to be above 32.2 °C for 3 consecutive days, the city of Boston opens community cooling centers.[150]

There are several other case scenarios in which the body temperature may be elevated, though. Exercise, especially when performed by untrained individuals in high ambient temperatures, can produce high levels of heat and fatigue.[151,152] The magnitude of the rise in body temperature depends on the intensity of the exercise and is largely independent of the environmental temperature.[142,153] In a study by Gonzáles-Alonso *et al*., cyclists exercised to hyperthermic fatigue experienced core temperatures of about 40.2 °C, while their skin temperatures were maintained at less than 37.2 °C.[152] As this temperature is lower than the VPTT of the proposed sensor implant, normal levels of exercise may have little effect on sensor operation. If the sensor system is affected during periods of intense exercise, the most likely outcome would be reduced analyte

diffusion owing to the deswelling of the hydrogel at temperatures above the VPTT. This could be avoided by incorporating a calibration for temperature. As long as the duration of the thermal elevation is relatively short, it should not have a significant effect on the "self-cleaning" properties.

One other case scenario that may arise is fever. The febrile response typically increases the body temperature from 0.5 to 3°C.[142] During the course of the fever, the sensor hydrogel could remain in the collapsed state. If this occurs for an extended period of time, there may be a temporary build-up of cells around the sensor, causing a need for recalibration.

Other Considerations

Because this particular sensor is intended for use in diabetic patients, there may be several other factors to consider. One of the potential complications of diabetes involves complications with vascular disease. The vascular responses of diabetic patients are significantly reduced compared to non-diabetic subjects.[154,155] Additionally, glucose has a vasoconstricting effect, while insulin promotes vasodilation.[156,157] The potential effects of these factors on the system could be investigated in the future.

Material Design

In order to promote maximum diffusion in the hydrogel "resting state", a thermoresponsive material was designed to have a VPTT slightly above body

temperature. Several methods are commonly used to alter the VPTT, including adjusting the pH or adding surfactants, both of which would be physiologically infeasible.[158,159] The other widely used technique is the introduction of a comonomer.[160-162]

One of the most extensively used hydrophilic comonomers is acrylic acid (AAc).[160-165] PNIPAAm-*co*-AAc has been shown to have a higher water content than plain PNIPAAm above the VPTT and demonstrates a smaller change in volume.[162] In order to increase the VPTT to slightly above body temperature, acrylic acid was included into the PNIPAAm precursor solution. After optimizing for swelling, diffusion, and strength, the formulas were determined as follows: (A) PNIPAAm aqueous solution was composed of 12.5 wt% NIPAAm monomer, .2wt% BIS cross-linker, 1 wt% Irgacure-2959 photoinitiator, and 1 wt% polysiloxane colloidal nanoparticles, based on total precursor solution weight. (B) Acrylic acid comonomer was substituted for 10 wt% of the total monomer composition. The swelling profile for each of these can be seen in Figure 5.2.

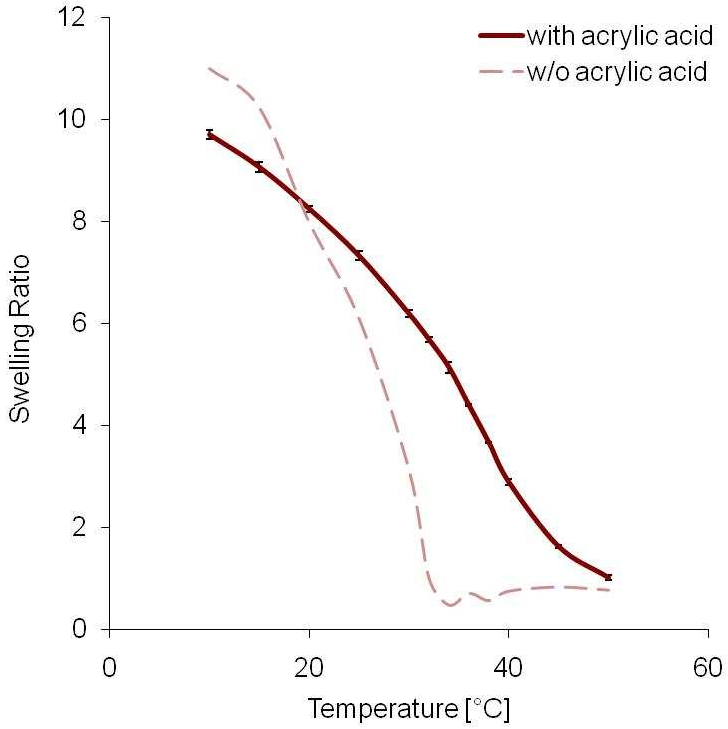

Figure 5.2. The equilibrium swelling profile with regards to temperature for PNIPAAm hydrogels with and without acrylic acid

The addition of acrylic acid increases the VPTT, but the transition broadens significantly compared to the hydrogels without the comonomer. A less gradual change in swelling is more desirable to achieve maximum self-cleaning potential with a small temperature change. Another concern is the highly pH sensitive nature of acrylic acid. Though the body closely regulates acidity, the local environment around a wound healing site can experience minor fluctuations.

In order to raise the VPTT while maintaining a sharper swelling transition, a hydrophilic comonomer, *N*-vinylpyrrolidone (NVP), was added to the PNIPAAm precursor solution.

In addition to the main design constraint of the transition temperature, the other components of the hydrogel were also considered with regard to impact on swelling, diffusion, and mechanical strength. Monomer concentration has a large influence on swelling ratio. Typically, the more "solids" included in the hydrogel composition, the lower the total degree of swelling. The cross-linker affects the hydrogel structure and elasticity. Additional cross-linker agent increases cross-linking and strength while decreasing diffusion and the maximum degree of swelling. Kuckling *et al*. showed that low BIS cross-linker contents (1 and 2 mol %) created homogeneous and transparent gels, while higher levels of cross-linker created cloudy (4 and 6 mol %) and opaque (8 and 10 mol %), heterogeneous hydrogels.[166] A design of experiments (DOE) analysis was performed using JMP statistical software to optimize the formula by varying the hydrogel components as described in Table 5.1.

Table 5.1. The compositions were varied by altering the percentage of three components

Component	Range
Total Monomer	10-15 wt%
NVP	1-2 wt%
BIS	0.2-1 wt%

Each potential combination of components was analyzed base on maximum swelling ratio, diffusion, and mechanical strength to predict the most desirable formula for use in

the temperature range of interest. Figure 5.3 shows the prediction profile based on the results of a set of 16 predetermined hydrogel compositions measured in triplicate.

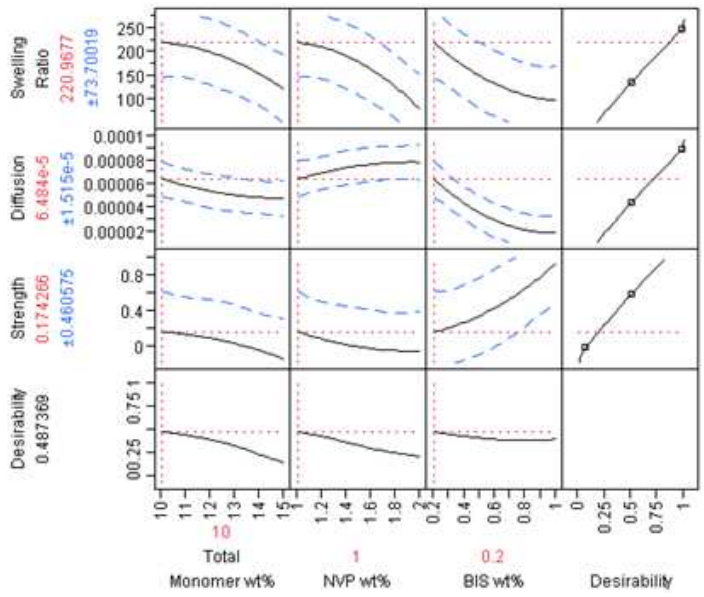

Figure 5.3. JMP statistical analysis to determine maximum desirability of swelling ratio, diffusion, and strength based on total monomer, comonomer, and cross-linker concentrations

As hypothesized, higher total monomer concentrations and higher cross-linker amounts led to decreased diffusion, while increasing the amount of hydrophilic NVP led to increased diffusion due to the additional hydration of the hydrogels. Conversely, increasing the comonomer concentration led to a decrease in strength, while adding more cross-linker strengthened the gels. Finally, the swelling ratio, which takes into consideration the change in volume between 35 and 39 °C, was maximized at low concentrations of each of the components. Taking each of these properties into

consideration, the optimal composition was determined to be 9 wt% NIPAAm monomer, 1 wt% NVP comonomer, 87.8 wt% water, 0.2 wt% BIS cross-linker, 1 wt% nanoparticles (wt % solids of nanoparticles with respect to total precursor solution wt), and 1 wt% Irgacure photoinitiator.

Material Characteristics

The end goal of the design of this material is to prevent long term cell adhesion via changes in surface swelling and hydrophobicity. The hydrogel composition was optimized such that it will exhibit large changes in hydration between body temperature and a slightly elevated "activated" temperature. In order to view the morphological differences between the swollen and deswollen states, the hydrogel samples were maintained in PBS at either 4 ℃ or 50 ℃ for at least 24 hours to promote swelling or contraction. They were then flash frozen in liquid N_2 to maintain morphology and freeze-dried in a lyophilizer (Labconco CentriVap Gel Dryer System, Kansas City, MO) for 6 hours at -40 ℃ to completely remove any water from the hydrogels and preserve hydrogel structure and volume.[167,168] Cross-sections were sputter-coated with gold and visualized with a field emission scanning electron microscope (Quanta 600 FE-SEM, FEI, Hillsboro, OR; FE-SEM acquisition was supported by the NSF DBI-0116835, the VP for Research Office, and the Texas Engineering Experiment Station). Figure 5.4 shows that the hydrogels that were maintained in a swollen state below the VPTT exhibited a homogeneous, expanded network, while those that were maintained in a

deswollen state above the VPTT were homogeneous, but had a much more contracted mesh.

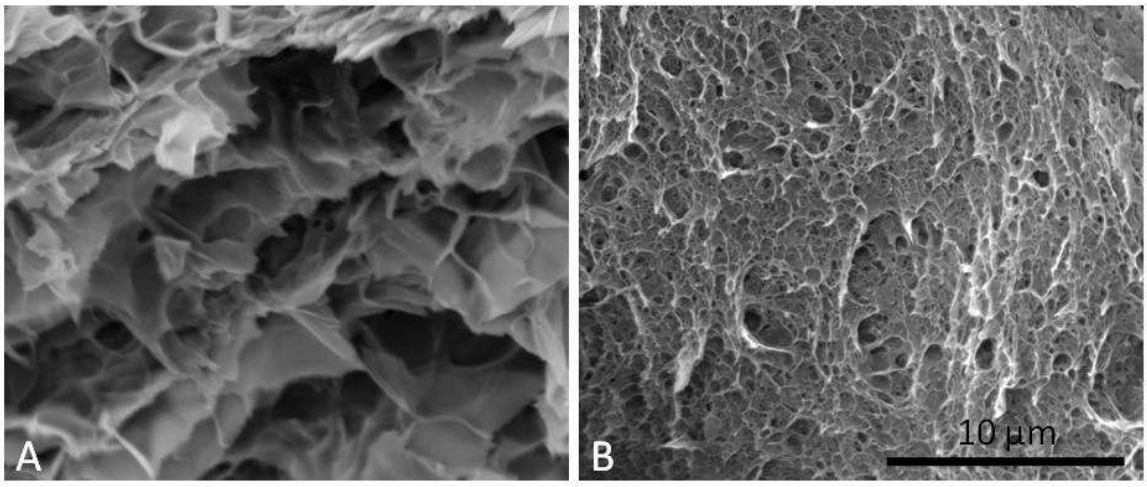

Figure 5.4. SEM micrographs of hydrogels displaying A) swollen morphology after conditioning below the VPTT at 4 °C and B) collapsed morphology after conditioning above the VPTT at 50 °C

Internal Environment

Both the external and internal environments must be considered for optimal design creation. Characterization of the VPTT of PNIPAAm hydrogels is typically conducted in DI water, but it is important to analyze the functionality of an implantable sensor under physiological conditions, particularly with respect to pH and salinity. Designed to be implanted in the subcutaneous tissue, the sensor will be bathed in interstitial fluid. The human body can control the pH of blood and interstitial fluid to within a tenth of a pH unit of 7.4.[169] Since the pH of DI water is about 7, a slightly more basic solution should be used for more accurate testing. PNIPAAm has been considered a slightly pH sensitive

material.[170,171] However, other work supports the idea that the changes seen are in fact due to other factors such as a copolymer or the salts used in the preparation of the pH buffer solutions, and not necessarily to the change in pH.[158,172]

The VPTT of PNIPAAm can be changed with the addition of various salts via a salting out effect that causes a decrease in the transition temperature.[158,159,173,174] The type of salt, valence, size of the anions, and the concentration have a strong influence on the effect. The salting out may be due to a combination of several effects, including changes of the water structure in the hydration layer surrounding the polymer and changes of the interactions between the polymer and the solvent. The addition of electrolytes changes the normal hydrogen bonded water structure, disrupting the highly oriented water molecules, resulting in an increase in the hydrophobicity of the PNIPAAm and a subsequent decrease in the VPTT.[159]

Table 5.2. VPTT of the hydrogels with and without the comonomer NVP in either water or PBS

	T_o [°C]	T_{max} [°C]
(A) With NVP, in PBS	34.59 ± 0.69	37.44 ± 1.52
(B) With NVP, in water	38.08 ± 0.25	41.82 ± 0.12
(C) Without NVP, in PBS	30.38 ± 1.84	31.74 ±1.72
(D) Without NVP, in water	32.79 ± 0.26	34.85 ± 0.12

Given the known effect of pH, salts, and electrolytes on the VPTT of PNIPAAm, studies were conducted on nanocomposite hydrogel samples soaked in both DI water as well as phosphate buffered saline (PBS). The impact of PBS can be seen in Table 5.2 as hydrogels saturated in PBS displayed a lower VPTT in terms of onset (T_o) and maximum (T_{max}) temperatures of the endothermic peaks. The volume phase transition temperature (VPTT) of the hydrogels was determined using differential scanning calorimetry (DSC, TA Instruments Q100, New Castle, DE). After soaking in either DI water or PBS at room temperature for at least 24 hours to equilibrate, the hydrogels were blotted with filter paper to remove the excess liquid and sealed in a hermetic pan. The temperature was cycled between -50 °C and 50 °C at a rate of 3 °C/min with the reported data occurring in the 2nd cycle. In addition to the effects seen in the presence of PBS, the inclusion of the comonomer also has a large impact on the VPTT. The hydrogels that incorporate NVP exhibit higher transition temperatures. Thus, the hydrogels will exist in a hydrated, swollen state with increased diffusion at body temperature when implanted in the body.

Equilibrium Swelling

The extent of swelling and deswelling of the hydrogels were determined via equilibrium swelling measurements from 10 to 50 °C in both water and in PBS with a pH of 7.4 in order to simulate the internal environment of the implantable sensor. The hydrogel slabs were submerged in either solution at a specific temperature for 24 hours and then the wet

weight (w_{wet}) was measured. The dry weight (w_{dry}) was measured after the hydrogels had been dehydrated in an oven at 40 °C for 24 hours. The swelling ratio is defined as:

$$SR = \frac{w_{wet} - w_{dry}}{w_{dry}}$$

As seen in the previous DSC measurements of VPTT, Figure 5.5 shows that the VPTT occurred at slightly lower temperature for hydrogels soaked in PBS, whereas the presence of NVP increased the VPTT due to its hydrophilic nature. Upon implantation, swelling of the hydrogel membrane would enhance diffusion in the resting state at 35 °C. At ~39 °C in PBS, the hydrogel containing NVP produced the most significant deswollen state. The large extent of deswelling in the range between body temperature and the “activated” temperature is expected to maximize the self-cleaning mechanism, presumably increasing the likelihood of cell detachment upon temperature cycling.

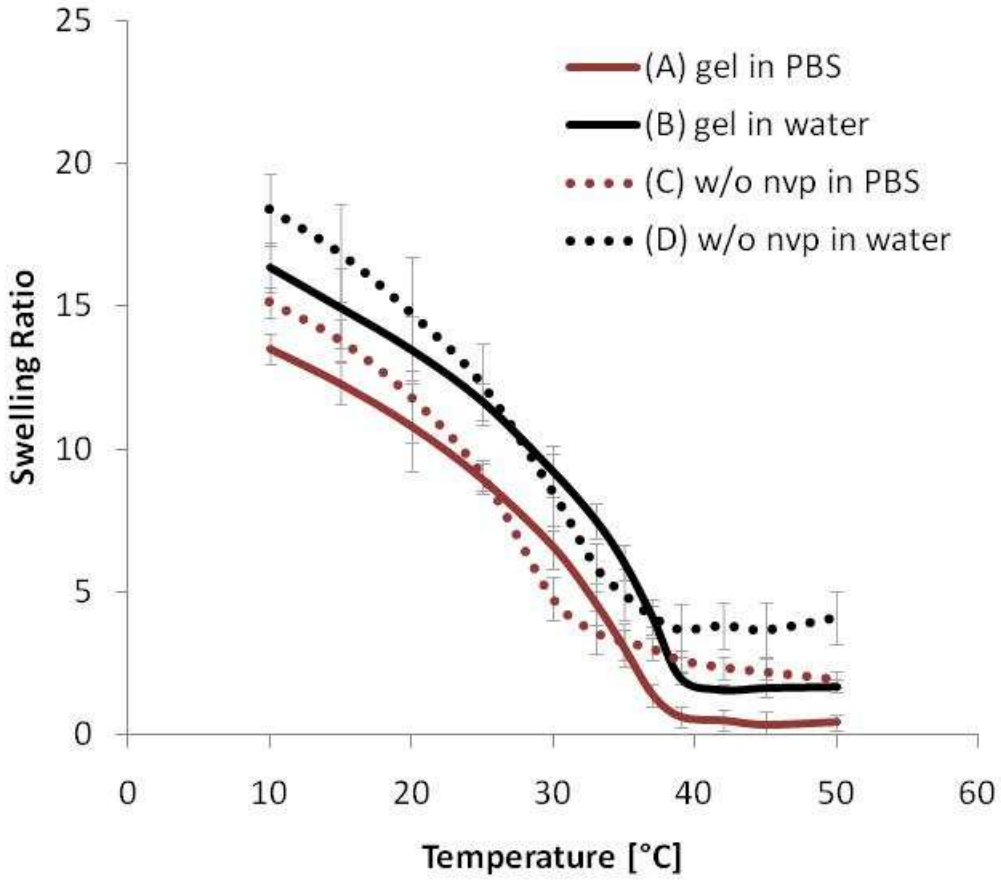

Figure 5.5. Equilibrium swelling ratios as a function of temperature for the hydrogels in PBS (A), hydrogels in water (B), hydrogels without the NVP comonomer in PBS (C), and hydrogels without NVP in water (D)

Swelling and Deswelling Kinetics

Deswelling and swelling kinetics were examined by measuring the change in hydrogel diameter at regular time intervals while sequentially heating or cooling hydrogel discs from 35 °C (below the VPTT) to 39 °C (above the VPTT). Hydrogel discs were created with an 8 mm punch at room temperature. The samples were submerged in PBS at either 35 or 39 °C for 24 hours to equilibrate and then switched to the opposite temperature at

time zero. The diameter was measured over time using a digital caliper. Whereas swelling began rapidly upon cooling, deswelling appeared to be slower, as shown in Figure 5.6. This may be due in part to the limitations of the measurement process. The diameters of the hydrogels during deswelling may have increased during the physical measurement at room temperature due to reswelling even though each measurement lasted only a few seconds. Also, as pointed out in the previous chapter, the surface of the hydrogel may immediately deswell, effectively forming a skin that inhibits the transport of water from the center of the gels.[119,175] Enhanced deswelling may be effected with methods such as modification of the polymerization conditions, poration, and freeze-drying that may be useful if a quicker transition is necessary.[168,176-178]

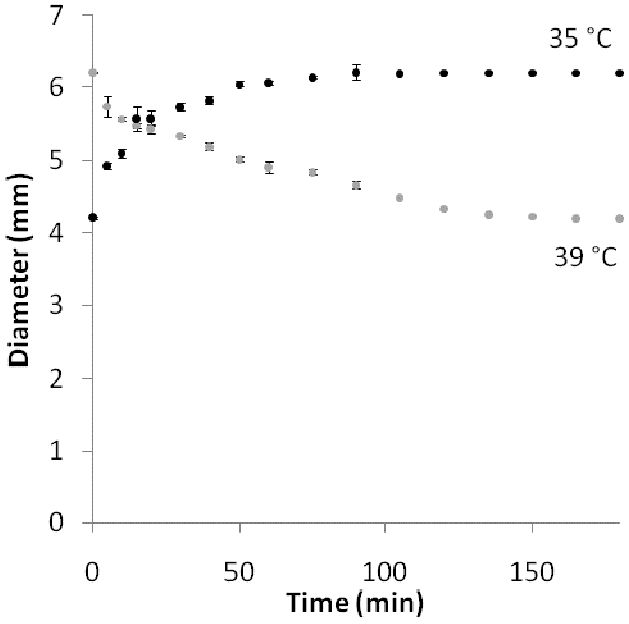

Figure 5.6. Phase transition over time showing swelling upon cooling to 35 °C and deswelling when the hydrogels were heated to 39 °C

Glucose Diffusion

The diffusion through the hydrogels was studied using glucose as an example analyte. A side-bi-side diffusion cell was used to monitor the glucose transport through the gels. The donor chamber was filled with glucose solution and the receptor chamber contained DI water at the beginning of the experiment. The solutions were stirred to provide even analyte distribution and a water jacket was used to maintain a consistent temperature. Samples were taken every 20 minutes from the receptor chamber and the glucose concentration was measured using a YSI 2700 Select Biochemistry Analyzer (YSI Incorporated, Yellow Springs, OH). The average thickness of each of the gels was measured with a DMA Q800 (TA Instruments, New Castle, DE) and the diffusion coefficients were calculated for each case using Fick's second law of diffusion, as outlined previously in Chapter IV.

Table 5.3 shows the effect of temperature on the diffusion coefficients of hydrogels that were created with and without the comonomer NVP. Without the addition of NVP, the diffusion rate decreases significantly with temperature. If it were to be implanted in the body, the diffusion rate could be prohibitive when the external heating device is activated to promote cleaning of the hydrogel surface. By including NVP in the hydrogels, the diffusion rate is significantly improved at the temperatures of interest. Glucose diffusion through the dermal layer of skin has been previously measured as 2.64 x 10^{-6} cm^2/s and as 0.075 x 10^{-6} cm^2/s through the epidermis.[49] Furthermore, Sharkawy *et al*. have shown that densely fibrous, avascular tissues forming around implanted

materials reduce diffusion by 50% compared to rates measured in the subcutis, potentially increasing the sensor lag time by threefold.[107] Though the NVP-inclusive hydrogels experience a slight decrease in diffusion rate at the activated temperature, their self-cleaning properties may provide significant improvement of long-term diffusion rates *in vivo*.

Table 5.3. The effect of temperature on diffusion coefficients of hydrogels with and without the comonomer NVP [cm^2/s]

Temperature [°C]	Without NVP	With NVP
30	$1.09 \pm 0.39 \times 10^{-6}$	$1.33 \pm 0.18 \times 10^{-6}$
35	$0.193 \pm 0.06 \times 10^{-6}$	$1.24 \pm 0.15 \times 10^{-6}$
39	$0.0483 \pm 0.01 \times 10^{-6}$	$0.785 \pm 0.30 \times 10^{-6}$

Mechanical Properties

Mechanical robustness is desired for an implanted sensor membrane to permit easy insertion and removal, as well as promote integrity during residence in the body. Although swelling enhances diffusion, it also leads to reduced mechanical strength. The high water content typical of hydrogels increases flexibility, minimizing the local tissue irritation that could occur with a stiffer material, but can also contribute to reduced mechanical integrity.[131] The mechanical properties of an implant are typically designed to match that of the local environment. In the case of a subcutaneous implant that is not load-bearing, the main physical requirements are that the implant be able to maintain its

functionality throughout its useful lifetime and then be able to be fully removed. Many methods for improving hydrogel strength do so by reducing the extent of swelling.[179] For instance, PNIPAAm hydrogels formed at temperatures below 20 °C are morphologically homogeneous whereas those formed at higher temperatures are heterogeneous.[180-183] At temperatures above ~ 20 °C, newly formed insoluble PNIPAAm chains phase separate such that subsequent cross-linking leads to the formation of a macroscopic network of loosely interconnected highly cross-linked polymer rich domains and lightly cross-linked polymer poor domains. Heterogeneous PNIPAAm hydrogels display greater swelling but are mechanically weaker compared to the corresponding homogeneous hydrogel. To maintain mechanical integrity, homogeneous hydrogels were prepared for this study. Furthermore, polysiloxane colloidal nanoparticles have been incorporated to improve the mechanical properties of the nanocomposite hydrogels without affecting the volume phase transition temperature.[134] For compression and tensile tests, measures were taken to avoid dehydration of the specimens that would falsely increase mechanical rigidity and strength.

In order to assess the effects of temperature on the mechanical properties of the nanocomposite hydrogels, dynamic mechanical analysis (DMA) and tensile testing was performed at 35 °C (below the VPTT) and at 39 °C (above the VPTT). DMA was performed in the compression mode using a DMA Q800 (TA Instruments, New Castle, DE) equipped with a parallel-plate compression clamp with a bottom diameter of 40 mm and a top diameter of 15 mm. Hydrogel discs were prepared with a diameter of 13 mm

using a punch, clamped between the parallel plates, and silicone oil was placed around the exposed edges to prevent dehydration during the testing process. The hydrogel discs were allowed to equilibrate for 5 minutes at 25 °C and then were evaluated in multi-frequency-strain mode (1 to 100 Hz).

Analysis of tensile strength was performed using a DMA Q800 operating in tension mode. Specimens with a ring geometry were prepared using a tubular mold (ID = 3 mm, OD = 7.5 mm). Individual rings of ~3 mm width were cut from the central portion of the appropriate hydrogel tube using a clean razor blade and sample dimensions were measured using a digital caliper. Each hydrogel ring was blotted with filter paper and loaded onto the outside of custom aluminum bars that were fixed in the DMA tension clamps so that the upper and lower bars were located inside the ring. The hydrogels were subjected to a constant strain (1 mm/min) until breaking at the center of one side of the ring. Stress was determined using the measured force divided by the cross-sectional area of two rectangles with dimensions based on the ring width and wall thickness. The tensile modulus, ultimate tensile strength (UTS) and % strain at break were determined. The tensile modulus was obtained from the slope of the linear part of the stress-strain curve. The UTS was designated as the maximum stress prior to failure. Percent strain at break was calculated by dividing the measured displacement by the gauge length, which was found by subtracting the ring wall thickness from the outer diameter. Results reported are the average of measurements from three specimens cut from the central portion of the same hydrogel tube.

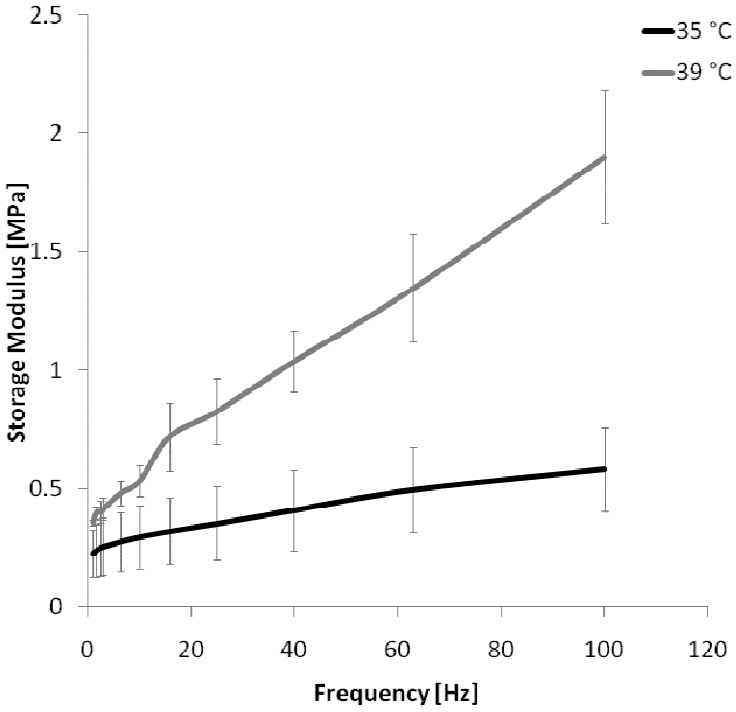

Figure 5.7. Storage modulus of the nanocomposite PNIPAAm-co-NVP hydrogels at 35 and 39 °C measured in compression mode

In DMA, the storage modulus, G', is related to the stiffness or rigidity of the material.[184] Figure 5.7 shows the relationship between G' and temperature for the nanocomposite hydrogels. As expected, the deswollen hydrogels at 39 °C exhibited a higher G' at all frequencies compared to the swollen hydrogels at 35 °C due to the lower water content of the former samples. The tensile modulus, ultimate tensile strength (UTS), and percent strain at break also increased for the deswollen hydrogel, as shown in Table 5.4. The constantly changing hydrogel stiffness between the resting and activated temperatures may contribute to cell detachment upon thermal cycling. Materials with modulus values

much greater than the surrounding tissue are known to cause local irritation and an increased host response. Though the mechanical properties of specialized connective tissue such as bone, cartilage, and tendon have been extensively studied, much less information is available regarding the behavior of loose connective tissue in humans. Iatridis *et al.* determined that the equilibrium tensile modulus of subcutaneous rat tissue is approximately 2.75 kPa.[185] Thus, the modulus of the hydrogel in the deswollen as well as the swollen state are similar to soft tissue and would be expected to minimize local tissue irritation.

Table 5.4. Tensile properties of the hydrogels

	35 °C	**39 °C**
Modulus [kPa]	2.0 ± 0.4	8.5 ± 1.1
UTS [kPa]	89.2 ± 27.9	353.7 ± 46.2
% strain at break	68.3 ± 7.1	78.8 ± 5.8

Self-Cleaning via Cell Release

The effects of a variable thermal environment on cell adhesion were studied using GFP-labeled H2B 3T3 mouse fibroblast cells. Hydrogels and polystyrene controls were sterilized by exposure to 70% ethanol for 45 minutes. The samples were then washed three times with sterile Dulbecco's PBS for 30 minutes each and placed in DMEM overnight. The samples were inoculated with GFP-H2B 3T3 mouse fibroblast cells maintained in DMEM with 10% fetal calf serum and antibiotics. The samples were then randomly assigned to one of two groups. The control group was maintained at a constant

temperature of 35 °C while the variable group was cycled between 35 and 39 °C every hour. Samples of each material and group were removed daily and imaged (Nikon Eclipse TE 2000-S) to obtain an average cell count.

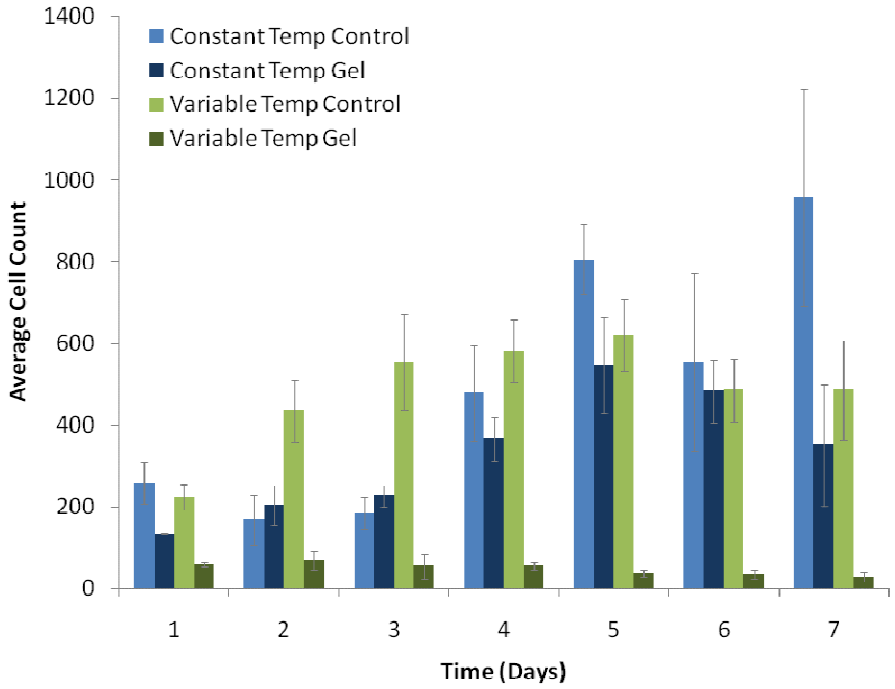

Figure 5.8. Cell adhesion over time for hydrogels and controls maintained at either constant or variable temperatures

Figure 5.8 shows that in the constant temperature group, the number of cells increased throughout the week. The control samples have more cell attachment at the end of the week than the gels, potentially due to the hydrogels remaining in a relatively hydrophilic state while cells tend to grow well on more hydrophobic surfaces. The control specimens that experienced variable temperatures exhibited increasing cell numbers over time,

showing that implementing thermal cycling by this protocol does not destroy cells. The slight decrease in cell count between days 5 and 6 is attributed to cells that may have been disturbed when the used cell culture media was exchanged for fresh DMEM. The "activated" time required to completely detach cells from PNIPAAm films depends on cell types and physiochemical properties of the specific hydrogel.[186] The hydrogels that were subject to thermal cycling showed very little cell adhesion over the duration of the study, demonstrating the possibility of using this system to promote self-cleaning of an implantable sensor.

Conclusions

In an effort to design an implant material that can overcome the host response to a foreign body while maintaining sufficient levels of analyte diffusion and mechanical strength, the composition of a PNIPAAm-based thermoresponsive nanocomposite hydrogel was optimized for *in vivo* conditions. During the design process, the site specific environment including factors such as local temperature and salinity were considered, and JMP statistical analysis was used to create the optimal formulation. By incorporating a hydrophilic comonomer, NVP, the volume phase transition temperature was raised such that at body temperature the hydrogel exists in the swollen state, thus permitting increased glucose diffusion through the hydrogel to the enclosed sensor. The "self-cleaning" mechanism of the hydrogel membrane is activated by cyclically raising the temperature above the VPTT and subsequently cooling to body temperature. Even though the diffusion rate is slightly lower in the "active" state, the addition of NVP

significantly improves glucose transfer. During deswelling, the dynamic compression modulus, G', as well as tensile modulus increased. This increase in hydrogel rigidity should contribute to diminished adhesion of cells as well as the change in surface hydrophilicity during thermal cycling. Over a period of 7 days, it was found that thermally cycled hydrogels experienced very low levels of cell attachment throughout the course of the study. Though further research is needed to determine the necessary duty cycle to promote optimal diffusion while limiting cell adhesion and to assess *in vivo* functionality, the *in vitro* cell adhesion rates are promising.

CHAPTER VI

SENSOR IMPLANT IMPLEMENTATION

Sensing System

In order to take a glucose-sensitive assay from a cuvette to the body, thorough design must occur, taking into consideration all of the normal site specific conditions and possibilities for problems. Implementing the self-cleaning membrane discussed in the previous chapters involves the introduction of an internal component to sense glucose in the interstitial fluid as well as an external device to measure the fluorescence signal and regulate the hydrogel temperature. Figure 6.1 shows the schematic of the proposed system. The interface device is relatively simple, with a large LCD screen and only three buttons, keeping in mind the aging target population. Stylistically, the device is a cross between a watch and a glucometer, promoting discretion and potentially increasing patient use in public. Additionally, the size has been minimized for comfort and portability. Typical outer dimensions of a wrist-wearable medical device are about 60 x 50 x 15 mm.[187] In order to house the multitude of components, mechanical and electrical codesign is necessary throughout the development phase. High-density packaging (HDP) and 3D integration (3DI) technologies may be useful for creating highly integrated nanochips with high speeds and miniscule dimensions.[188,189] The housing of the device should render it shockproof, conforming to IP 65 class according to IEC 60529, Degrees of Protection Provided by Enclosures.[187] Additionally, the interface between the patient and the device must be biocompatible. While the implant may need to be replaced on a

regular basis, the external device should have a field life of approximately four years in order to be eligible for reimbursement by many health insurance companies.[187]

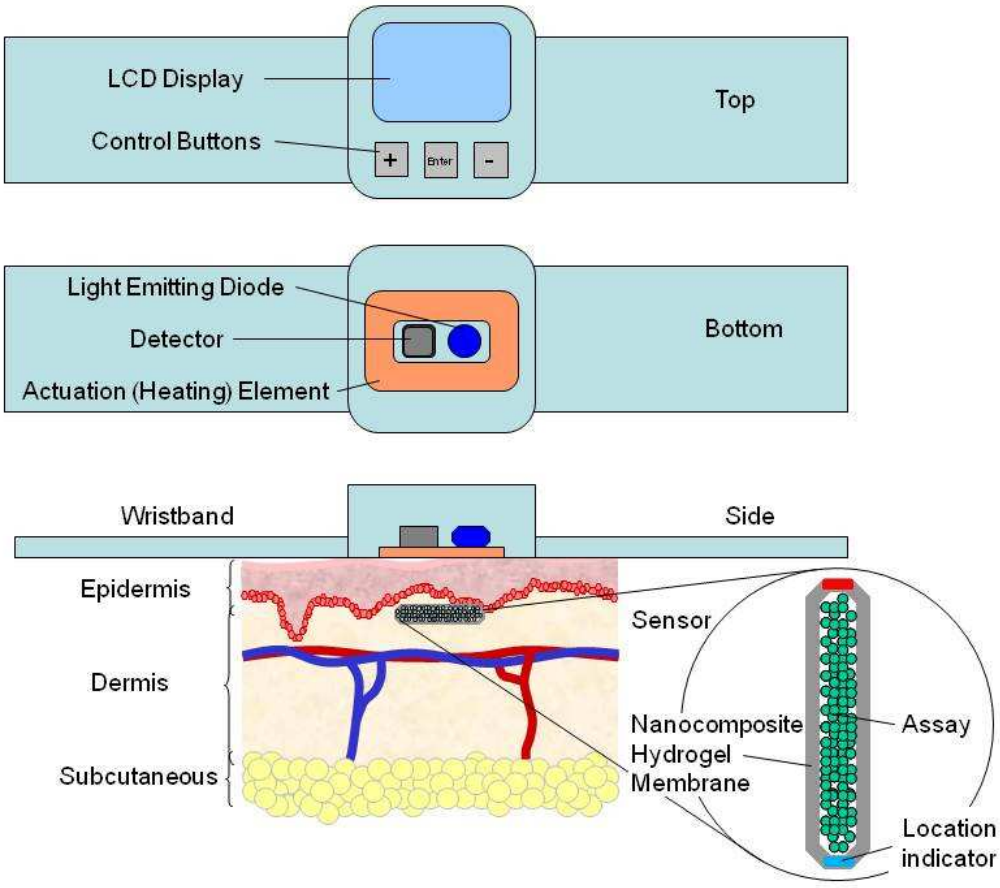

Figure 6.1. Schematic of the proposed system with optics for analyte detection and a heating element for activating "self-cleaning" of the implant

The underside of the device contains an optical system, comprised of an LED and photodetector, as well as a heating element, all of which should ideally be low-power to extend battery life and increase safety. The heating element is transparent to allow for

light transmission to and from the optical components (Thermal-clear transparent heater, Minco, Minneapolis, MN). Clear, flexible heaters were developed for military applications such as laser sights, cockpit displays, and pilot helmets, specifically because LCD screens do not function well at low temperatures.[190] They are useful for this application because they can simultaneously occupy the same space as the optical devices, minimizing the size of the system and the affected skin surface area. Additionally, the flexibility of the heaters allows the device to fit snugly against the forearm for maximum heat conduction.

One potential concern for a system such as this is cost. While the initial implantation and upfront fee for the device may be more expensive than the average glucometer, there are no disposable components such as test strips that need to be purchased for each test. Also, by providing the potential for increased glycemic control, overall health expenses may decrease as long-term complications are minimized. The annual cost difference between well-monitored and poorly monitored diabetic patients is about €2000 (~$2800) per year.[187]

Heat Propagation

In order to determine the effects of heating at the skin surface to raise the implanted hydrogel above the VPTT and trigger the self-cleaning response, it is useful to model the temperature distribution throughout the system. Figure 6.2 shows the tissue geometry in one dimension beginning with the epidermis at the surface and progressing through the

highly vascularized dermis and into the fatty subcutaneous tissue. Heat may be produced by the heater at the surface as well as by the metabolic processes of the body. If the sensor is inserted just below the epidermis, the heat only has to travel through one 80 μm layer to activate the self-cleaning of the hydrogel sensor.

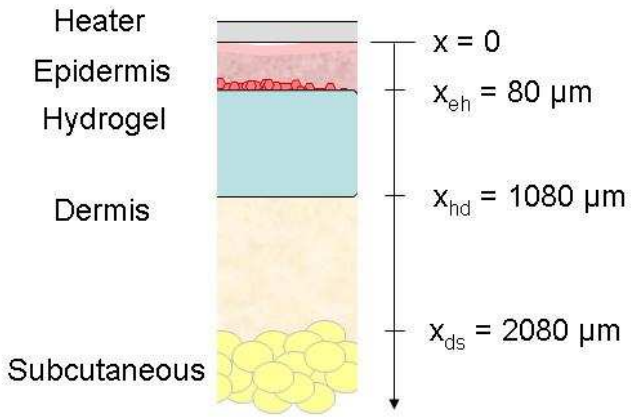

Figure 6.2. Model of one-dimensional tissue geometry

From a thermal point of view, biological systems consist of a different tissue layers and a complex network of blood vessels that distribute heat through the surrounding media. The temperature distributions within each tissue layer can be derived using the bioheat transfer equation.

$$\underbrace{\rho c \frac{\partial T}{\partial t}}_{\substack{\text{change} \\ \text{in storage}}} = \underbrace{k\nabla^2 T}_{\text{conduction}} + \underbrace{\rho_b c_b \omega_b \left(T_b - T\right)}_{\substack{\text{convection} \\ \text{due to blood flow}}} + \underbrace{Q}_{\substack{\text{metabolic} \\ \text{heat generation}}}$$

where ρ, ρ_b are densities of tissue and blood in kg/m^3, c, c_b are the specific heats of tissue and blood in J/kg·K, T, T_b are the temperatures of tissue and blood in K, t is time, k is the heat conductivity of tissue in W/m·K, ω_b is the flow rate of blood in m^3/m^3·sec, and Q is the metabolic rate in J/m^3·sec.[89,191] The thermal properties of each of the skin components can be seen in Table 6.1.[192]

Table 6.1. Thermal properties of skin tissue components

Component	***k* (W/m·K)**	**ρ[kg/m^3]**	***c* [J/kg·K]**
Epidermis	0.34	1,120	3,200
Dermis	0.41	1,090	3,500
Blood	0.55	1,060	3,600

The arterial blood temperature measured at the distal portion of the brachial artery in the forearm is about 36.63 °C and blood flow was found to be 6.2 ml/min·100 ml tissue, which is approximately 0.00103 m^3/m^3·sec.[193] The density of the hydrogel sensor is 1,032 kg/m^3 and the specific heat is around 8,500 J/kg·K.[194,195] Figure 6.3 shows the thermal profile as heat is applied to the surface of the epidermis. The heat travels quickly through the thin epidermal layer, while the highly vascularized dermis tends to remain closer to the core body temperature.

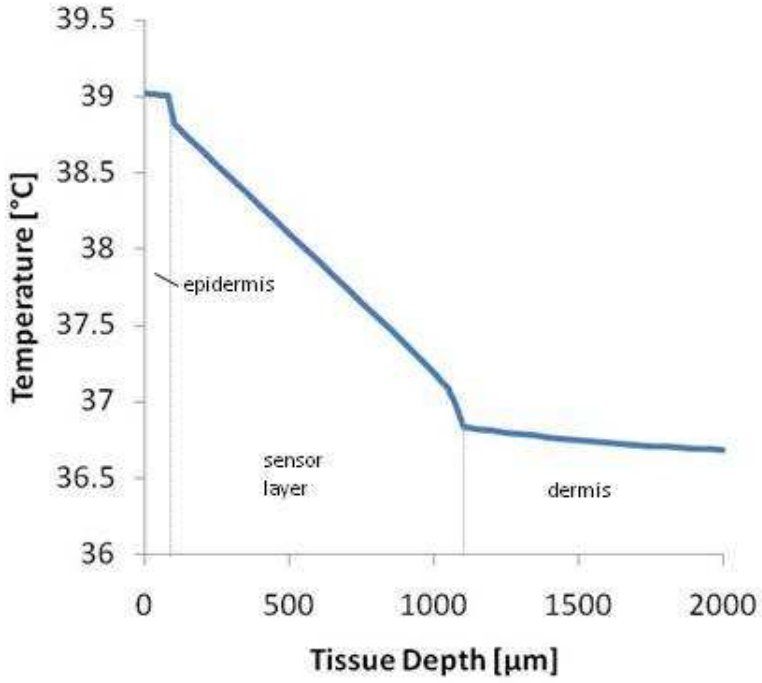

Figure 6.3. Thermal profile as heat is applied

Ice application with compression has been shown to have a greater rate of cooling than treatment without compression.[196] This may be applicable for the implementation of this device as compression may be applied by the watchband, aiding conduction and reducing the amount of time that the heater must be activated, thereby prolonging battery life.

Light Propagation

Light must also propagate through the tissue to reach the sensor. Skin properties can vary widely from person to person depending on genetics and environment. Pigments such as melanin, oxyhemoglobin, deoxyhemoglobin, carotenoids, and bilirubin are

involved in producing skin color.[197,198] Most biological tissues are strongly scattering or turbid, but optical absorption is relatively weak in the range of about 650 to 1300 nm, which is called the optical or therapeutic window.[199] Figure 6.4 shows the increased levels of absorption at wavelengths below the optical window due to tissue constituents such as protein, melanin, and hemoglobin. Water is one of the primary absorbers at wavelengths above the optical window, along with collagen at higher wavlenghts.[200] In the key optical window range, the typical absorption coefficient is about 0.1 to 1 cm^{-1}, which means that a photon can travel from 1 to 10 cm before it is absorbed.[201] Heating causes an increase in cutaneous blood flow and vasodilation, while cooling causes vasoconstriction and closing of capillary shunts. Because light scattering by human skin is linearly dependent on temperature, the optical signal may need to be calibrated at both body temperature and the elevated activated temperature.[202]

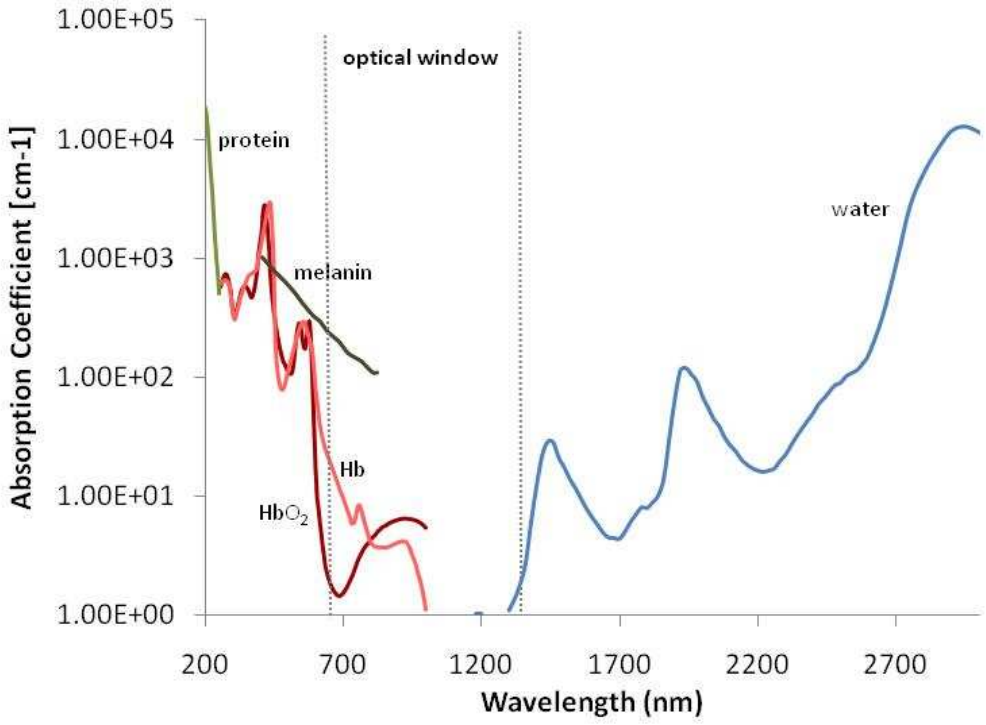

Figure 6.4. Absorption spectra of several main tissue components

Photon migration in a biological tissue such as skin can be numerically simulated using the Monte Carlo method.[203] The trajectory of each photon is modeled as a persistent random walk in which the direction of the step is dependent on the previous step. At boundaries, a photon is either reflected or passes across the boundary. Monte Carlo calculates probability distributions for each type of interaction (scattering or absorption), randomly sampling variables, and as the name implies, is like throwing the dice.

The optical properties and thickness of the skin and sensor layers used in the modeling are shown in Table 6.2.[204-209] Each layer is treated as a flat, homogenous material with a

semi-infinite geometry compared to that of the beam size. The original Monte Carlo code was generated by Mark A. Mackanos of VaNTH and modified by Alex Abraham.

Table 6.2. Optical properties of skin model layers

Layer	Thickness [μm]	n	μ_a [mm^{-1}]	μ_s [mm^{-1}] 488 nm	μ_s [mm^{-1}] 700 nm	g
Stratum corneum	10	1.50	0.2	40	20	0.9
Epidermis	80	1.34	0.15	35	10	0.85
Sensor layer	1000	1.508	0.1	35	28	0.6
Papillary dermis	100	1.40	0.7	30	12	0.8
Upper blood net dermis	80	1.39	1.0	35	15	0.9
Dermis	1500	1.40	0.7	27	12	0.76
Deep blood net dermis	200	1.39	1.0	35	15	0.95
Subcutaneous fat	5000	1.44	0.3	15	5	0.8

Theoretically, the implanted sensor would be as small as possible to enable easy delivery and minimal tissue disruption. However, Figure 6.5 shows the correlation between sensor thickness and signal intensity. As the sensor size is minimized, the emission also decreases as there is less area for fluorophore to interact with the light. One potential way to improve the signal would be to use a higher excitation power, but there are tradeoffs with battery life. Also, the current regulations set by the American National Standard for Safe Use of Lasers (ANSI Z136.1) limit the maximum permissible exposure limits in terms of power and time, depending on the chosen light source. For

example, when using a continuous wave HeNe laser, 2.5 x 10^{-3} W/cm^2 is permissible for 0.25 seconds, while only 293 x 10^{-6} W/cm^2 is allowed for a duration of 600 seconds.[210] Another method to potentially increase the intensity of the signal is to increase the assay concentration. There is an optimal amount of fluorophore for tagging the assay, above which, quenching or a decrease in the dynamic range may be experienced. However, high quantities of the labeled assay could be introduced to the sensor implant, provided that there is still enough room for sufficient binding and unbinding motility. The detection process is reversible and does not consume the analyte so an increase in assay should not be physiologically problematic.

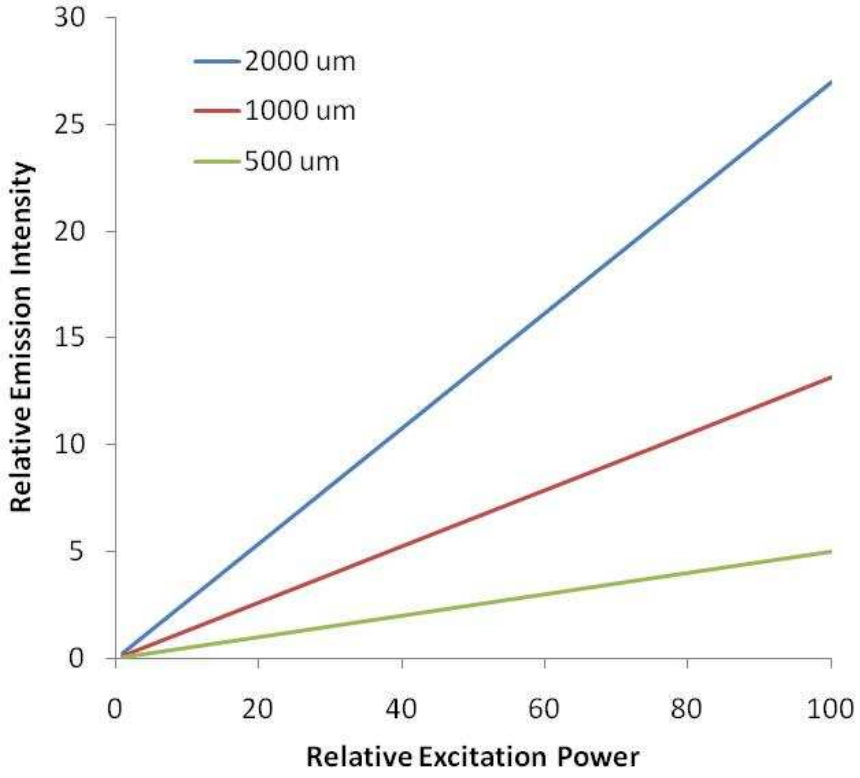

Figure 6.5. Dependence of signal intensity on excitation power and sensor thickness

Another factor to consider is implant depth. The sensor must be located below the epidermis for long term use because the surface of the skin is constantly sloughed off as it regenerates. On the other hand, increased depth leads to a significant decrease in signal strength, as shown in Figure 6.6. Additionally, the sensor membrane becomes harder to heat as the heat must penetrate farther into the tissue and the thermal equilibrating effects of the deeper vasculature become more prominent. Ideally, the surface of the implant would be located directly under the epidermal layer for optimal optical and thermal outcomes.

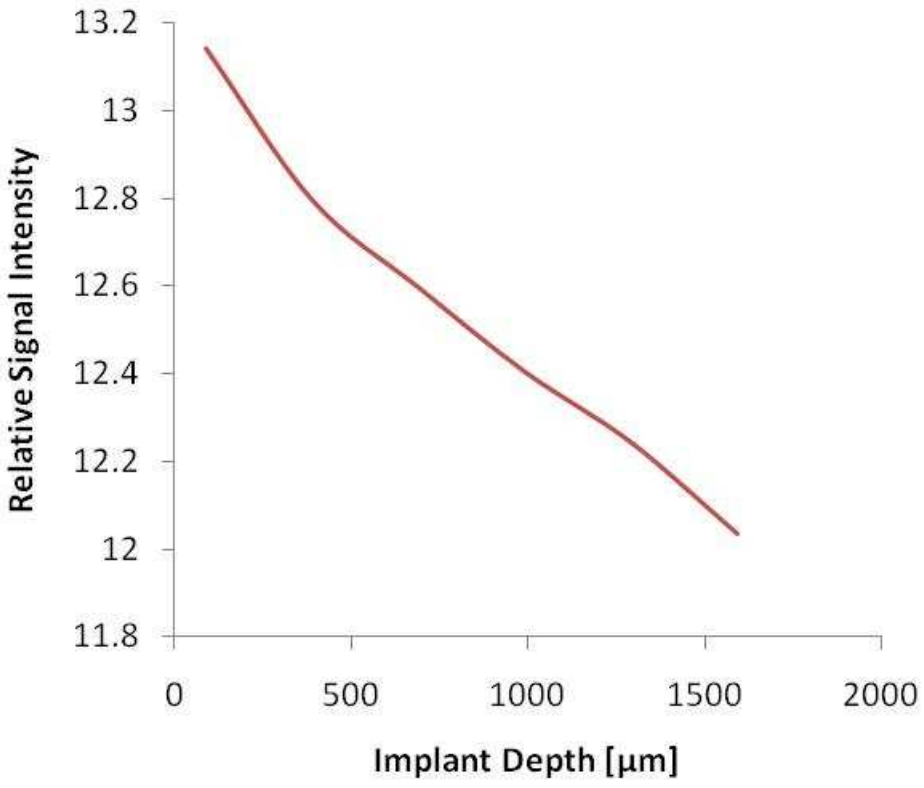

Figure 6.6. Relationship between implant depth and signal intensity

Sensor Implant

It can be useful to model a new design after previous cases that have been successful. In humans, common implants include microchips, radiation implants, and contraceptives. Hormonal contraceptive implants in particular have been widely studied, including Norplant, Jadelle, and Implanon, which have been approved for use in Europe, North America, and several other countries.[211] Each of these implants is comprised of at least one cylindrical rod ranging in volume from about 125 mm^3 to 211 mm^3, as shown in Table 6.3.

Table 6.3. Physical properties of common contraceptive implants

	Number of Implants	Diameter	Length
Norplant	6	2.4 mm	34 mm
Jadelle	2	2.5 mm	43 mm
Implanon	1	2 mm	40 mm

The proposed self-cleaning implant will also have a cylindrical rod shape. The form is easy to manufacture using a glass mold consisting of a hollow tube with a solid rod in the center. After polymerization, the assay is loaded into the center of the implant and the ends are capped with additional polymer. Highly angular polymer surfaces have shown to induce the highest enzyme activity and cellular response upon implantation.[212] Therefore, even the ends of the hydrogel tubes will be rounded, as shown in Figure 6.7.

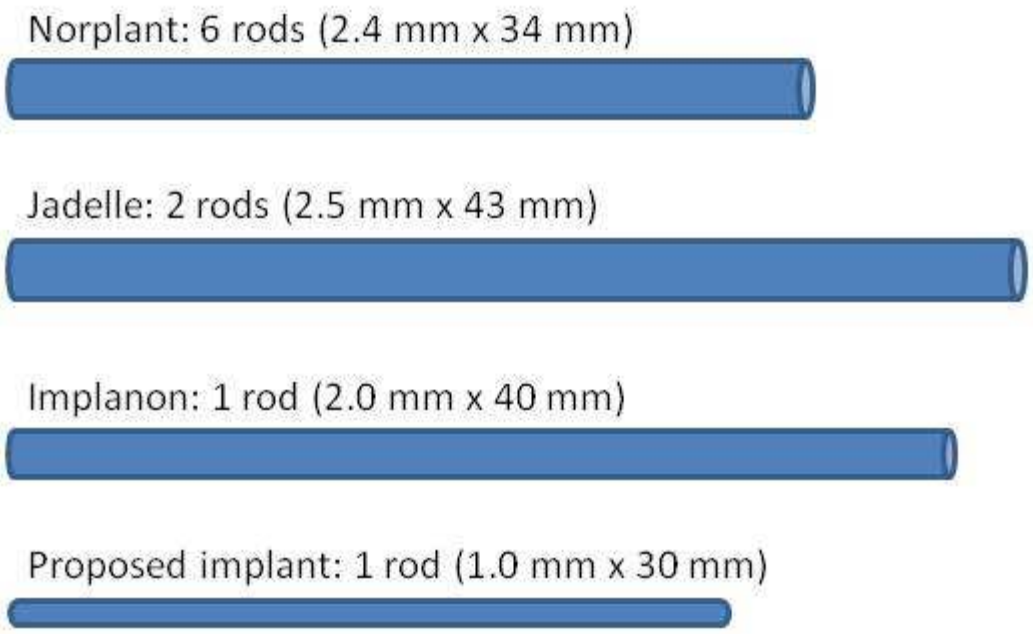

Figure 6.7. Comparative sizes of implants

Another positive aspect to the rod shape design is potential ease of implantation via a needle-type injection device. The delivery process would be similar to that of the insertion of hormonal contraceptive implants such as Norplant or Implanon.[213] The applicator device can be seen in Figure 6.8. After cleaning the insertion site with antiseptic, a local anesthetic can be applied if needed. The needle tip is inserted just under the skin and the obturator is released as the cannula is retracted back along the length of the obturator, leaving the sensor in place.[214] If necessary, saline could be injected first, creating a pocket in the tissue in which to implant the sensing device.

In order to remove the implant after the assay is no longer effective, a small incision would be made at the tip of the rod. The implant would be manipulated toward the incision, grasped with forceps, and gently removed. A new sensor could be inserted before the incision is closed.

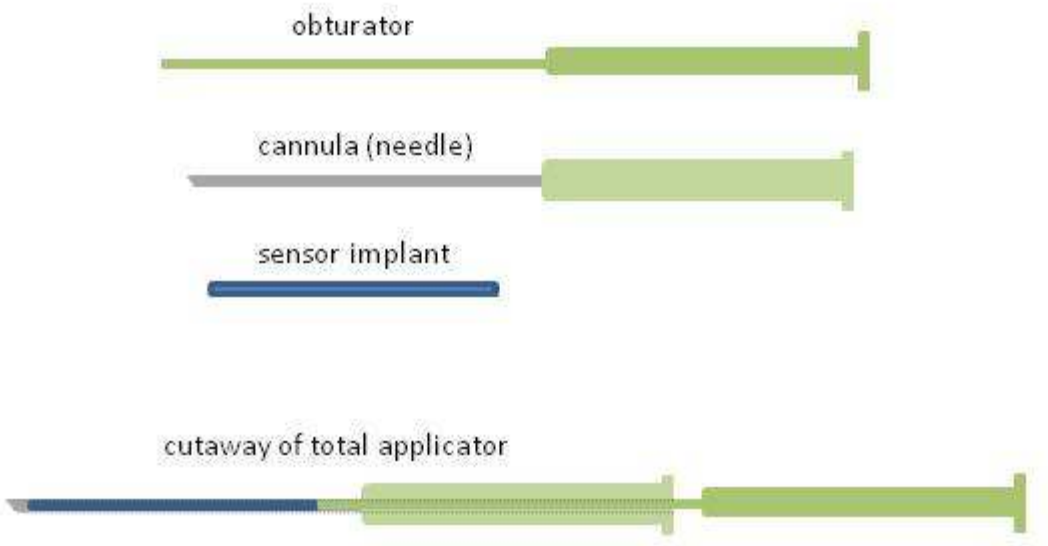

Figure 6.8. Applicator device for sensor implantation

The insertion and removal process have been described as easy, typically taking less than 1 and 4 minutes to achieve, respectively.[213] One of the concerns during device delivery was accidental non-insertion whereby the rod either remains in the applicator or falls out prior to insertion.[214] This should be recognized immediately as the fluorescence signal would be detected upon implantation. Furthermore, location indicator dyes would be incorporated into the end caps of the sensor rod, as shown in Figure 6.1, to distinguish

position. If the distance between the locators appears smaller than expected, the rod may have been implanted on an angle and needs to be adjusted before use. The average removal time is slightly higher than implantation times due to the potential for more complications.[213] Because the hormonal contraceptive implants are detected through palpation, many problems stemmed from difficulty in locating the implant, particularly when it was too deeply embedded in the tissue. The presence of the locator indicator dyes should prevent this problem. Another issue that was experienced by several patients was implant adhesion to underlying tissue accompanied by a thick fibrotic sheath. This will hopefully be avoided because of the self-cleaning nature of the hydrogel material. The only issue seen in the removal of Implanon that may be problematic is the possibility of breakage. The hydrogel would then have to be removed in several pieces and the assay solution could be released into the body if it is not embedded in microspheres. Though there has been concern about the toxicity of Concanavalin A, Ballerstadt *et al*. have recently shown that small amounts of Con A pose little or no health risk in the event of sensor rupture.[215] The most likely outcome of a situation in which the implant fractured upon removal would be switching the location of the new implant to the opposite forearm so as to avoid signal interference with any fluorophore temporarily left in the local area.

Regulatory Standards

In the United States, regulations for medical devices are derived from five principle laws that include the Federal Food, Drug and Cosmetic Act of 1938, Medical Device

Amendments of 1976, Safe Medical Devices Act of 1990, Medical Device Amendments of 1992, and FDA Modernization Act of 1997 (Section 204).[216] Devices are classified in one of three categories as shown in Table 6.4 and regulation increases with higher class number. Most Class I devices are exempt from Premarket Notification 510 (k), but it is required for most Class II devices. The majority of Class III devices require a more intensive Premarket Approval.[217]

Table 6.4. Classification of medical devices

Category	Description	Distribution
Class I	General controls	Over-the-counter
Class II	Performance standards and special controls	Physician-controlled
Class III	Premarket approval	Clinical use only

According to the Food and Drug Administration (FDA) product classification database, both noninvasive and invasive glucose sensors are currently listed as Class III devices. Class III devices are those that support or sustain human life, are of substantial importance in preventing impairment of human health, or which present a potential risk. Products requiring premarket approval (PMA) are either high risk devices that pose a significant risk of illness or injury or are devices found not substantially equivalent to approved Class I and II devices.[217] The PMA process is the most stringent type of device marketing application, requiring sufficient clinical data as evidence to support the claims and assure that the device is safe and effective for its intended use.

In addition to regulations set by the FDA, standards relating to biomedical materials and devices are set by the International Standards Organization (ISO) and the American Society for the Testing of Materials (ASTM). These include ISO 10993: Biological evaluation of medical devices and F748 issued by the F04 ASTM committee on medical and surgical devices and materials.[218] These standards provide guidelines for performance characteristics and can be used to characterize a device as part of the safety review for PMA.

Summary

In an attempt to translate a glucose-sensitive assay from the research laboratory to clinical use, several implementation design concepts were considered. A system design was proposed that includes both heating and optical elements for self-cleaning and analyte monitoring, respectively. The ideal implant placement for both thermal and optical purposes is at minimal tissue depth, but it must be located below the epidermal layer for long-term stability. For ease of implantation and minimal local tissue irritation, the sensor size should be minimized. However, there is a tradeoff with signal strength. This could potentially be overcome by adjusting the excitation power and assay concentration. The implant design has been modeled after currently used hormonal contraceptive implants. The cylindrical shape allows for easy deliver and removal by a trained clinician in a matter of a few minutes. Though the Class III classification of glucose-sensing devices requires a stringent PMA process for approval, the numerous

laboratory tests that have been and will be conducted on these materials will help ensure the safety and efficacy of this device.

CHAPTER VII

SUMMARY

Review of Results

Diabetes is a disease in which the body does not produce or properly use insulin, leading to abnormal glucose levels in the body and a significantly increased potential for long-term complications. Continuous glucose monitoring (CGM) has been shown to increase glycemic control in diabetic patients, leading to overall improved health outcomes. However, currently available CGM systems are invasive and limited to short-term use between 3 and 7 days. Fluorescence-affinity sensing has demonstrated potential for fast, reagentless, minimally invasive glucose measurement. The purpose of this research was to help advance a glucose-sensitive assay from cuvette to clinical use. To this end, several main objectives were identified including improving the assay encapsulation to increase sensor response and developing a membrane to prolong sensor implant efficacy and lifespan.

Microporation of poly(ethylene glycol) (PEG) spheres was used to create cavities of solution in which analytes may freely diffuse and interact with the sensing elements. This process allows for the use of a fine hydrogel mesh size to minimize leaching, thereby increasing sensor lifetime, without limiting the mobility of the assay components to bind and unbind, promoting both functionality and stability of the encapsulated sensors.

A “self-cleaning” sensor implant membrane was developed with temperature-dependent surface hydrophobicity that limits cellular adhesion in response to thermal cycling around the volume phase transition temperature (VPTT). However, the original nanocomposite PNIPAAm hydrogel formulation had a VPTT around 33-34 °C, resulting in a gel that is in a collapsed state at body temperature, limiting diffusion. The VPTT was increased by introducing a hydrophilic comonomer, *N*-vinylpyrrolidone (NVP) and the new formulation was optimized with regard to diffusion, mechanical strength, and cell releasing capabilities under physiological conditions.

Recommendations

Several aspects can be considered for future work to continue this research. The concepts that make the microporated spheres effective would be improved by the use of fully hollow spheres. There have been some advances using layer-by-layer self assembly to achieve this, but as of yet, the process appears to be too harsh to retain complete assay functionality.

In terms of improving the self-cleaning membrane, various nanoparticle sizes could be studied. Smaller particles may lead to increased optical clarity, allowing higher concentrations to be used in the precursor solution, thereby increasing the hydrogel mechanical strength. Furthermore, testing in PBS showed deviations in performance from those observed in DI water. To more closely study potential effects under physiological conditions, characterization could be done in interstitial fluid.

Additionally, the duty cycle of the heating system could be optimized by studying the minimal amount of activated time necessary to promote an effectively clean surface for maximum sensor performance while simultaneously allowing sufficient glucose transport through the membrane. Finally, cell culture has been used to assess the potential of these materials, but *in vivo* studies are necessary to determine the actual performance characteristics needed for long-term use. Though there is much work to be done, overall, this system is a promising start in an effort to achieve an effective sensor implant for minimally invasive continuous glucose sensing.

REFERENCES

1. Ahmed AM. History of diabetes mellitus. Saudi Med J 2002;23(4):373-378.

2. Geddes CD, Lakowicz JR, editors. Glucose sensing. Volume 11. New York: Springer; 2006.

3. National Diabetes Information Clearinghouse. Diabetes overview, NIH publication no. 06-3873. Bethesda, MD: National Institutes of Health; 2006.

4. Centers for Disease Control and Prevention. National diabetes fact sheet: General information and national estimates on diabetes in the United States, 2007. Atlanta, GA: U.S. Department of Health and Human Services, Centers for Disease Control and Prevention; 2008.

5. Wild S, Roglic G, Green A, Sicree R, King H. Global prevalence of diabetes. Diabetes Care 2004;27(5):1047-1053.

6. World Health Organization. Diabetes fact sheet; November 2008. Report nr 312.

7. World Health Organization. World Health Organization website at www.who.int/topics/diabetes_mellitus/en/; accessed September 2009.

8. Kirtland KA, Li YF, Geiss LS, Thompson TJ. State-specific incidence of diabetes among adults -- participating states, 1995 -- 1997 and 2005 -- 2007. MMWR 2008;57(43):1169-1173.

9. American Diabetes Association. Pre-diabetes. American Diabetes Association website at www.diabetes.org/diabetes-basics/prevention/pre-diabetes/; accessed September 2009.

10. Del Prato S. A call to action: The UN Resolution on diabetes. Int J Clin Pract 2007;61(157):1-4.

11. United Nations General Assembly, 61st Session. UN Resolution 61/225: World Diabetes Day. Signed 20 December 2006.

12. Wagner EH, Sandhu N, Newton KM, McCulloch DK, Ramsey SD, Grothaus LC. Effect of improved glycemic control on health care costs and utilization. J Amer Med Assoc 2001;285(2):182-189.

13. Diabetes Research Group. The effects of intensive treatment of diabetes on the development and progression of long-term complications in insulin-dependent diabetes mellitus. New Engl J Med 1993;329:977-986.

14. Silink M. United Nations Resolution 61/225: What does it mean to the diabetes world? Int J Clin Pract 2007;61(157):5-8.

15. Newman JD, Turner APF. Home blood glucose biosensors: A commercial perspective. Biosens Bioelectron 2005;20:2435-2453.

16. Clark LC, Lyons C. Electrode systems for continuous monitoring in cardiovascular surgery. Ann NY Acad Sci 1962;102:29-45.

17. Dungan K, Chapman J, Braithwaite SS, Buse J. Glucose measurement: Confounding issues in setting targets for inpatient management. Diabetes Care 2007;30(2):403-409.

18. Skeie S, Thue G, Nerhus K, Sandberg S. Instruments for self-monitoring of blood glucose: Comparisons of testing quality achieved by patients and a technician. Clin Chem 2002;48(7):994-1003.

19. Thomas LE, Kane MP, Bakst G, Busch RS, Hamilton RA, Abelseth JM. A glucose meter accuracy and precision comparison: The FreeStyle Flash versus the Accu-Chek Advantage, Accu-Chek Compact Plus, Ascensia Contour, and the BD Logic. Diabetes Technol Ther 2008;10(2):102-110.

20. American Diabetes Association. Standards of medical care in diabetes - 2008. Diabetes Care 2008;31(Supplement 1):S12-S54.

21. Subramanian SL, Hirsch IB. The utility and recent advances in self-monitoring of blood glucose in type 1 diabetes. Diabetes Technol Ther 2008;10(Supplement 1):S43-S50.

22. Bode BW, Sabbah HT, Gross TM, Fredrickson LP, Davidson PC. Diabetes management in the new millennium using insulin pump therapy. Diabetes Metab Res 2002;18(S1):S14-S20.

23. Cheyne E, Kerr D. Making 'sense' of diabetes: Using a continuous glucose sensor in clinical practice. Diabetes Metab Res 2002;18:S43-S48.

24. Florida Department of Health Diabetes Prevention & Control Program. Diabetes fact sheet. Florida Department of Health website at www.doh.state.fl.us/Family/DCP/factsheet.html; accessed September 2009.

25. Raccah D, Sulmont V, Reznik Y, Guerci B, Renard E, Hanaire H, Jeandidier N, Nicolino M. Incremental value of continuous glucose monitoring when starting pump therapy in patients with poorly controlled type 1 diabetes: The realtrend study. Diabetes Care published online ahead of print at care.diabetesjournals.org/content/early/2009/09/16/dc09-0750, September 18, 2009.

26. Bode BW, Gross TM, Thornton KR, Mastrototaro JJ. Continuous glucose monitoring used to adjust diabetes therapy improves glycosylated hemoglobin: A pilot study. Diabetes Res Clin Pr 1999;46(3):183-190.

27. Juvenile Diabetes Research Foundation Continuous Glucose Monitoring Study Group. Continuous glucose monitoring and intensive treatment of type 1 diabetes. New Engl J Med 2008;359(14):1464-1476.

28. Juvenile Diabetes Research Foundation Continuous Glucose Monitoring Study Group. Sustained benefit of continuous glucose monitoring on HbA1c, glucose profiles, and hypoglycemia in adults with type 1 diabetes. Diabetes Care published online ahead of print at care.diabetesjournals.org/content/early/2009/08/03/dc09-0846, August 12, 2009.

29. Hovorka R, Wilinska ME, Chassin LJ, Acerini CL, Dunger DB. The artificial pancreas: Making headway. Pract Diab Int 2007;24(2):56-58.

30. Tamada JA, Lesho M, Tierney MJ. Keeping watch on glucose: New monitors help fight the long-term complications of diabetes. IEEE Spectrum April 2002:52-57.

31. Renard E. Implantable closed-loop glucose-sensing and insulin delivery: The future for insulin pump therapy. Curr Opin Pharmacol 2002;2:708-716.

32. Wentholt IME, Hoekstra JBL, Zwart A, DeVries JH. Pendra goes Dutch: Lessons for the CE mark in Europe. Diabetologia 2005;48:1055-1058.

33. Bao JZ, Davis CC, Schmukler RE. Frequency domain impedance measurements of erythrocytes. Constant phase angle impedance characteristics and a phase transition. Biophys J 1992;61(5):1427-1434.

34. Beving H, Eriksson G. Dielectric spectroscopy of human blood. Eur J Surg 1994;574:87-89.

35. Zhao TX, Lockner D. Electrical impedance and erythrocyte sedimentation rate. Biochim Biophys Acta 1993;1153(2):243-248.

36. Pfutzner A, Caduff A, Larbig M, Schrepfer T, Forst T. Impact of posture and fixation technique on impedance spectroscopy used for continuous and noninvasive glucose monitoring. Diabetes Technol Ther 2004;6(4):435-441.

37. Flacke F. Practical aspects of using the PENDRA device. 40th Annual Meeting of the EASD, Munich, Germany, available online at www.diabetes-symposium.org/index.php?menu=view&id=136; presented May 9, 2004.

38. Weinzimer SA. PENDRA: The once and future noninvasive continuous glucose monitoring device. Diabetes Technol Ther 2004;6(4):442-444.

39. Girardin CM, Huot C, Gonthier M, Delvin E. Continuous glucose monitoring: A review of biochemical perspectives and clinical use in type 1 diabetes. Clin Biochem 2009;42(3):136-142.

40. Maran A, Poscia A. Continuous subcutaneous glucose monitoring: The GlucoDay system. Diabetes Nutr Metab 2002;15(6):429-433.

41. Ricci F, Moscone D, Palleschi G. Ex vivo continuous glucose monitoring with microdialysis technique: The example of GlucoDay. IEEE Sens J 2008;8(1):63-70.

42. Kubiak T, Worle B, Kuhr B, Nied I, Glasner G, Hermanns N, Kulzer B, Haak T. Microdialysis-based 48-hour continuous glucose monitoring with GlucoDay: Clinical performance and patients' acceptance. Diabetes Technol Ther 2006;8(5):570-575.

43. The Menarini Group. Continuous glucose monitoring: GlucoDay. Menarini Group website at www.menarini.com/diagnostic_uk/uk/diagnostic/products/continuous_glucose_monitoring/introduction; accessed September 2009.

44. Kerr D, Fayers K. Continuous real-time glucose monitoring systems: Time for a closer look. Pract Diab Int 2008;25(1):37-41.

45. Wolpert HA. The nuts and bolts of achieving end points with real-time continuous glucose monitoring. Diabetes Care 2008;31(Supplement 2):S146-S149.

46. Cengiz E, Tamborlane WV. A tale of two compartments: Interstitial versus blood glucose monitoring. Diabetes Technol Ther 2009;11(Supplement 1):S11-S16.

47. Brauker J. Continuous glucose sensing: Future technology developments. Diabetes Technol Ther 2009;11(s1):S25-S36.

48. United States Patent and Trademark Office. Patent full-text and image database. website at patft.uspto.gov/netahtml/PTO/search-bool.html; accessed September 2009.

49. Tuchin VV, editor. Handbook of optical sensing of glucose in biological fluids and tissues. Boca Raton, FL: CRC Press; 2009.

50. Oliver NS, Toumazou C, Cass AEG, Johnston DG. Glucose sensors: A review of current and emerging technology. Diabetic Med 2009;26(3):197-210.

51. Lakowicz JR. Principles of fluorescence spectroscopy. New York: Springer; 2006.

52. Ballerstadt R, Schultz JS. Competitive-binding assay method based on fluorescence quenching of ligands held in close proximity by a multivalent receptor. Anal Chim Acta 1997;345(1):203-212.

53. Chowdhury TK, Weiss AK, editors. Concanavalin A. 2nd ed. Volume 55. New York: Plenum Press; 1975.

54. Wikimedia Commons. Con A tetramer. website at commons.wikimedia.org/ wiki/File:ConA_Tetramer.png; accessed September 2009.

55. Meadows DL. A fiber optic biosensor for glucose monitoring based on fluorescence energy transfer, Ph.D. Dissertation, University of Michigan, Ann Arbor, MI, 1988.

56. Bittiger H, Schnebli HP. Concanavalin A as a tool. London: John Wiley & Sons; 1976.

57. Schultz JS, Mansouri S, Goldstein IJ. Affinity sensor - a new technique for developing implantable sensors for glucose and other metabolites. Diabetes Care 1982;5(3):245-253.

58. Meadows D, Schultz JS. Fiber-optic biosensors based on fluorescence energy-transfer. Talanta 1988;35(2):145-150.

59. Meadows DL, Schultz JS. Design, manufacture and characterization of an optical-fiber glucose affinity sensor-based on an homogeneous fluorescence energy-transfer assay system. Anal Chim Acta 1993;280(1):21-30.

60. Ballerstadt R, Schultz JS. A fluorescence affinity hollow fiber sensor for continuous transdermal glucose monitoring. Anal Chem 2000;72(17):4185-4192.

61. Russell RJ, Pishko MV, Gefrides CC, McShane MJ, Cote GL. A fluorescence-based glucose biosensor using concanavalin A and dextran encapsulated in a poly(ethylene glycol) hydrogel. Anal Chem 1999;71(15):3126-3132.

62. Ibey BL, Beier HT, Yadavalli VK, Rounds RM, Cote GL, Pishko MV. Competitive binding assay for glucose based on glycodendrimer-fluorophore conjugates. Anal Chem 2005;77(21):7039-7046.

63. Ibey BL. Enhancement of a fluorescent sensor for monitoring glucose concentration in diabetic patients, Ph.D. Dissertation, Texas A&M University, College Station, TX, 2006.

64. Ballerstadt R, Polak A, Beuhler A, Frye J. In vitro long-term performance study of a near-infrared fluorescence affinity sensor for glucose monitoring. Biosens Bioelectron 2004;19(8):905-914.

65. Moschou EA, Sharma BV, Deo SK, Daunert S. Fluorescence glucose detection: Advances toward the ideal in vivo biosensor. J Fluoresc 2004;14(5):535-547.

66. Yadavalli VK, Koh WG, Lazur GJ, Pishko MV. Microfabricated protein-containing poly(ethylene glycol) hydrogel arrays for biosensing. Sens Actuat B - Chem 2004;97(2-3):290-297.

67. O'Neal DP, Meledeo MA, Davis JR, Ibey BL, Gant VA, Pishko MV, Cote GL. Oxygen sensor based on the fluorescence quenching of a ruthenium complex immobilized in a biocompatible poly(ethylene glycol) hydrogel. IEEE Sensors 2004;4(6):728-734.

68. Kim SH, Kim B, Yadavalli VK, Pishko MV. Encapsulation of enzymes within polymer spheres to create optical nanosensors for oxidative stress. Anal Chem 2005;77(21):6828-6833.

69. Russell RJ, Pishko MV, Simonian AL, Wild JR. Poly(ethylene glycol) hydrogel-encapsulated fluorophore-enzyme conjugates for direct detection of organophosphorus neurotoxins. Abstr Pap Am Chem S 2000;219:U107-U107.

70. Zguris J, Pishko MV. pH sensitive fluorescent poly(ethylene) glycol hydrogel microstructures for monitoring in cell culture systems. Sens Lett 2005;3(3):206-210.

71. Heo J, Crooks RM. Microfluidic biosensor based on an array of hydrogel-entrapped enzymes. Anal Chem 2005;77(21):6843-6851.

72. Sharma S, Johnson RW, Desai TA. Ultrathin poly(ethylene glycol) films for silicon-based microdevices. Appl Surf Sci 2003;206(1-4):218-229.

73. Harris JM, Zalipsky S, editors. Poly(ethylene glycol): Chemistry and biological applications. Volume 680. Washington, D.C.: American Chemical Society; 1997.

74. Rihova B. Biocompatibility of biomaterials: Hemocompatibility, immunocompatibility and biocompatibility of solid polymeric materials and soluble targetable polymeric carriers. Adv Drug Deliver Rev 1996;21(2):157-176.

75. Quinn CAP, Connor RE, Heller A. Biocompatible, glucose-permeable hydrogel for in situ coating of implantable biosensors. Biomaterials 1997;18(24):1665-1670.

76. Russell RJ, Axel AC, Shields KL, Pishko MV. Mass transfer in rapidly photopolymerized poly(ethylene glycol) hydrogels used for chemical sensing. Polymer 2001;42(11):4893-4901.

77. Mellott MB, Searcy K, Pishko MV. Release of protein from highly cross-linked hydrogels of poly(ethylene glycol) diacrylate fabricated by UV polymerization. Biomaterials 2001;22(9):929-941.

78. Kurdikar DL, Peppas NA. The volume shrinkage, thermal and sorption behavior of polydiacrylates. Polymer 1995;36(11):2249-2255.

79. Ibey BL, Meledeo MA, Gant VA, Yadavalli V, Pishko MV, Cote GL. In vivo monitoring of blood glucose using poly(ethylene glycol) microspheres. Proc SPIE 2003;4965:1-6.

80. Barone PW, Parker RS, Strano MS. In vivo fluorescence detection of glucose using a single-walled carbon nanotube optical sensor: Design, fluorophore properties, advantages, and disadvantages. Anal Chem 2005;77(23):7556-7562.

81. Chinnayelka S, McShane MJ. Glucose-sensitive nanoassemblies comprising affinity-binding complexes trapped in fuzzy microshells. J Fluoresc 2004;14(5):585-595.

82. Chinnayelka S, McShane MJ. Microcapsule biosensors using competitive binding resonance energy transfer assays based on apoenzymes. Anal Chem 2005;77(17):5501-5511.

83. Chen J, Park H, Park K. Synthesis of superporous hydrogels: Hydrogels with fast swelling and superabsorbent properties. J Biomed Mater Res 1999;44(1):53-62.

84. Oxley HR, Corkhill PH, Fitton JH, Tighe BJ. Macroporous hydrogels for biomedical applications: Methodology and morphology. Biomaterials 1993;14(14):1064-1072.

85. Badiger MV, McNeill ME, Graham NB. Porogens in the preparation of microporous hydrogels based on poly(ethylene oxides). Biomaterials 1993;14(14):1059-1063.

86. Filmon R, Retailleau-Gaborit N, Grizon F, Galloyer M, Cincu C, Basle MF, Chappard D. Non-connected versus interconnected macroporosity in poly(2-hydroxyethyl methacrylate) polymers. An x-ray microtomographic and histomorphometric study. J Biomat Sci - Polym E 2002;13(10):1105-1117.

87. Yadavalli VK, Russell RJ, Pishko MV, McShane MJ, Cote GL. A Monte Carlo simulation of photon propagation in fluorescent poly(ethylene glycol) hydrogel microsensors. Sens Actuat B - Chem 2005;105(2):365-377.

88. Canal T, Peppas NA. Correlation between mesh size and equilibrium degree of swelling of polymeric networks. J Biomed Mater Res 1989;23:1183-1193.

89. Datta AK. Biological and bioenvironmental heat and mass transfer. New York: Marcel Dekker; 2002.

90. Peppas NA, Bures P, Leobandung W, Ichikawa H. Hydrogels in pharmaceutical formulations. Eur J Pharm Biopharm 2000;50:27-46.

91. Liu L, Sheardown H. Glucose permeable poly (dimethyl siloxane) poly (N-isopropyl acrylamide) interpenetrating networks as ophthalmic biomaterials. Biomaterials 2005;26(3):233-244.

92. Shewhart W. Economic control of quality of manufactured product. Princeton, NJ: Van Nostrand; 1931.

93. Evered D, Whelan J, editors. Fibrosis (Ciba Foundation Symposium 114). London: Pitman; 1985.

94. Ratner BD, Hoffman AS, Schoen FJ, Lemons JE, editors. Biomaterials science: An introduction to materials in medicine. 2nd ed. San Diego, CA: Elsevier; 2004.

95. Black J. Biological performance of materials: Fundamentals of biocompatibility. Boca Raton, FL: CRC Press; 2006.

96. Stocum DL. Wound repair, regeneration and artificial tissues. Austin, TX: R.G. Landes; 1995.

97. Silver FH, Christiansen DL. Biomaterials science and biocompatibility. New York: Springer-Verlag; 1999.

98. Anderson JM. Biological responses to materials. Annu Rev Mater Res 2001;31:81-110.

99. Ratner BD, Bryant SJ. Biomaterials: Where we have been and where we are going. Annu Rev Biomed Eng 2004;6:41-75.

100. Frost M, Meyerhoff ME. In vivo chemical sensors: Tackling biocompatibility. Anal Chem 2006;78(21):7370-7377.

101. Shtilman MI. Polymeric biomaterials: Part I polymer implants. Boston: VSP; 2003.

102. Zaikov GE (ed). Polymers in medicine. Commack, NY: Nova Science; 1998.

103. Williams DF, editor. Definitions in biomaterials. Volume 4. Amsterdam: Elsevier; 1987.

104. Ratner BD. Reducing capsular thickness and enhancing angiogenesis around implant drug release systems. J Control Release 2002;78(1-3):211-218.

105. Moussy F, Reichert WM. Biomaterials community examines biosensor biocompatibility. Diabetes Technol Ther 200;2(3):473-477.

106. Rebrin K, Fischer U, Hahn von Dorsche H, von Woetke T, Abel P, Brunstein E. Subcutaneous glucose monitoring by means of electrochemical sensors: Fiction or reality? J Biomed Eng 1992;14(1):33-40.

107. Sharkawy AA, Klitzman B, Truskey GA, Reichert WM. Engineering the tissue which encapsulates subcutaneous implants. I. Diffusion properties. J Biomed Mater Res 1997;37(3):401-412.

108. Dungel P, Long N, Yu B, Moussy Y, Moussy F. Study of the effects of tissue reactions on the function of implanted glucose sensors. J Biomed Mater Res A 2008;85A(3):699-706.

109. Wisniewski N, Rajamand N, Adamsson U, Lins PE, Reichert WM, Klitzman B, Ungerstedt U. Analyte flux through chronically implanted subcutaneous polyamide membranes differs in humans and rats. Am J Physiol Endocrinol Metab 2002;282(6):E1316-1323.

110. Wisniewski N, Reichert M. Methods for reducing biosensor membrane biofouling. Colloid Surface B 2000;18(3-4):197-219.

111. Park H, Park K. Hydrogels in bioapplications. In: Ottenbrite RM, Huang SJ, Park K, editors. Hydrogels and Biodegradable Polymers for Bioapplications. Washington, DC: American Chemical Society; 1996.

112. Kopecek J. Hydrogel biomaterials: A smart future? Biomaterials 2007;28(34):5185-5192.

113. Jilie K, Li M. Smart hydrogels. In: Galaev I, Mattiasson B, editors. Smart Polymers: Applications in Biotechnology and Biomedicine. Boca Raton, GL: CRC Press; 2008. p 247-268.

114. Freitag R (ed). Synthetic polymers for biotechnology and medicine. Austin, TX: Eurekah; 2003.

115. Tanaka T. Dynamics of critical concentration fluctuations in gels. Phys Rev A 1978;17(2):763-766.

116. Hoffmann J, Plötner M, Kuckling D, Fischer W-J. Photopatterning of thermally sensitive hydrogels useful for microactuators. Sensor Actuat A - Phys 1999;77(2):139-144.

117. Harmon ME, Tang M, Frank CW. A microfluidic actuator based on thermoresponsive hydrogels. Polymer 2003;44(16):4547-4556.

118. Ramanan RMK, Chellamuthu P, Tang L, Nguyen KT. Development of a temperature-sensitive composite hydrogel for drug delivery applications. Biotechnol Prog 2006;22(1):118-125.

119. Bae YH, Okano T, Hsu R, Kim SW. Thermo-sensitive polymers as on-off switches for drug release. Makromol Chem - Rapid Comm 1987;8:481-485.

120. Brazel CS, Peppas NA. Pulsatile local delivery of thrombolytic and antithrombotic agents using poly(N-isopropylacrylamide-co-methacrylic acid) hydrogels. J Control Release 1996;39:57-64.

121. Dinarvand R, D'Emanuele A. The use of thermoresponsive hydrogels for on-off release of molecules. J Control Release 1995;36(3):221-227.

122. Twaites BR, de las Heras Alarcón C, Cunliffe D, Lavigne M, Pennadam S, Smith JR, Górecki DC, Alexander C. Thermo and pH responsive polymers as gene

delivery vectors: Effect of polymer architecture on DNA complexation in vitro. J Controll Release 2004;97(3):551-566.

123. Schmaljohann D, Oswald J, Jorgensen B, Nitschke M, Beyerlein D, Werner C. Thermo-responsive PNiAAm-g-PEG films for controlled cell detachment. Biomacromolecules 2003;4(6):1733-1739.

124. Yamada N, Okano T, Sakai H, Karikusa F, Sawasaki Y, Sakurai Y. Thermo-responsive polymeric surfaces: Control of attachment and detachment of cultured cells. Makromol Chem - Rapid Comm 1990;11:571-576.

125. Schmaljohann D. Thermo-responsive polymers and hydrogels in tissue engineering. E-Polymers 2005(21).

126. Shimizu T, Yamato M, Isoi Y, Akutsu T, Setomaru T, Abe K, Kikuchi A, Umezu M, Okano T. Fabrication of pulsatile cardiac tissue grafts using a novel 3-dimensional cell sheet manipulation technique and temperature-responsive cell culture surfaces. Circ Res 2002;90(3):e40.

127. Alarcon CDH, Pennadam S, Alexander C. Stimuli responsive polymers for biomedical applications. Chem Soc Rev 2005;34:276-285.

128. Wu XY, Zhang Q, Arshady R. Stimuli sensitive hydrogels: Polymer structure and phase transition. In: Arshady R, editor. Introduction to Polymeric Biomaterials. London: Citus; 2003. p 157-194.

129. Chaterji S, Kwon IK, Park K. Smart polymeric gels: Redefining the limits of biomedical devices. Prog Polym Sci 2007;32:1083-1122.

130. Heskins M, Guillet JE. Solution properties of poly(N-isopropylacrylamide). J Macromol Sci A 1968;2(8):1441-1455.

131. Lu H-F, Targonsky ED, Wheeler MB, Cheng Y-L. Thermally induced gelable polymer networks for living cell encapsulation. Biotechnol Bioeng 2007;96(1):146-155.

132. Zhang X-Z, Wu D-Q, Chu C-C. Synthesis, characterization and controlled drug release of thermosensitive IPN-PNIPAAm hydrogels. Biomaterials 2004;25:3793-3805.

133. Stoica F, Miller AF, Alexander C, Saiani A. Thermo-responsive PNIPAAm copolymers with hydrophobic spacers. Macromol Symp 2007;251(1):33-40.

134. Hou Y, Matthews AR, Smitherman AM, Bulick AS, Hahn MS, Hou H, Han A, Grunlan MA. Thermoresponsive nanocomposite hydrogels with cell-releasing behavior. Biomaterials 2008;29(22):3175-3184.

135. Singh D, Kuckling D, Choudhary V, Adler HJ, Koul V. Synthesis and characterization of poly(N-isopropylacrylamide) films by photopolymerization. Polym Advan Technol 2006;17(3):186-192.

136. McShane MJ, Russell RJ, Pishko MV, Cote GL. Glucose monitoring using implanted fluorescent microspheres. IEEE Eng Med Biol 2000;19(6):36-45.

137. Lee KK, Jung JC, Jhon MS. The synthesis and thermal phase transition behavior of poly(N-isopropylacrylamide)-b-poly(ethylene oxide). Polym Bull 1998;40:455-460.

138. Tanaka T, Fillmore DJ. Kinetics of swelling of gels. J Chem Phys 1979;70(3):1214-1218.

139. Lee S, editor. Encyclopedia of chemical processing. Boca Raton, FL: CRC Press; 2006.

140. Shen M, Martinson L, Wagner MS, Castner DG, Ratner BD, Horbett TA. PEO-like plasma polymerized tetraglyme surface interactions with leukocytes and proteins: in vitro and in vivo studies. J Biomat Sci - Polym E 2002;13(4):367-390.

141. Russell TP. Surface-responsive materials. Science 2002;297(5583):964-967.

142. Blatteis CM, editor. Physiology and pathophysiology of temperature regulation. River Edge, NJ: World Scientific; 1998.

143. Savage MV, Brengelmann GL. Control of skin blood flow in the neutral zone of human body temperature regulation. J Appl Physiol 1996;80(4):1249-1257.

144. Hardy JD, Du Bois EF, Soderstrom GF. Basal metabolism, radiation, convection and vaporization at temperatures of 22 to 35 °C.: Six figures. J Nutr 1938;15(5):477-497.

145. Werner J, Buse M. Temperature profiles with respect to inhomogeneity and geometry of the human body. J Appl Physiol 1988;65(3):1110-1118.

146. Ducharme MB, Tikuisis P. Forearm temperature profile during the transient phase of thermal stress. Eur J Appl Physiol 1992;64:395-401.

147. Montgomery LD, Williams BA. Effect of ambient temperature on the thermal profile of the human forearm, hand, and fingers. Ann Biomed Eng 1976;4:209-219.

148. Bouchama A, Knochel JP. Heat stroke. New Engl J Med 2002;346(25):1978-1988.

149. Ducharme MB, VanHelder WP, Radomski MW. Tissue temperature profile in the human forearm during thermal stress at thermal stability. J Appl Physiol 1991;71(5):1973-1978.

150. Rampulla J. Hyperthermia & heat stroke: Heat-related conditions. In: O'Connell JJ, editor. The Health Care of Homeless Persons. Boston: Boston Health Care for the Homeless Program; 2004. p 199-204.

151. Jessen C. Temperature regulation in humans and other mammals. Berlin: Springer-Verlag; 2001.

152. Gonzalez-Alonso J, Teller C, Andersen SL, Jensen FB, Hyldig T, Nielsen B. Influence of body temperature on the development of fatigue during prolonged exercise in the heat. J Appl Physiol 1999;86(3):1032-1039.

153. Schonbaum E, Lomax P, editors. Thermoregulation: Physiology and biochemistry. Volume 131. New York: Pergamon Press; 1990.

154. Khan F, Elhadd TA, Greene SA, Belch JJ. Impaired skin microvascular function in children, adolescents, and young adults with type 1 diabetes. Diabetes Care 2000;23(2):215-220.

155. Katz A, Ekberg K, Johansson BL, Wahren J. Diminished skin blood flow in type I diabetes: Evidence for non-endothelium-dependent dysfunction. Clin Sci 2001;101(1):59-64.

156. Forst T, Kunt T, Pohlmann T, Goitom K, Lobig M, Engelbach M, Beyer J, Pfutzner A. Microvascular skin blood flow following the ingestion of 75 g glucose in healthy individuals. Exp Clin Endocr Diab 1998;106(6):454-459.

157. Yki-Jarvinen H, Utriainen T. Insulin-induced vasodilatation: Physiology or pharmacology? Diabetologia 1998;41(4):369-379.

158. Geever LM, Nugent MJD, Higginbotham CL. The effect of salts and pH buffered solutions on the phase transition temperature and swelling of thermoresponsive pseudogels based on N-isopropylacrylamide. J Mater Sci 2007;42:9845-9854.

159. Eeckman F, Amighi K, Moes AJ. Effect of some physiological and non-physiological compounds on the phase transition temperature of thermoresponsive polymers intended for oral controlled-drug delivery. Int J Pharm 2001;222:259-270.

160. Erbil C, Aras S, Uyanik N. Investigation of the effect of type and concentration of ionizable comonomer on the collapse behavior of N-isopropylacrylamide copolymer gels in water. J Polym Sci Pol Chem 1999;37:1847-1855.

161. Feil H, Bae YH, Feijen J, Kim SW. Effect of comonomer hydrophilicity and ionization on the lower critical solution temperature of N-isopropylacrylamide copolymers. Macromolecules 1993;26(10):2496-2500.

162. Stile RA, Burghardt WR, Healy KE. Synthesis and characterization of injectable poly(N-isopropylacrylamide)-based hydrogels that support tissue formation in vitro. Macromolecules 1999;32(22):7370-7379.

163. Suzuki T, Ikkai F, Shibayama M. Structure and dynamics of N-isopropylacrylamide / acrylic acid copolymer gels prepared by cross-linker-free UV-induced polymerization. Macromolecules 2007;40(7):2509-2514.

164. Huglin MB, Liu Y, Velada JL. Thermoreversible swelling behaviour of hydrogels based on N-isopropylacrylamide with acidic comonomers. Polymer 1997;38(23):5785-5791.

165. Kratz K, Hellweg T, Eimer W. Influence of charge density on the swelling of colloidal poly(N-isopropylacrylamide-co-acrylic acid) microgels. Colloid Surface A 2000;170(2-3):137-149.

166. Kuckling D, Richter A, Arndt KF. Temperature and pH-dependent swelling behavior of poly(N-isopropylacrylamide) copolymer hydrogels and their use in flow control. Macromol Mater Eng 2003;288(2):144-151.

167. Bekiari V, Lianos P. Photophysical behavior of terpyridine-lanthanide ion complexes incorporated in a poly(N,N-dimethylacrylamide) hydrogel. Langmuir 2006;22:8602-8606.

168. Kato N, Gehrke SH. Microporous, fast response cellulose ether hydrogel prepared by freeze-drying. Colloids and Surfaces B: Biointerfaces 2004;38(3-4):191-196.

169. Campbell NA, Reece JB, Mitchell LG. Biology. Menlo Park, CA: Benjamin Cummings; 1999.

170. Hobabi MR, Hassanzadeh D, Azarmi S, Entezami AA. Effect of synthesis method and buffer composition on the LCST of a smart copolymer of N-isopropylacrylamide and acrylic acid. Polym Adv Technol 2007;18:986-992.

171. Pei Y, Chen J, Yang L, Shi L, Tao Q, Hui B, Li J. The effect of pH on the LCST of poly(N-isopropylacrylamide) and poly(N-isopropylacrylamide-co-acrylic acid). J Biomater Sci Polym E 2004;15(5):585-594.

172. Jones MS. Effect of pH on the lower critical solution temperatures of random copolymers of N-isopropylacrylamide and acrylic acid. Eur Polym J 1999;35(5):795-801.

173. Liu X-M, Wang LSL-S, Wang L, Huang J, He C. The effect of salt and pH on the phase-transition behaviors of temperature-sensitive copolymers based on N-isopropylacrylamide. Biomaterials 2004;25(25):5659-5666.

174. Eeckman F, Moes AJ, Amighi K. Evaluation of a new controlled-drug delivery concept based on the use of thermoresponsive polymers. Int J Pharm 2002;241:113-125.

175. Zhang J-T, Bhat R, Jandt KD. Temperature-sensitive PVA/PNIPAAm semi-IPN hydrogels with enhanced responsive properties. Acta Biomater 2009;5:488-497.

176. Lee W, Yen S. Thermoreversible hydrogels. XII. Effect of the polymerization conditions on the swelling behavior of the N-isopropylacrylamide gel. J Appl Polym Sci 2000;78:1604-1611.

177. Zhang XZ, Chu CC. Thermosensitive PNIPAAm cryogel with superfast and stable oscillatory properties. Chem Commun 2003:1446-1447.

178. Zhang XZ, Wang FJ, Chu CC. Thermoresponsive hydrogel with rapid response dynamics. J Mater Sci - Mater M 2003;14:451-455.

179. Anseth KS, Bowman CN, Brannon-Peppas L. Mechanical properties of hydrogels and their experimental determination. Biomaterials 1996;17(17):1647-1657.

180. Takata S-i, Norisuye T, Shibayama M. Preparation temperature dependence and effects of hydrolysis on static inhomogeneities of poly(acrylamide) gels. Macromolecules 1999;32(12):3989-3993.

181. Rathjen CM, Park C-H, Goodrich PR, Walgenbach DD. The effect of preparation temperature on some properties of a temperature-sensitive hydrogel. Polym Gels Netw 1995;3(2):101-115.

182. Sayil C, Okay O. The effect of preparation temperature on the swelling behavior of poly(N-isopropylacrylamide) gels. Polym Bull 2000;45(2):175-182.

183. Kayaman N, Kazan D, Erarslan A, Okay O, Baysal BM. Structure and protein separation efficiency of poly(N-isopropylacrylamide) gels: Effect of synthesis conditions. J Appl Polym Sci 1998;67(5):805-814.

184. Wicks ZW, Jones FN, Pappas SP, editors. Organic coatings science and technology. 2nd ed. New York: John Wiley & Sons; 1999.

185. Iatridis JC, Wu J, Yandow JA, Langevin HM. Subcutaneous tissue mechanical behavior is linear and viscoelastic under uniaxial tension. Connect Tissue Res 2003;44:208-217.

186. Chen B, Xu FJ, Fang N, Neoh KG, Kang ET, Chen WN, Chan V. Engineering cell de-adhesion dynamics on thermoresponsive poly(N-isopropylacrylamide). Acta Biomater 2008;4:218-229.

187. Scheffler M, Hirt E. Wrist-wearable medical devices: Technologies and applications. Med Device Technol 2003;14(7):26-30.

188. Tummala RR, Sundaram V, Fuhan L, White G, Hattacharya S, Pulugurtha RM, Swaminathan M, Dalmia S, Laskar J, Jokerst NM and others. High density packaging in 2010 and beyond. December 4-6, 2002. Proceedings of the 4th International Symposium on Electronic Materials and Packaging, Kaohsiung, Taiwan. p 30-36.

189. Roy Y. High density 3d integration. July 28-31, 2008. International Conference on Electronic Packaging Technology & High Density Packaging, Shanghai, China. p 1-10.

190. Williams B. The top five considerations in choosing flexible heaters for ruggedized display units. 2006. Military Embedded Systems website at www.mil-embedded.com/articles/authors/williams,b/; accessed September 2009.

191. Diller K, Shitzer A, editors. Macroscopic & microscopic heat and mass transfer in biomedical engineering. Belgrade: International Centre for Heat and Mass Transfer; 1992.

192. Jia W, Aguilar G, Verkruysse W, Franco W, Nelson JS. Improvement of port wine stain laser therapy by skin preheating prior to cryogen spray cooling: A numerical simulation. Laser Surg Med 2006;38(2):155-162.

193. Ducharme MB, Tikuisis P. In vivo thermal conductivity of the human forearm tissues. J Appl Physiol 1991;70(6):2682-2690.

194. Chern J-M, Lee W-F, Hsieh M-Y. Preparation and swelling characterization of poly(N-isopropylacrylamide)-based porous hydrogels. J Appl Polym Sci 2004;92(6):3651-3658.

195. Li Y, Tanaka T. Study of the universality class of the gel network system. J Chem Phys 1989;90(9):5161-5166.

196. Janwantanakul P. Cold pack/skin interface temperature during ice treatment with various levels of compression. Physiotherapy 2006;92(4):254-259.

197. Nordlund JJ, Boissy RE. The biology of melanocytes. In: Freinkel RK, Woodley DT, editors. The Biology of the Skin. New York: Parthenon; 2001. p 113-131.

198. Shimada M, Masuda Y, Yamada Y, Itoh M, Takahashi M, Yatagai T. Explanation of human skin color by multiple linear regression analysis based on the modified Lambert-Beer law. Opt Rev 2000;7(4):348-352.

199. Anderson RR, Parrish JA. The optics of human skin. The Journal of Investigative Dermatology 1981;77:13-19.

200. Jacques SL. Optical properties spectra. Oregon Medical Laser Center website at omlc.ogi.edu; accessed September 2009.

201. Warren W. Introduction to tissue imaging. Warren Research Group at Duke University website at www.chem.duke.edu/~wwarren/tissueimaging.php; accessed September 2009.

202. Yeh S, Hanna CF, Khalil OS. Monitoring blood glucose changes in cutaneous tissue by temperature-modulated localized reflectance measurements. Clin Chem 2003;49(6):924-934.

203. Wang LV, Wu H. Biomedical optics: Principles and imaging. Hoboken, NJ: Wiley; 2007.

204. McShane MJ. Design of an optical probe and signal processing for an implantable florescence-based glucose sensor, PhD dissertation, Texas A&M University, College Station, TX, 1999.

205. McShane MJ, Rastegar S, Pishko M, Cote GL. Monte Carlo modeling for implantable fluorescent analyte sensors. IEEE T Biomed Eng 2000;47(5):624-632.

206. Cheong W-F, Prahl SA, Welch AJ. A review of the optical properties of biological tissues. IEEE J Quantum Elect 1990;26(12):2166-2185.

207. Churmakov DY, Meglinski IV, Greenhalgh DA. Amending of fluorescence sensor signal localization in human skin by matching of the refractive index. J Biomed Opt 2004;9(2):339-346.

208. Materials Database Station. PolyInfo polymer database: poly(N-isopropylacrylamide). National Institute for Materials Science website at polymer.nims.go.jp; accessed September 2009.

209. Marquez G, Wang LV, Wang C, Hu Z. Development of tissue-simulating optical phantoms: poly-N-isopropylacrylamide solution entrapped inside a hydrogel. Phys Med Biol 1999;44:309-318.

210. ANSI. Safe use of lasers, standard z-136.1-1993. Orlando, FL: American National Standards Institute, Laser Institute of America; 1993.

211. Meirik O. Implantable contraceptives for women. Contraception 2002;65(1):1-2.

212. Matlaga BF, Yasenchak LP, Salthouse TN. Tissue response to implanted polymers: The significance of sample shape. J Biomed Mater Res 1976;10:391-397.

213. Levine JP, Sinofsky FE, Christ MF. Assessment of Implanon insertion and removal. Contraception 2008;78:409-417.

214. Fischer MA. Implanon: A new contraceptive implant. JOGNN 2008;37:361-368.

215. Ballerstadt R, Evans C, McNichols R, Gowda A. Concanavalin A for in vivo glucose sensing: A biotoxicity review. Biosens Bioelectron 2006;22(2):275-284.

216. Gad SC. Safety evaluation of medical devices. New York: Marcel Dekker; 2002.

217. U.S. Food and Drug Administration. Device advice: Device regulation and guidance. U.S. Department of Health & Human Services, FDA website at www.fda.gov/medicaldevices/deviceregulationandguidance/default.htm; accessed September 2009.

218. Batchelor AW, Chandrasekaran M, editors. Service characteristics of biomedical materials and implants. Volume 3. London: Imperial College Press; 2004.

VITA

Rebecca May Gant developed an interest in science and medicine when her younger brother was diagnosed with diabetes at the age of eight. Pursuing knowledge in these fields, she attended Cornell University and received her Bachelor of Science degree in biological engineering with a biomedical engineering minor in 2003. In order to build upon her learning with practical application, she continued on at Cornell, completing her Master of Engineering work in biological engineering in 2004 under the direction of Dr. Daniel Aneshansley. Following graduation, Rebecca traveled to Texas A&M University to enter the Optical Biosensing Laboratory. Working with Dr. Gerard Coté and Dr. Melissa Grunlan, she explored materials for encapsulating implantable glucose sensors for diabetes. After receiving her Doctor of Philosophy degree in biomedical engineering in December 2009, Rebecca hopes to continue working in the field of diabetes technology.

Rebecca can be reached by email at beckygant@tamu.edu or at the following address:

Department of Biomedical Engineering

Texas A&M University

Mail Stop 3120

College Station, TX 77843